Single-molecule approaches to unravel the mechanism of SMC proteins

Eeftens, Jorine

DOI
10.4233/uuid:e011fb5f-d2cf-4f1f-905d-d2f1e82630a2

Publication date
2017

Document Version
Final published version

Citation (APA)
Eeftens, J. (2017). *Single-molecule approaches to unravel the mechanism of SMC proteins*. [Dissertation (TU Delft), Delft University of Technology]. https://doi.org/10.4233/uuid:e011fb5f-d2cf-4f1f-905d-d2f1e82630a2

Single-molecule approaches to unravel the mechanism of SMC proteins

Single-molecule approaches to unravel the mechanism of SMC proteins

Proefschrift

ter verkrijging van de graad van doctor
aan de Technische Universiteit Delft,
op gezag van de Rector Magnificus prof. ir. K.C.A.M. Luyben,
voorzitter van het College voor Promoties,
in het openbaar te verdedigen op vrijdag 3 november 2017 om 15:00 uur

door

Jorine Mirjam Eeftens

Master of Science in Molecular Life Sciences,
Radboud Universiteit Nijmegen,
geboren te Breda, Nederland.

This dissertation has been approved by the

promotor: prof. dr. C. Dekker

Composition of the doctoral committee:

Rector Magnificus,	chairman
prof. dr. C. Dekker,	Technische Universiteit Delft
Independent members:	
Prof. dr. D.J. Sherratt,	University of Oxford
Prof. dr. ir. S. Tans,	Technische Universiteit Delft
dr. C. Joo,	Technische Universiteit Delft
dr. B. Rowland,	NKI Amsterdam
dr. F. Uhlmann,	The Francis Crick Institute
Prof. dr. N. Dekker,	Technische Universiteit Delft, reserve member
Other members:	
dr. C.H. Haering,	EMBL Heidelberg

Keywords: SMC proteins, cohesin, condensin, single-molecule biophysics, magnetic tweezers, DNA curtains, atomic force microscopy

Printed by: Gildeprint

Front & Back: Jorine Eeftens

Casimir PhD Series, Delft-Leiden 2017-36

ISBN 978-90-8593-320-5

An electronic version of this dissertation is available at
`http://repository.tudelft.nl/`.

Contents

I

Introduction

1

Preface

DNA in every living cell has to be organised in such a way that it fits inside the cell, but at the same time stays accessible for cellular processes. To achieve this, cells use proteins to organise the DNA. Members of the SMC (structural maintenance of chromosomes) family are important players in this process, conserved from bacteria to humans. In this introduction, we review the history of SMC proteins and their role in DNA organisation.

1

1.1. DNA organisation

Cells need a way to store their genetic information. The polymer DNA (deoxyribonucleic acid) fulfils this role, with all information encoded in its sequence. DNA has to be stored properly, but it also needs to be replicated, expressed, and repaired. Every cell in every organism deals with the challenge of organising its DNA to make this possible. To fit inside a cell with a size in the micrometer range, the meters-long DNA has to be compacted to a size that is several orders of magnitude smaller. In humans, for example, each cell contains a genome of about 2 meters of DNA, that has to fit inside a cell that is a few microns in size.

While in the compacted state, the DNA still needs to be accessible for cellular processes such as transcription, translation, and DNA repair. To achieve this, the DNA is organised into chromosomes. Prokaryotes commonly have only one chromosome, organised in the nucleoid: an irregularly shaped region that is not confined by a membrane. DNA segregation occurs in parallel with replication (for a review on bacterial chromosome organisation, see [1]). Eukaryotes have multiple, linear chromosomes that are organised in the cell nucleus. The nucleus is membrane-enclosed. Here, the processes of segregation and replication are separated in time. Besides the global folding to fit inside the cell nucleus, eukaryotic DNA needs a second level of compaction into mitotic chromosomes. All organisms use similar strategies for organising their DNA: supercoiling [2], and protein-assisted organisation [3].

DNA binding proteins or nucleoid/nuclear associated proteins (NAPs) are numerous, diverse, and unevenly understood. General common factors are 1) association with DNA, and 2) their ability to alter the trajectory of the DNA. They can do so by, for example, forming DNA bridges (e.g., Fis, H-NS), wrapping DNA around them (e.g., nucleosomes), or bending the DNA (e.g., HU). SMC proteins are known to interact with DNA and alter its shape, but we are still largely in the dark on their particular mechanism.

1.2. A short history of SMC proteins

Cohesin, condensin, Smc5/6, MukB, and BsSMC are nowadays known as members of the family of Structural Maintenance of Chromosomes. Originally, however, the SMC acronym stood for Stability of Mini-Chromosomes [4]. After discovering the involvement of *S. cerevisiae* Smc1 in chromosome segregation [5] and Smc2 in chromosome compaction, it was proposed that the original SMC acronym should be redefined as Structural Maintenance of Chromosomes [6], which indeed became the convention. We now know SMC proteins as large, ring-like complexes, consisting of a dimer of SMC proteins that are connected at a hinge, and a kleisin subunit, that bridges the ATPase heads of the SMC dimer. Until today, we are not aware of the existence of an organism that does not express an SMC protein [7].

The dynamic behaviour of chromosomes in the cell cycle has been described long ago, even before DNA was identified as the carrier of genetic information [8]. Sister chromatid cohesion (sister chromatids keeping together while microtubules exert pulling forces) and chromosome condensation (DNA compaction into mitotic chromosomes) were already observed as relevant processes by Walter Flemming, who drew pictures of both phenomena in detail at the end of the 19th century (Figure 1.1a). A few years later,

the names of the "phases" of mitosis were introduced. Now, we can visualise this process with microscopy (Figure 1.1b). A century later, cohesin and condensin were found essential players in this process, and in 1997, both complexes were named [9, 10].

Cohesin

Cohesion of sister-chromatids had long been recognised as an important event, and scientists already suspected that a protein factor was responsible for resisting microtubule forces, and subsequently destructing cohesion. Throughout the nineties, different pieces of the puzzle came together, and cohesin was identified.

The SMC1 gene was already described as encoding a head-rod-tail type of protein in the early nineties [5]. In a 1997 paper, Smc1, Smc3 and the kleisin Scc1 were identified as proteins that ensure chromosome cohesion [10]. Soon thereafter, it was found that cohesin indeed ensures proper attachment of microtubules [12], and cleavage of the Scc1 unit by separase was the event that triggered separation of sister chromatids [13, 14] (Figure 1.2). Besides this anaphase pathway, it was shown that most cohesin complexes are released from the DNA in prophase [15]. Proof that cohesin forms a ring came a few years later [16, 17], followed by studies showing that cohesin topological embraces DNA [18, 19]. Recently, topological loading was also shown *in vitro* [20, 21].

A major open question is: how does cohesin load onto the DNA? We know that cleavage of Scc1 by separase releases cohesin from DNA in at the onset of anaphase, but how does it release from DNA in the prophase pathway? *In vivo* cross-linking studies indicated that loading of cohesin onto DNA involves opening of the hinge domain [22], while the prophase DNA exit gate was proposed to be between Scc1 and the Smc3 coiled coil [23]. This dissociation pathway is regulated by the protein Wapl [24]. However, *in vitro* loading studies indicate that both loading and release involves ATP hydrolysis and opening of the Scc1-Smc3 interface [20].

Cohesin's role in gene expression was first discovered in yeast, where it was found at the boundaries of silenced chromatin [25]. The discovery that cohesin mediates transcription through association with CTCF binding sites, together with the invention of chromosome-capture techniques, opened up a new area of research [26, 27].

If cohesin is not functioning correctly, this can result in a range of diseases and defects. A number of developmental disorders originate from genetic mutations in cohesin. These disorders are termed cohesinopathies, and typically result in a range of developmental effects like mental retardation, growth defects, and deformed limbs [28]. Cohesion needs to resist in female oocytes for decades, from birth till maturity, and loss of this cohesion can result in aneuploidy [29]. Similarly, most cancer cells have an abnormal number of chromosomes. It is therefore not surprising that cohesin subunits and regulators are mutated in about 7% of all cancers [30].

Condensin

In 1994, Hirano and colleagues identified the *Xenopus* proteins XCAP-C and XCAP-E as necessary for chromosome condensation *in vitro* [31] (Figure 1.3). During submission of their manuscript, they learned that XCAP-C and XCAP-E were the *Xenopus* homologues of condensin [32]. It was almost a decade later that it was discovered that vertebrates

1

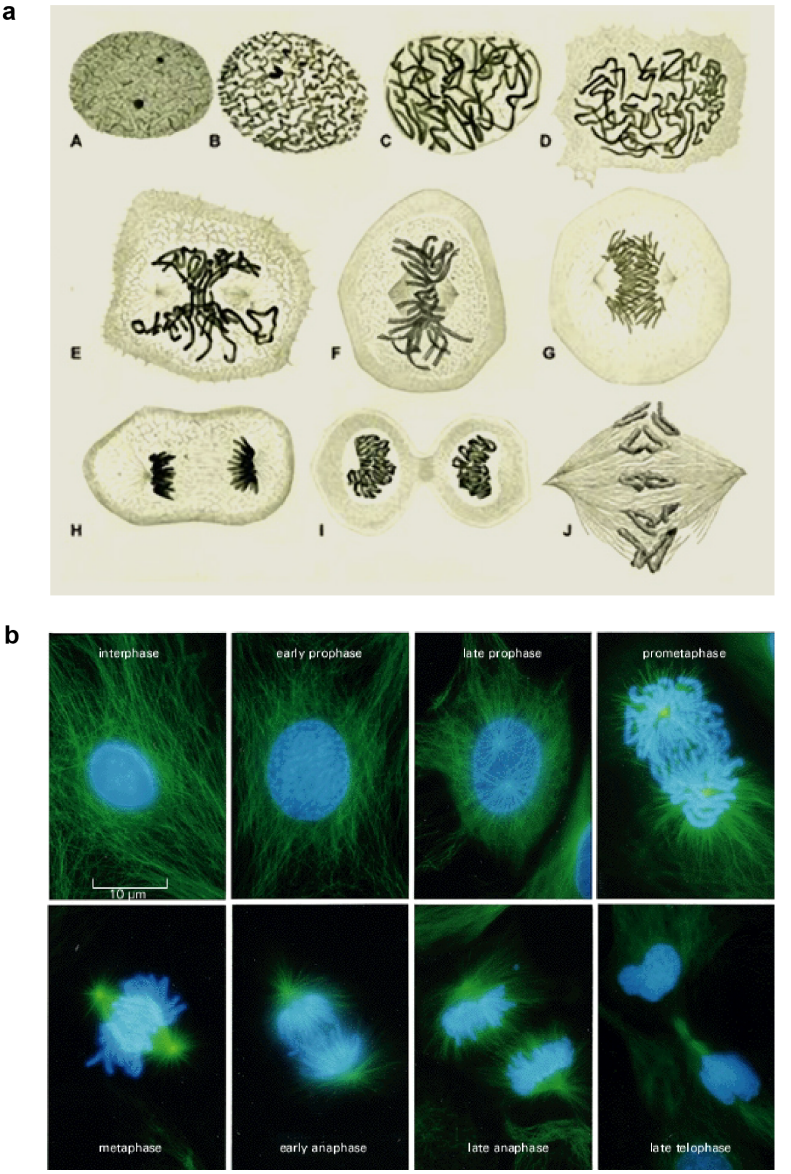

Figure 1.1: **Visualisation of mitosis. a.** Walter Flemming's drawings of mitosis from the year 1882. He documented the processes of compaction into mitotic chromosomes (A to E) as well as the alignment and separation of sister chromatids (F to J). Image adapted from [8]. **b.** Microscopy images of a cell in mitosis. Once the nuclear envelope breaks down, the DNA (stained in blue) goes from a blob that fills the entire nucleus to neatly packed chromosomes. The sister chromatids stay cohesed while the microtubules (in green) are pulling on them, until separation in anaphase. From [11].

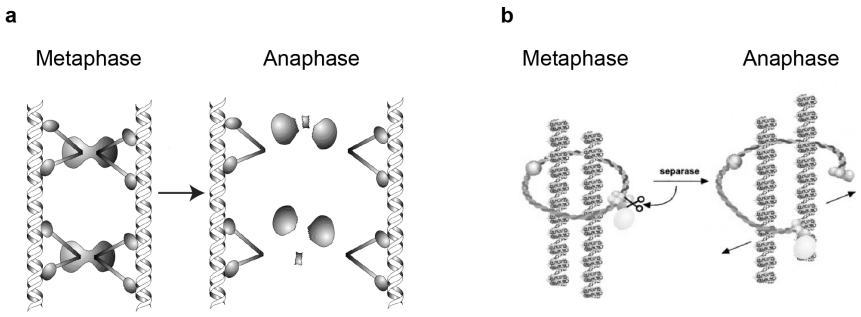

Figure 1.2: **Models for sister chromatid cohesion and release. a.** In 1999, it was already known that sister-chromatid separation was triggered by cleavage of the Scc1 cohesin subunit, but the geometry of the full cohesin complex was unknown. Image adapted from [13]. **b.** In 2002, it was discovered that cohesin formed a ring. Image adapted from [16]

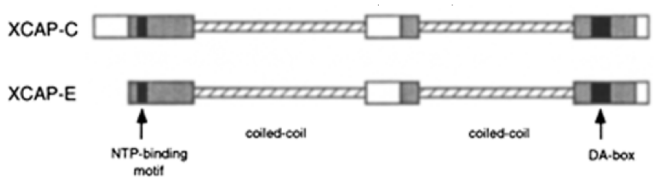

Figure 1.3: **Condensin structure as pictured in 1994.** XCAP-E and XCAP-E were later identified as Smc2 and Smc4. The DA box and NTP binding domain together form the Walker A/Walker B ATPase heads. From [31].

cells possess two condensin complexes (condensin I and condensin II) that have the same SMC-dimer but different non-SMC subunits [33].

A few years after cohesin, condensin was shown to bind DNA topologically, too [34, 35]. The role of ATP hydrolysis is still enigmatic, but it has been shown that condensin can associate with DNA in the absence of ATP [36, 37]. In addition, it was shown that condensin's HEAT repeats bind DNA directly [38]. How the condensin loads onto the DNA is still unknown. Crosslinking of the subunit interfaces (like for cohesin) is an experiment that still has to be done.

Other SMC complexes

Interestingly, although identified in 2000, the Smc5/6 complex does not yet have a name that associates with its function. It is also the least well understood [39]. Like cohesin and condensin, Smc5/6 links DNA by forming a ring consisting of an SMC-dimer and a kleisin subunit [40]. The complex was originally identified as involved in DNA repair, but Smc5/6's function might be more diverse [41]. Interestingly, it is the only SMC complex that contains subunits with catalytic activity besides the ATPase heads [42].

This thesis focusses on eukaryotic SMC proteins. Historically, the eukaryotic proteins were the first to be classified as parts of the SMC family, but homology to prokaryotic proteins was found around the same time [43]. The *Bacillus* homologue was found in 1996

[44], and identified a few years later as indeed a member of the SMC family [45]. Meanwhile, MukB was found to be required for chromosome partioning in *E. coli* in 1991 [46]. ATPase activity and binding to DNA was soon found in a follow-up paper [47], where electron micrographs showed the characteristic hinge/coiled-coil/head structure. Interestingly, it wasn't until an important imaging study from 1998 that MukB was considered a member the SMC family [48].

1.3. In this thesis

Decades of research have shown that SMC proteins are essential for all forms of life. How they use their remarkable ring-like structure and ATPase activity is still fascinating the field. Many questions remain unanswered. What is the general conformation of the SMC complexes? What is the role of ATP binding and hydrolysis? What mechanism do SMC proteins use to organise DNA? How does all of this differ between different complexes and species?

Currently, the mechanism of SMC proteins is an essential, yet still poorly understood process in cell biology. A review from 1995 already contained the same statement that we still use today: "Mechanistic studies of SMC function should help unravel the mysteries of chromosome dynamics." [49]. In this thesis, we approach this open question from a single-molecule perspective.

In Part I of this thesis, a general introduction is given and the history of SMC proteins is reviewed. More specifically, we look at the insights obtained with biophysical methods in **chapter 2**.

Part II of this thesis focuses on the structure and mechanism of the condensin complex. In **chapter 3**, the topology of condensin's Smc2-Smc4 dimers is probed with high-speed atomic force microscopy. We show that the coiled coils are flexible, and that the SMC dimers can adopt various conformations. In **chapter 4**, we use DNA curtains to demonstrate that condensin is a mechanochemical motor that translocates along the DNA. The translocation proceeds with a velocity of ~60 basepairs per second, and is only observed in the presence of hydrolysable ATP. **Chapter 5** describes our results from a magnetic tweezers assay where we monitor condensin mediated compaction in real-time. We show that compaction proceeds with distinct steps of ~200nm. Our results indicate that condensation requires two distinct steps: electrostatic interaction of condensin with DNA, followed by ATP-hydrolysis-driven topological interaction and compaction.

Part III of this thesis works towards force spectroscopy on the cohesin complex. **Chapter 6** describes a new method for attachment of biomolecules in magnetic tweezers: copper-free click chemistry. Development of this technique was necessary for the experiments conducted in **chapter 7**, where we attempt to probe the rupture force of a single cohesin complex with force spectroscopy. We describe our methods for designing the experiment, show preliminary data, and end with recommendations and outlook for pursuing this project.

References

[1] A. Badrinarayanan, T. B. Le, and M. T. Laub, *Bacterial Chromosome Organization and Segregation,* Annual Review of Cell and Developmental Biology **31**, 171 (2015).

[2] N. Gilbert and J. Allan, *Supercoiling in DNA and chromatin,* Current Opinion in Genetics & Development **25**, 15 (2014).

[3] S. C. Dillon and C. J. Dorman, *Bacterial nucleoid-associated proteins, nucleoid structure and gene expression,* Nature Reviews Microbiology **8**, 185 (2010).

[4] V. L. Larionov, T. S. Karpova, N. Y. Kouprina, and G. A. Jouravleva, *A mutant of Saccharomyces cerevisiae with impaired maintenance of centromeric plasmids,* Current Genetics **10**, 15 (1985).

[5] A. V. Strunnikov, V. L. Larionov, and D. Koshland, *SMC1: an essential yeast gene encoding a putative head-rod-tail protein is required for nuclear division and defines a new ubiquitous protein family.* The Journal of cell biology **123**, 1635 (1993).

[6] A. V. Strunnikov, E. Hogan, and D. Koshland, *SMC2, a Saccharomyces cerevisiae gene essential for chromosome segregation and condensation, defines a subgroup within the SMC family.* Genes & development **9**, 587 (1995).

[7] N. Cobbe and M. M. S. Heck, *The Evolution of SMC Proteins: Phylogenetic Analysis and Structural Implications,* Molecular Biology and Evolution **21**, 332 (2003).

[8] Walther Flemming, *Zellsubstanz, Kern und Zelltheilung* (1882).

[9] T. Hirano, R. Kobayashi, and M. Hirano, *Condensins, chromosome condensation protein complexes containing XCAP-C, XCAP-E and a Xenopus homolog of the Drosophila Barren protein.* Cell **89**, 511 (1997).

[10] C. Michaelis, R. Ciosk, and K. Nasmyth, *Cohesins: Chromosomal Proteins that Prevent Premature Separation of Sister Chromatids,* Cell **91**, 35 (1997).

[11] B. Alberts, A. Johnson, J. Lewis, M. Raff, K. Roberts, and P. Walter, *Molecular biology of the cell (garland science, new york, 2002),* There is no corresponding record for this reference (1997).

[12] T. Tanaka, J. Fuchs, J. Loidl, and K. Nasmyth, *Cohesin ensures bipolar attachment of microtubules to sister centromeres and resists their precocious separation.* Nature cell biology **2**, 492 (2000).

[13] K. Nasmyth, F. Uhlmann, and F. Lottspeich, *Sister-chromatid separation at anaphase onset is promoted by cleavage of the cohesin subunit Scc1,* Nature **400**, 37 (1999).

[14] F. Uhlmann, D. Wernic, M. A. Poupart, E. V. Koonin, and K. Nasmyth, *Cleavage of cohesin by the CD clan protease separin triggers anaphase in yeast.* Cell **103**, 375 (2000).

[15] I. C. Waizenegger, S. Hauf, A. Meinke, and J. M. Peters, *Two distinct pathways remove mammalian cohesin from chromosome arms in prophase and from centromeres in anaphase.* Cell **103**, 399 (2000).

[16] C. H. Haering, J. Löwe, A. Hochwagen, and K. Nasmyth, *Molecular Architecture of SMC Proteins and the Yeast Cohesin Complex,* Molecular Cell **9**, 773 (2002).

[17] S. Gruber, C. H. Haering, and K. Nasmyth, *Chromosomal Cohesin Forms a Ring,* Cell **112**, 765 (2003).

[18] D. Ivanov and K. Nasmyth, *A topological interaction between cohesin rings and a circular minichromosome.* Cell **122**, 849 (2005).

[19] C. H. Haering, A.-M. Farcas, P. Arumugam, J. Metson, and K. Nasmyth, *The cohesin ring concatenates sister DNA molecules.* Nature **454**, 297 (2008).

[20] Y. Murayama and F. Uhlmann, *Biochemical reconstitution of topological DNA binding by the cohesin ring.* Nature **505**, 367 (2014).

[21] Y. Murayama and F. Uhlmann, *DNA Entry into and Exit out of the Cohesin Ring by an Interlocking Gate Mechanism,* Cell **163**, 1628 (2015).

[22] S. Gruber, P. Arumugam, Y. Katou, D. Kuglitsch, W. Helmhart, K. Shirahige, and K. Nasmyth, *Evidence that loading of cohesin onto chromosomes involves opening of its SMC hinge.* Cell **127**, 523 (2006).

[23] P. J. Huis in 't Veld, F. Herzog, R. Ladurner, I. F. Davidson, S. Piric, E. Kreidl, V. Bhaskara, R. Aebersold, and J.-M. Peters, *Characterization of a DNA exit gate in the human cohesin ring,* Science (New York, N.Y.) **346**, 968 (2014).

[24] S. Kueng, B. Hegemann, B. H. Peters, J. J. Lipp, A. Schleiffer, K. Mechtler, and J.-M. Peters, *Wapl Controls the Dynamic Association of Cohesin with Chromatin,* Cell **127**, 955 (2006).

[25] D. Donze, C. R. Adams, J. Rine, and R. T. Kamakaka, *The boundaries of the silenced HMR domain in Saccharomyces cerevisiae.* Genes & development **13**, 698 (1999).

[26] K. S. Wendt, K. Yoshida, T. Itoh, M. Bando, B. Koch, E. Schirghuber, S. Tsutsumi, G. Nagae, K. Ishihara, T. Mishiro, K. Yahata, F. Imamoto, H. Aburatani, M. Nakao, N. Imamoto, K. Maeshima, K. Shirahige, and J.-M. Peters, *Cohesin mediates transcriptional insulation by CCCTC-binding factor.* Nature **451**, 796 (2008).

[27] J. Dekker, K. Rippe, M. Dekker, and N. Kleckner, *Capturing Chromosome Conformation,* Science **295**

(2002).

[28] J. Liu and I. D. Krantz, *Cohesin and Human Disease,* Annual Review of Genomics and Human Genetics **9**, 303 (2008).

[29] T. Chiang, F. E. Duncan, K. Schindler, R. M. Schultz, and M. A. Lampson, *Evidence that Weakened Centromere Cohesion Is a Leading Cause of Age-Related Aneuploidy in Oocytes,* Current Biology **20**, 1522 (2010).

[30] A. Losada, *Cohesin in cancer: chromosome segregation and beyond,* Nature reviews Cancer **14**, 389 (2014).

[31] T. Hirano and T. J. Mitchison, *A heterodimeric coiled-coil protein required for mitotic chromosome condensation in vitro,* Cell **79**, 449 (1994).

[32] N. Saitoh, I. G. Goldberg, E. R. Wood, and W. C. Earnshaw, *ScII: An Abundant Chromosome Scaffold Protein Is a Member of a Family of Putative ATPases with an Unusual Predicted Tertiary Structure,* The Journal of Cell Biology **127**, 303 (1994).

[33] T. Ono, A. Losada, M. Hirano, M. P. Myers, A. F. Neuwald, and T. Hirano, *Differential Contributions of Condensin I and Condensin II to Mitotic Chromosome Architecture in Vertebrate Cells,* Cell **115**, 109 (2003).

[34] S. Cuylen, J. Metz, and C. H. Haering, *Condensin structures chromosomal DNA through topological links.* Nature structural & molecular biology **18**, 894 (2011).

[35] R. Gandhi, P. J. Gillespie, and T. Hirano, *Human Wapl Is a Cohesin-Binding Protein that Promotes Sister-Chromatid Resolution in Mitotic Prophase,* Current Biology **16**, 2406 (2006).

[36] K. Kimura and T. Hirano, *ATP-Dependent Positive Supercoiling of DNA by 13S Condensin: A Biochemical Implication for Chromosome Condensation,* Cell **90**, 625 (1997).

[37] D. F. Hudson, S. Ohta, T. Freisinger, F. Macisaac, L. Sennels, F. Alves, F. Lai, A. Kerr, J. Rappsilber, and W. C. Earnshaw, *Molecular and genetic analysis of condensin function in vertebrate cells.* Molecular biology of the cell **19**, 3070 (2008).

[38] I. Piazza, A. Rutkowska, A. Ori, M. Walczak, J. Metz, V. Pelechano, M. Beck, and C. H. Haering, *Association of condensin with chromosomes depends on DNA binding by its HEAT-repeat subunits.* Nature Structural & Molecular Biology **21**, 560 (2014).

[39] M. I. Fousteri and A. R. Lehmann, *A novel SMC protein complex in Schizosaccharomyces pombe contains the Rad18 DNA repair protein.* The EMBO journal **19**, 1691 (2000).

[40] T. Kanno, D. G. Berta, and C. Sjögren, *The Smc5/6 Complex Is an ATP-Dependent Intermolecular DNA Linker,* Cell Reports **12**, 1471 (2015).

[41] A. Kegel and C. Sjögren, *The Smc5/6 complex: more than repair?* Cold Spring Harbor symposia on quantitative biology **75**, 179 (2010).

[42] E. A. Andrews, J. Palecek, J. Sergeant, E. Taylor, A. R. Lehmann, and F. Z. Watts, *Nse2, a component of the Smc5-6 complex, is a SUMO ligase required for the response to DNA damage.* Molecular and cellular biology **25**, 185 (2005).

[43] S. M. Notarnicola, M. A. McIntosh, and K. S. Wise, *A Mycoplasma hyorhinis protein with sequence similarities to nucleotide-binding enzymes.* Gene **97**, 77 (1991).

[44] A. Oguro, H. Kakeshita, H. Takamatsu, K. Nakamura, and K. Yamane, *The effect of Srb, a homologue of the mammalian SRP receptor α-subunit, on Bacillus subtilis growth and protein translocation,* Gene **172**, 17 (1996).

[45] R. A. Britton, D. C. Lin, and A. D. Grossman, *Characterization of a prokaryotic SMC protein involved in chromosome partitioning.* Genes & development **12**, 1254 (1998).

[46] H. Niki, A. Jaffé, R. Imamura, T. Ogura, and S. Hiraga, *The new gene mukB codes for a 177 kd protein with coiled-coil domains involved in chromosome partitioning of E. coli.* The EMBO journal **10**, 183 (1991).

[47] H. Niki, R. Imamura, M. Kitaoka, K. Yamanaka, T. Ogura, and S. Hiraga, *E.coli MukB protein involved in chromosome partition forms a homodimer with a rod-and-hinge structure having DNA binding and ATP/GTP binding activities.* The EMBO journal **11**, 5101 (1992).

[48] T. E. Melby, *The Symmetrical Structure of Structural Maintenance of Chromosomes (SMC) and MukB Proteins: Long, Antiparallel Coiled Coils, Folded at a Flexible Hinge,* The Journal of Cell Biology **142**, 1595 (1998).

[49] T. Hirano, T. J. Mitchison, and J. R. Swedlow, *The SMC family: from chromosome condensation to dosage compensation,* Current Opinion in Cell Biology **7**, 329 (1995).

2

Biophysical approaches to clarify the mechanism of SMC proteins

Structural Maintenance of Chromosome (SMC) complexes are vital regulators of chromosome architecture, and essential in all domains of life from bacteria to humans. For decades, the field has been debating how these SMC protein complexes are able to mechanistically use their intricate ring-like structure to structurally organize DNA. Single-molecule biophysical techniques might be key to resolve the molecular mechanism of SMC proteins. This review provides an overview of insights obtained so far with such biophysical methods.

J.M. Eeftens and C. Dekker, *submitted* (2017)

Genomes of different organisms vary greatly in size, from a million to hundred billion base pairs, but all share the challenge that they need to be squeezed into a micron-size cell that is many orders of magnitude smaller than the length of the DNA. The spatial organization of the genome within cells is an intriguing scientific question of strong current interest. DNA needs to be strongly compacted, but at the same time organized in such a way that it is still accessible for processes such as transcription and repair. Structural Maintenance of Chromosome (SMC) protein complexes are the key players in the spatiotemporal organization and maintenance of DNA from bacteria to humans. They are essential for many chromosomal processes such as compaction, chromosome segregation, DNA repair, and gene regulation [1–3].

SMC protein complexes have a unique structural organization, which is characterized by a ring shape consisting of three proteins along its circumference: two SMC proteins complemented by a kleisin subunit (Figure 2.1a). The main part of the SMC subunits involves a ~50nm long antiparallel coiled coil, connecting a hinge domain on one end with ATPase heads on the other end. The SMC heads are ABC transporter ATPases, characterized by WalkerA and WalkerB motifs. All SMC rings associate with different subunits and co- factors to form functional complexes (Fig.2.1bc) [4].

The ring-like structure is very well conserved, and thus of vital importance for the function of SMC proteins. Prokaryotes only have a single type of SMC complex. The well-characterized BsSMC in *Bacillus subtilis*, for example, contains a homodimer of SMC proteins and the kleisin protein ScpA, whereas sub-families of γ-proteobacteria (e.g. *E. coli*) have an SMC complex called MukBEF (Fig. 2.1b). The structure of MukBEF slightly deviates from the other SMC complexes, as the MukF kleisin domain forms dimers, thus allowing the formation of multimers of SMC complexes [5]. Deletion or mutation of Smc or MukBEF leads to severe chromosomal defects, including disruption of nucleoid structure and failure to segregate sister chromatids [6–9].

In eukaryotes, the SMC complex has evolved to three types of protein complexes that are all essential, but that have different, partially overlapping functions: cohesin, condensin, and Smc5/6 (Fig. 2.1c). Cohesin is responsible for faithful chromosome segregation during cell division, as it holds sister chromatids together while they align under the tension of the mitotic spindle (Fig. 2.2a) [10]. Most of the cohesin is removed from the chromosome arms in prophase, but some stays bound at centromeres until the onset of anaphase, when its kleisin Scc1 is cleaved by separase to release the cohesion [10, 11]. In addition, cohesin plays an important role in gene expression (Fig. 2.2b, recently reviewed in Ref.[12]). Condensin is the main factor in mitotic chromosome assembly (Fig. 2.2a). Most eukaryotes have two condensin complexes, Condensin I and Condensin II, that work together to ensure proper DNA compaction and segregation[13]. Like cohesin, condensin also has non-mitotic chromosome functions, such as gene regulation, dosage compensation, DNA damage response, and DNA repair [1, 14, 15]. Finally, the Smc5/6 complex is the least well-understood SMC complex. It is needed for double-strand break repair, while while it also has a role in chromosome segregation [16–19].

2.1. SMC proteins in chromosome organization

The spatial organization of the genome is a topic of intense current study [20]. Genome mapping studies have provided ample evidence for topological domains and loop for-

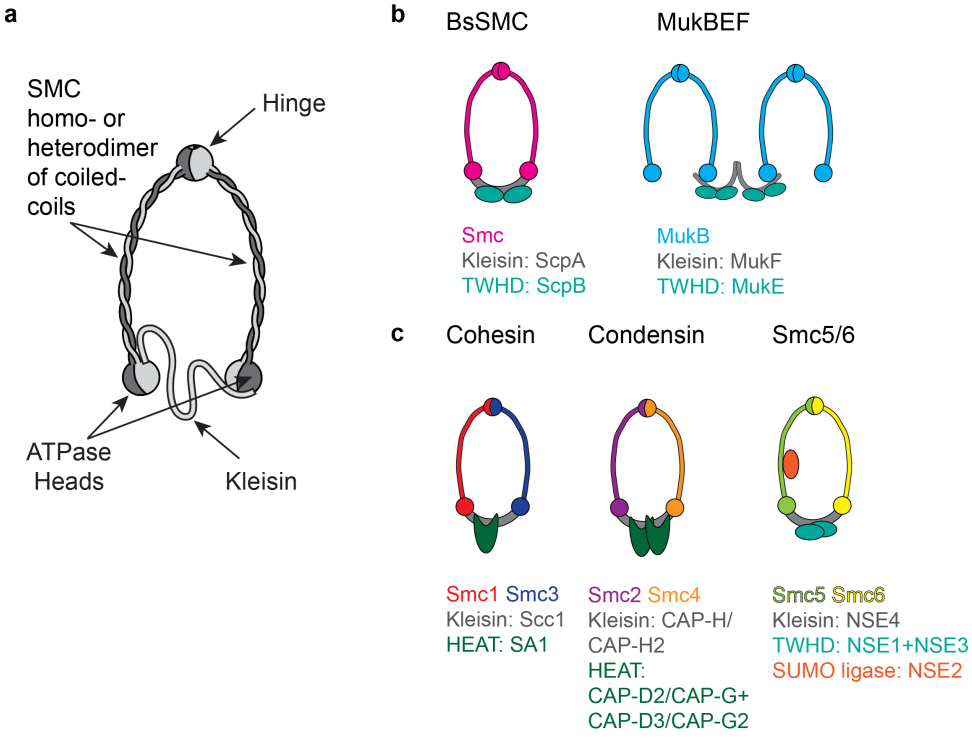

Figure 2.1: **Architecture of SMC complexes a.** General architecture of SMC complexes. SMC complexes consist of two SMC proteins that mutually connect at the hinge. In prokaryotes, this is a homodimer, whereas eukaryote complexes contain a heterodimer. The other ends of the SMC proteins, the ?heads?, exhibit ATPase activity. A kleisin subunit completes the ring. **b.** Overview of prokaryotic SMC complexes. **c.** Overview of eukaryotic SMC complexes. The names for the human proteins are listed.

mation. How exactly such loops are established and stabilized is still unclear, but SMC proteins are the main candidates for directing these processes. A topological embrace of DNA, where the SMC complex encompasses one or more DNA molecules, is thought to be the basis for the function of the ring-shaped SMC complexes, and this unique principle has been the starting point for many studies on the molecular mechanism [21–24]. Chromosome-conformation-capture methods (more generally, Hi-C methods) have recently provided great insights in understanding the three-dimensional organization of chromosomes, and the role of SMC proteins therein [25–27]. The mechanism of loop formation by SMC proteins has also been extensively investigated with computer simulations.

The classic, most simple model for chromosome organization by SMC complexes is that random DNA-DNA crosslinks are formed which can be established by trapping DNA inside the SMC ring [28, 29]. Using condensin, DNA compaction could be achieved by grabbing two DNA strands and connecting them together inside the condensin ring (Fig. 2.2c). Linking could be realized by a single SMC ring, or by two mutually interacting SMC rings. The same principle can be applied to cohesin in the context of loop formation and sister- chromatid cohesion. A stochastic non-specific linking does not explain how chromosomes arrange into elongated loop structures, instead of an entangled random-blob spatial arrangement and mutually cross-linked sister chromatids. To test if crosslinking suffices to compact DNA into chromosomes, a computer-simulation study modeled chromosome compaction as stochastic pairwise bonding between condensin molecules that connect distant DNA sites [30]. This pairwise interaction model condensed the DNA accurately and matched the Hi-C data, indicating that this simple model can go a long way to explain basic features of DNA compaction.

Recently, an alternative model, the so-called loop-extrusion model, gained a lot of attention (Fig. 2.2d) [31–33]. In this model, an SMC protein binds DNA, initiates formation of a loop, and translocates DNA through its ring to form an extending DNA loop [34, 35]. Such a principle could be employed by condensin to compact DNA into mitotic chromosomes, or by cohesin to establish loop formation in TADs. For example, cohesin might halt and anchor the loop when it encounters two CTCF sites. Alipour and Marko first simulated a 1D model with condensin as a loop-extruding enzyme machine that employs two DNA- binding sites per protein [31]. The assumption was that each binding site moves along the DNA, away from the other binding site, in an ATP-hydrolysis-dependent manner. This drives the extrusion of a loop. The authors found that under certain association and dissociation conditions, two possible outcomes could result: either formation of loops of variable size with gaps in between, or a stack of proteins anchoring a single loop. This model was recently applied on a larger scale in two independent studies [26, 34]. While these modeled general "extrusion factors", it was speculated that these factors in fact could be cohesin molecules. Sanborn et al assumed that each SMC extruder would stop extruding upon recognition of a CTCF motif of the correct directionality [26]. This led to formation of stable loops in a manner that was consistent with the experimental Hi-C data that were reported in the same paper. A second study by Fudenberg et al. came to the same conclusion [34]. Yet another large-scale study took parameters from experimental studies to model DNA compaction with condensin as the loop-extruding factor [36]. Depending on parameters, these simulations showed

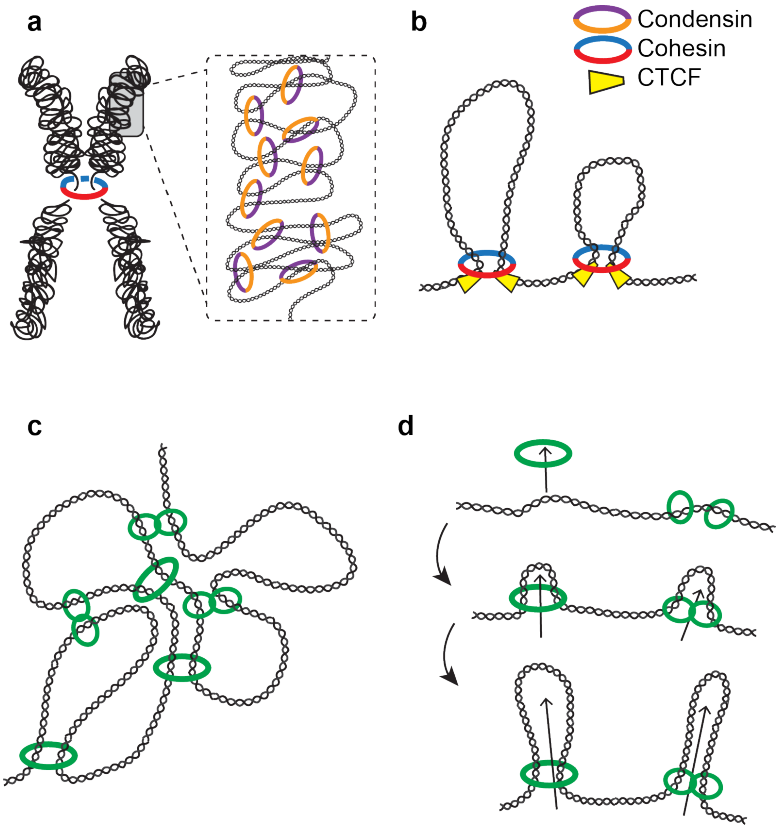

Figure 2.2: **Main mechanisms of SMC complexes. a.** Schematic depicting some of the main biological functions of cohesin and condensin. Condensin compacts the DNA into mitotic chromosomes, while cohesin holds sister chromatids together at metaphase. **b.** Cohesin acts as a boundary element for topological associating domains that are encoded in CTCF-binding sites. **c.** The random crosslinking model. An SMC complex links DNA together by trapping two DNA strands inside its ring. This looping can be achieved by a single SMC complex or by two interacting SMC complexes. **d.** The loop extrusion model. DNA gets trapped inside one or two SMC complexes upon which a DNA loop further extrudes.

either loops separated by gaps, or tightly stacked loop-arrays (the latter consistent with Hi-C data). The authors showed that one condensin per 10-30kb could lead to loop sizes consistent with Hi-C data. Loop extrusion by condensin was also shown to be able to compact chromatin into the dense structure characteristic for sister chromatids [37].

Although the random-crosslinking and loop-extrusion are exemplary for the two major classes of models, many more variations have been proposed throughout the years, including clustering-, translocation-, and supercoiling-based models [38–42]. Many questions remain to be answered for unraveling the mechanism of the SMC protein complexes such as proposed in these various models. At a mechanistic level, we are still in the dark on how exactly SMC complexes interact with DNA. For example: what conformational changes occur within SMC complexes? What is the role of ATP binding and hydrolysis? What is the dynamics of loading and unloading? Is loop extrusion really the all-explaining mechanism? Where are SMC complexes loaded, what drives their processivity, and how do they know when to stop? How does cohesin recognize CTCF orientation? And if all these questions can be addressed: is this mechanism the same for all SMC proteins? How do cohesin, condensin, and Smc5/6 differ? How are these eukaryotic SMC proteins different compared to their prokaryotic counterparts? To what extent is the molecular mechanism different between organisms? Despite numerous cell-biology and biochemical studies in the past decades, many questions thus remain and there is a need for new approaches. As the nature of the most important questions is mechanistic, we feel that single-molecule biophysical techniques are particularly fit to address these issues [43].

Excitingly, in the last five years, a lot of progress has been made on purification of several SMC complexes, enabling researchers to do more in vitro type of work [44]. While virtually impossible to deduce from bulk experiments, the mechanical properties of proteins can be probed with various biophysical techniques at the level of individual molecules. The mechanical properties of SMC complexes are of particular interest from a biophysical perspective. SMC rings must withstand external forces in the cell throughout various stages of the cell cycle, such as segregation, and thus must be strong and stable in their association with DNA [45]. Forces can be applied and probed with methods such as magnetic tweezers (Fig. 2.3c), optical tweezers, and atomic force microscopes. The two most common techniques used to visualize SMC complexes at the single-molecule scale are transmission electron microscopy (TEM, Fig. 2.3a) and atomic force microscopy (AFM, Fig. 2.3b). Visualization of protein-DNA interactions is also possible with optical techniques such as DNA flow stretching (Fig. 2.3d) [46] and DNA curtains (Fig. 2.3e)[47]: techniques that rely on visualizing a stretched DNA molecule with fluorescence microscopy. With Fluorescent Resonance Energy Transfer (FRET), the interaction between two molecules, or two sites within the same molecule, can be investigated (Fig. 2.3f) [48]. Some of the possibilities and limitations of these techniques are summarised in Table 1. Below, we review results obtained with these single-molecule techniques on SMC protein complexes.

Table 1
Possibilities and limitations of single-molecule techniques.

Technique	Possibilities	Limitations
TEM	Near atomic level imaging, i.e., very high resolution	Surface technique, imaging in vacuum, static snapshots, potential artefacts in sample preparation and contrast enhancement
AFM	High resolution (nm-scale) imaging of molecules in air or in liquid, no need for labeling	Surface technique, static snapshots
High-speed AFM	Observing dynamics with nm-scale resolution in liquid. Acquisition of videos at a rate of up to ~20 images per second	Surface technique
Magnetic tweezers	Controlled application of force and torque, accurate measurement of DNA end-to-end distance	No visualisation of proteins acting on DNA
DNA flow-stretching	Visualisation of fluorescently labeled proteins on stretched, immobilised DNA	Limited optical resolution
DNA curtains	Visualisation of many DNA molecules in parallel, i.e., high throughout	Limited optical resolution
FRET	Sensitive measurements of local dynamics of spots within proteins by monitoring the proximity of two fluorescently labeled sites	Incorporation of fluorescent tags at position of interest can be challenging, limited size range (up to ~10nm)

2.2. Single-molecule imaging of SMC complexes

Their large, multi-subunit architecture make SMC complexes difficult to purify, and structural information is hard to obtain [49]. Throughout the years, parts of SMC subunits have been crystalized, though crystal structures of full SMC complexes are not available (for a recent review on crystallography, see Ref.[49]). Accordingly, most of the information that we have on global SMC architecture is from real-space imaging techniques such as atomic force microscopy and electron microscopy.

TEM can yield high quality images using low-wavelength electrons (Fig. 2.3a). An electron source emits electrons that are focused into a thin beam that hits the sample (stained with for example heavy metals for increased contrast), where some electrons are scattered, while most travel through, creating a "shadow image" of the sample. Potential artifacts can occur in the sample preparation by transferring proteins from solution to air to vacuum, a challenge which recently has largely been overcome by cryo-EM [50] (which, to our knowledge, has not been applied to SMC complexes yet).

In AFM, a sharp tip at the end of a cantilever scans the surface of the sample of interest, oscillating near its resonance frequency (Fig. 2.3b). The oscillation of the tip is changed as the tip interacts with the sample, and the deflection is detected by a photo diode. This information is then translated into a topological image with nanometer resolution. Conventional AFM can be used to take high-resolution static snapshots of molecules on a surface. Due to recent technical advances, it is now also possible to observe the motion of single molecules in real-time with high- speed AFM, that can acquire images at a video rate of 20 images per second [51, 52]. In AFM, there is no need for labeling or staining the sample, but a fundamental limitation of both EM and AFM is that

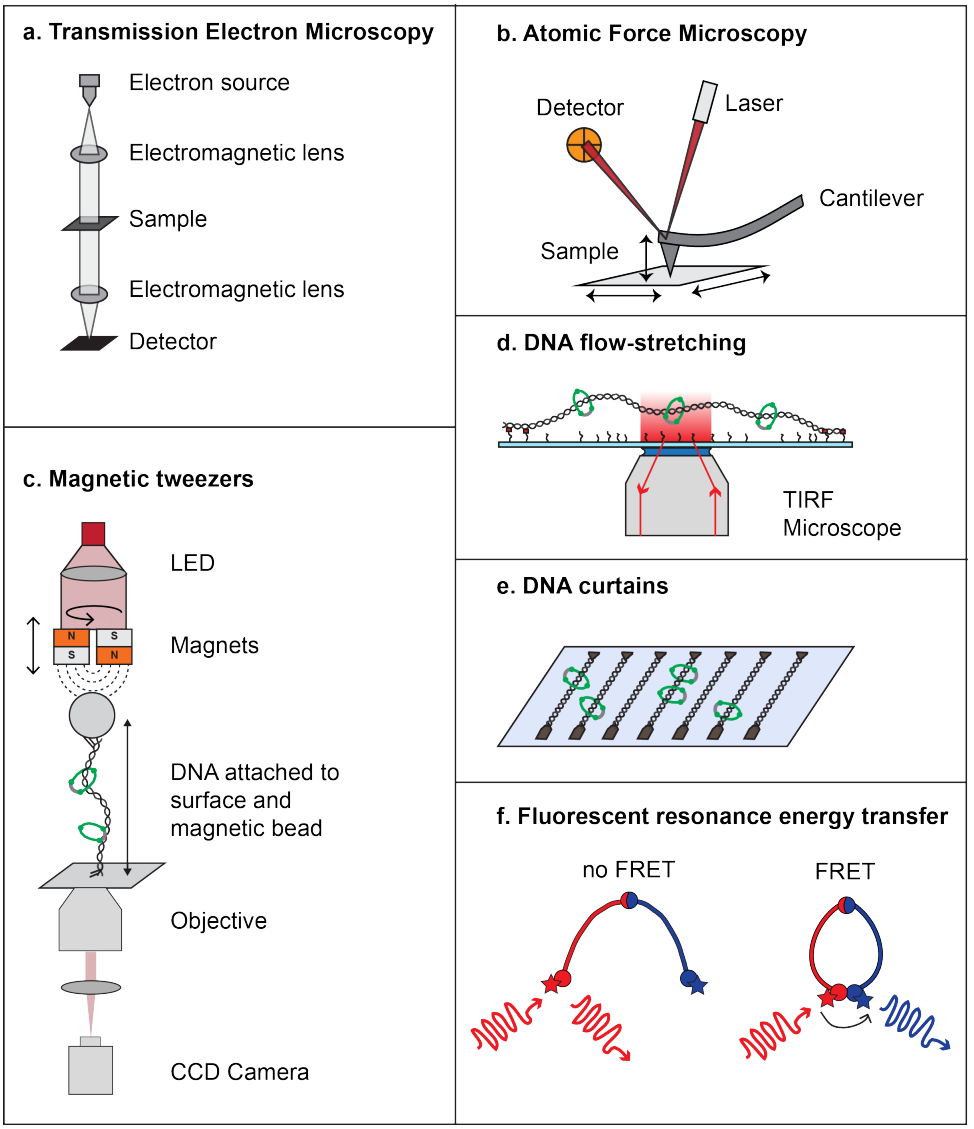

Figure 2.3: **Schematics of common single-molecule techniques a.** Transmission electron microscopy (TEM). **b.** Atomic Force microscopy (AFM). **c.** Magnetic tweezers. **d.** DNA flow-stretching. **e.** DNA curtains. **f.** Fluorescent resonance energy transfer.

proteins need to be bound to a surface for visualization. We note that some caution is needed when interpreting images from most EM and AFM reports, as these techniques dry the molecules, which possibly can kinetically trap them into a non physiological conformation.

Despite these potential caveats, imaging techniques have provided a number of valuable insights. 1) the structure of SMC subunits, 2) the shape and dynamics of full SMC complexes, and 3) their interaction with DNA. Specifically, researchers have tried to classify the shape of the SMC dimers and complexes using the letter system depicted in Figure 2.4a. This is of interest because the shape may relate directly to the SMC function: interaction between the heads will close the loop, interaction between heads and hinge may indicate an intermediate for loading, stiff rods could indicate that the SMC dimers are clamped onto DNA, etc. So far, the imaging efforts have yielded widely scattered results for different species of SMC complexes and varying conditions.

The first images of SMC proteins appeared in the early nineties, when bacterial MukB dimers were visualized with low-angle rotary-shadowing EM [53]. This was the first publication that reported the globular structures (heads and hinge) separated by coiled-coil segments, establishing a key step in determining the structure of SMC proteins. Several years later, higher- resolution EM imaging of MukB and BsSmc dimers revealed another crucial characteristic of SMC proteins: the antiparallel arrangement of the coiled coils, that brings the C- and N-terminals together at the head [54]. EM studies also showed that MukE and MukF bind to the MukB heads [55]. MukB dimers and BsSMC dimers were mostly observed in I-shaped and V-shaped conformations [53–58], and occasionally in Y- or O-shapes (Fig. 2.4b) [59]. Similar I- and V-shaped conformations were later found for the full BsSmc-ScpAB complex [60, 61].

One of the unanswered questions for SMC proteins is: do they mutually interact and cooperate? Interestingly, MukBEF complexes were shown form either fiber-form multimers or rosette shapes [55]. Similar rosette structures were also observed in liquid AFM for BsSMC [56], while multimers were observed with dry AFM [59]. After incubation with plasmid DNA, MukB complexes were shown to form large networks that appeared to consist of many catenated plasmids [62]. SMC clusters, however, appear to be much less prominent for eukaryotic SMCs. A live-cell imaging study used PALM (Photo Activated Localization Microscopy) super-resolution microscopy to probe the architecture of MukBEF complexes in vivo [63]. Despite their different molecular weights, all subunits displayed the same diffusion coefficient indicating that they were moving as a whole. Single-molecule fluorescent-particle tracking estimated a stoichiometry of 4:4:2 molecules for MukB:E:F, and functional units that consisted of 8-10 such MukBEF complexes.

Importantly, the first EM studies on eukaryotic SMC complexes confirmed that cohesin and condensin share the same head-coiled-coil-hinge structure [64]. Another important finding was that the anti-parallel coiled coils of cohesin Smc1/Smc3 dimers are intramolecular, thus folding back on themselves, and not two SMC proteins that are mutually coiled together along their entire length [65]. By imaging individual Smc1 or Smc3 proteins, it was shown that each of them forms an elongated structure with a globular structure on both sides of the coiled-coil, revealing that cohesin thus consists of one Smc1 arm and one Smc3 arm that mutually connect at the hinge.

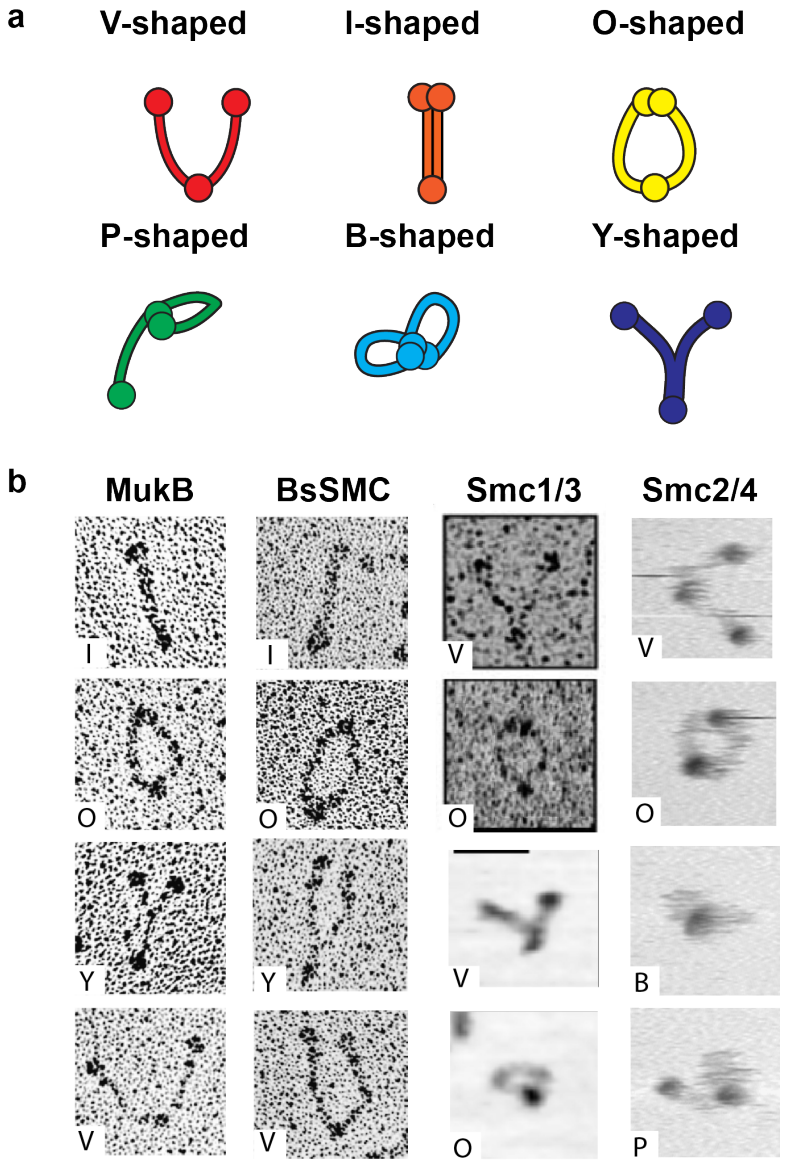

Figure 2.4: **Images of SMC complexes. a.** Classification of shape observations with a letter system. **b.** Images of various complexes, showing differences and similarities between species and techniques. Best-quality images are selected. MukB and BsSMC: EM images adapted from [54]. Smc1/3: EM images from [65], dry AFM images from [66]. Smc2/4 dimers: stills from high-speed AFM movies obtained from [67]. The letter in each panel indicates the letter-shape identified, as tabulated in panel a.

Cohesin and condensin (both dimers and holocomplexes) were imaged for a variety of species. Budding yeast Smc1/Smc3 dimers in the presence of ATP were reported to be in both V- and O-shapes (Fig. 2.4b), but mutants deficient in ATP binding showed less head engagement, suggesting that ATP binding influences the interaction between the cohesin heads [66, 68]. An AFM study in liquid reported I-shaped cohesin dimers, and the authors suggested that both coiled coils were in fact mutually intertwined in this I-shape [69]. Interestingly, deacetylated cohesin showed a higher occurrence of V- and Y-shaped Smc1/Smc3 dimers, suggesting that modifications such as acetylation influence the orientation, possibly also for condensin [64]. The majority of full cohesin complexes (human and yeast) was found to be in a V-, O- or Y-shape (Fig, 2.4b) [65, 68, 70]. In some cases, kinks in the coiled coils were observed. Several groups have attempted to visualize the interaction of condensin with DNA. With electron spectroscopic imaging [41], *Xenopus* condensin was visualized to interact with plasmid DNA in an ATP-hydrolysis dependent matter. Remarkably, the DNA appeared to be wrapped around the heads, which occurred only in the presence of ATP [71]. This led to the proposal of a model in which condensin, creates supercoils by wrapping DNA around the ATPase heads [41].

It is likely that different conformations exist for the same SMC complex, depending on the function and stage in the cell cycle, and that these conformational changes are dynamic. Condensin Smc2/Smc4 dimers imaged with high-speed AFM in liquid at physiological conditions indeed showed complexes that switched between various conformations over time [67]. The dimers were observed to switch between V-, O-, B- and P-shape, while I- shaped condensin dimers were not detected. While the existence of the head- hinge interaction has been predicted, this is the only report on B- and P- shapes so far [72, 73]. Furthermore, this study revealed that the coiled-coils are flexible, with a persistence length of only ~4nm [67]. This indicates that condensin has the structural flexibility to change conformation and engage in chromatin embrace. Cohesin was also imaged with high-speed AFM, showing that the coiled coils were flexible and that the molecules change their configuration within imaging time, but no quantification was given [69].

Out of all SMC complexes, the architecture and function of Smc5/6 is the least well studied. Remarkably, to our knowledge, there has not been any imaging or single-molecule study of the Smc5/6 complex. Visualization of this complex and its arrangement of subunits would greatly aid our understanding of its structure, but the bottleneck will be the purification of a clean and complete complex [17, 23].

In conclusion, the abundance of imaging studies has not resulted in the determination of a uniform conformation of SMC complexes, as the results are found to vary between groups, species, imaging techniques, and sample preparation methods. In fact, these studies have shown that these flexible complexes can adopt many different conformations.

2.3. Force spectroscopy with magnetic tweezers

The reorganization of DNA by SMC proteins can be studied in real time using single-molecule tweezers. Magnetic tweezers are exceptionally suitable to apply a force clamp on a molecule, monitor changes in DNA length upon protein binding, as well as to study DNA supercoiling induced by SMC complexes [74]. In magnetic tweezers, a DNA molecule

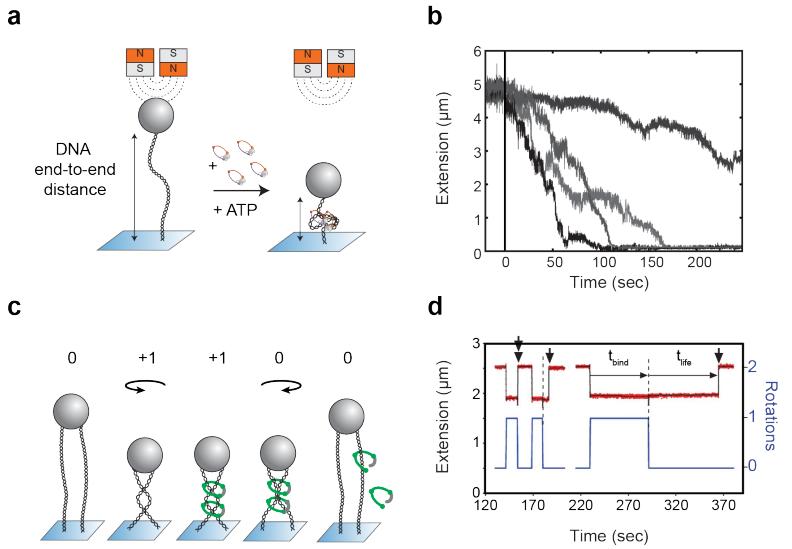

Figure 2.5: **SMC-mediated DNA compaction in magnetic tweezers. a.** Basic principle of the magnetic tweezers assay to monitor DNA compaction: A DNA molecule is stretched between a magnetic bead and a surface. Upon addition of condensin, the DNA is compacted and the end-to- end distance of the DNA decreases. Adapted from [75]. **b.** DNA compaction by the *S cerevisiae* condensin complex, in the presence of ATP. Different shades of gray represent different DNA molecules in the same experiment. Adapted from [75]. **c.** Schematic representation of the time sequence in the magnetic-tweezers DNA-bridging experiment. DNA bridges were introduced by rotating beads that have two attached DNA molecules, in the presence of MukB. Subsequently, the bead was untwisted to zero rotations to attempt to remove bridges. **d.** DNA extension (red) decreases as the magnets make one turn (blue), and recovers to the initial extension in the absence of protein (double arrow). In the presence of MukB, a delay in this recovery is observed (arrows, t_life) which was attributed to a MukB-induced bridge that was released after some time t_life.

is tethered between a surface and a magnetic bead (Fig. 2.3c). An external magnet is used to manipulate the bead, and thus the molecule. Rotation or vertical movement of the magnets can, respectively, apply torque and force to the molecule. Note that in this technique, the read-out is the z-position of the bead, which can be very precise, allowing a very accurate measurement of the DNA end-to-end length. A limitation of conventional magnetic tweezer techniques is that the proteins acting on DNA cannot be visualized.

Magnetic tweezers have been used to monitor the end-to-end distance of a DNA molecule as it gets shortened by compacting SMCs (Fig. 2.5a). A pioneering study with condensin holocomplex extracted from mitotic *Xenopus leavis* cells showed compaction and decompaction in large steps (±70nm) upon addition of ATP. Compaction was not observed in the absence of ATP, and only very weak compaction was seen when condensin from interphase cells was used [76]. Although no compaction was observed in the absence of ATP, condensin did interact with DNA in an ATP-independent fashion. Applying forces >10pN reversed compaction. Similar results were found in a recent magnetic tweezers study on the *S. cerevisiae* complex (Fig. 2.5b)[75] that showed compaction in large steps (~200nm), and revealed how the rate of compaction depends on protein

concentration, ATP concentration, and applied force. Compaction was found to be reversible with high salt, but condensin remained bound, indicating topological loading. Interestingly, although previously reported in biochemical studies [39–41], both magnetic tweezers studies on eukaryotic condensin failed to detect a putative supercoiling activity for condensin.

The *E.coli* MukB dimer similarly showed compaction of DNA against low forces in a stepwise manner, with steps of ~70nm [77]. Addition of the subunits MukE and MukF decreased the rate of compaction. The authors argued that MukB formed clusters that could resist forces up to 10pN. ATP had no effect on compaction rate but shortened the time before initiation of compaction. Two DNA molecules were attached to one magnetic bead, probing the ability of MukB to form a bridge between two DNA molecules (Fig. 2.5c,d) [78]. Interestingly, the probability that an SMC complex would form a bridge was increased in the presence of ATP, and decreased for an ATPase mutant.

Surprisingly, budding yeast's Smc1/3 dimer (i.e. not the full complex but merely the cohesin dimer) was reported to compact DNA in an stepwise manner (130nm steps) as well [70]. This compaction was not dependent on ATP and compaction still occurred when a headless variant (i.e. without the ATPase heads) was used, but not when the hinge was replaced. Note that protein aggregation can also lead to a reduced end-to-end distance of a DNA molecule in magnetic tweezers, calling for caution in interpretation results.

We note that all the step sizes reported so far in these SMC-induced DNA condensation studies are strikingly large (70-200 nm), much larger than for common DNA-translocating motor proteins such as helicases, translocases or polymerases which typically move in 1-bp increments [79–82]. In fact, these large steps are similar to or even larger than the size of the SMC complexes themselves, which measure maximum 70nm along their longest axis [64]. A similar size suggests conformational changes at the scale of the full SMC complex itself, while even larger steps are puzzling, yet consistently found in different studies. Such very large steps may involve the concerted action of multiple SMC complexes, or bursts of fast sequential steps of a single SMC complex - clearly a direction of further future research.

2.4. Fluorescent imaging techniques

The interaction between SMC complexes and DNA can be visualized with fluorescent imaging techniques. Typically, the DNA and the protein of interest are fluorescently labeled. In a flow-stretching experiment, a linear DNA molecule is stretched out along a PEGylated glass slide, and SMC complexes may bind to spots on the DNA (Fig. 2.3d). With the DNA curtain technique, DNA is attached to freely diffusing lipids that, upon applying a flow, diffuse towards micro-fabricated barriers, where "curtains" are formed (Fig. 2.3e). An advantage of DNA curtains is that many DNA molecules can be visualized in parallel, making it easier to build statistics in these single-molecule experiments. The drawbacks of both techniques are the limited optical resolution (typically >300nm), and the fact that conformational changes (such as compaction) in the DNA are difficult to observe when the DNA is fixated at both ends.

Using single-molecule imaging on flow stretched DNA, fluorescently labeled individual BsSMC complexes were shown to have two types of behavior when bound to DNA:

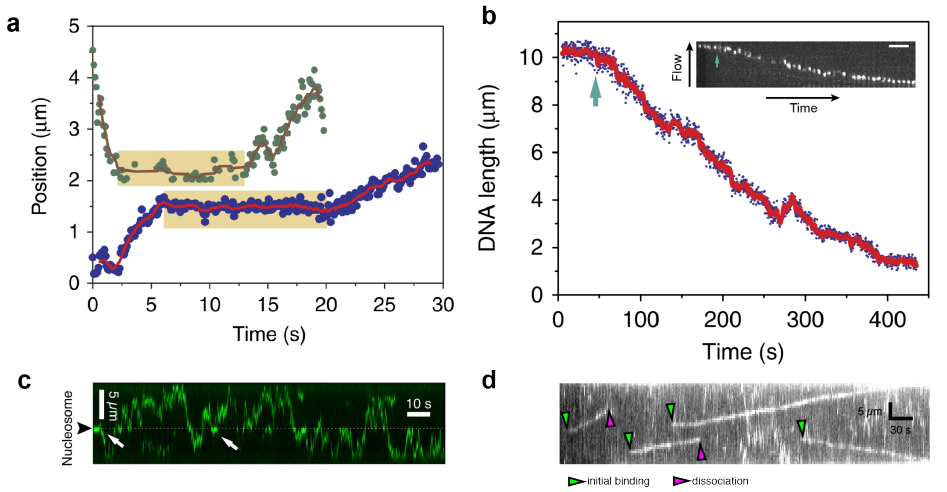

Figure 2.6: **SMC motion on flow-stretched DNA. a.** Individual BsSMC complexes slide on DNA, switching between static binding at one spot and random one-dimensional diffusion along the DNA. Adapted from [42]. **b.** At high concentrations, BsSmc complexes cluster and compact DNA. Kymograph shows the quantum-dot-labeled end of a DNA molecule (see inset) that is compacted. Adapted from [42]. **c.** Obstacles (in this case nucleosomes) restrict the mobility of cohesin. Cohesin is seen to transiently pause at the nucleosome, but it is able to diffuse past it. Adapted from [83]. **d.** Kymograph showing motor action of condensin as complexes bind and slide along DNA in an ATP-dependent linear motion over very long length scales (>10 μm). Adapted from [84].

static binding and one-dimensional Brownian diffusion (Fig. 2.6a) [42]. At higher concentrations, clusters of BsSMC were able to compact the DNA against the flow on a single tethered curtain (Fig. 2.6b). The presence of ATP had only a marginal influence on the compaction rate, while the presence of non-SMC subunits ScpA and ScpB reduced clustering on DNA. Interestingly, a headless mutant also showed local bending of the DNA. The authors suggested that the ATPase domains are required for cooperative clustering, while single BsSMC dimers might bend the DNA, thereby locally compacting the DNA.

Two studies on cohesin showed a similar diffusive behavior for motion along the DNA. A DNA curtain study on *S.pombe* cohesin found a diffusion constant of $3.8\pm0.2\mu m^2/s$ at 500mM salt [83], which is similar to that found for human cohesin on flow-stretched DNA ($1.7\pm0.1\mu m^2/s$) [85]. These values correspond well to an in vivo estimate for the diffusion of cohesin ($3.0\pm0.2\mu m^2/s$) [86]. Both studies found that ATP or a cohesin loading complex were not necessary for cohesin loading and diffusion. Cohesin remained associated with DNA at high salt concentrations, consistent with biochemical experiments and highly suggestive of a topological-embrace model [87].

Both studies also aimed to probe cohesin's ability to diffuse past obstacles of various sizes. DNA-bound obstacles with a size up to ~10nm could be passed without problems, but complexes >20nm could not be overcome. Cohesin was found to occasionally pause upon encountering a nucleosome, but it could diffuse over it (Fig. 2.6c). Interestingly, the majority of cohesin failed to pass the transcriptional regulator CTCF, which serves as a boundary element in vivo [85]. Both the bacterial DNA translocase FtsK and the

T7 RNAP could push the cohesin ring along the DNA. Although the eukaryotic cohesin would not encounter these bacterial complexes in vivo, it does indicate that cohesin can in principle be displaced by polymerases.

A third study probed the dynamics of *Xenopus* cohesin on flow-stretched DNA [88]. In contrast to the results reviewed above, these authors claim that cohesin diffusion is dependent on ATP as well as on the cohesin-loading complex Scc2-Scc4. The movement they observed was consistent with random diffusion rather than active linear translocation. The presence or Wapl-Pds5 (required for cohesin removal in prophase) was found to reduce cohesin's diffusional motion, an effect that was antagonised by acytelation of cohesin.

Recently, a DNA curtain study showed that the *S. cerevisiae* condensin complex is a mechanochemical molecular motor that translocates on DNA (Fig. 2.6d) [84]. The translocation was ATP dependent, persisted for very long distances (>10kb), and showed an average velocity of ~60 basepairs per second. Strikingly, condensin was also able to co-translocate a second DNA molecule along the DNA curtains. These findings show that condensin has a DNA-translocating motor domain, which is an essential ingredient for DNA compaction in a mechanism such as loop extrusion. Although loop extrusion is mostly mentioned in the context of cohesin, eukaryotic condensin is so far the only SMC protein for which motor activity is reported.

Single-molecule FRET techniques were also used to study the dynamics of SMC complexes. The spatial proximity of two fluorescently labeled sites (with separated excitation and emission spectra) can be determined with FRET. This principle relies on the energy transfer by excitation of one fluorophore (donor) to the nearby second fluorophore (acceptor). The efficiency of this transfer is strongly dependent on to the distance between the donor and acceptor, making this technique a very sensitive tool to study inter- and intramolecular interactions, for distances of up to ~10 nm. Incorporation of the suitable fluorescent tags into the proteins of interest at the position of choice can, however, be challenging.

The association of cohesin's head domains was probed with FRET in live cells of budding yeast [89]. A high FRET value was found constitutively throughout the cell cycle, indicating that the ATPase heads are in close proximity of each other at most times. No interactions between the hinge and the heads were detected, indicating that if this interaction exists in vivo, it is very transient. No associations between among different cohesin complexes could be detected in this in vivo assay. The proximity of the coiled-coils of both MukB and BsSMC was also probed in vitro with FRET [57]. A truncated form of BsSMC showed a high FRET efficiency, whereas a MukB fragment showed low FRET, consistent with an I-shape and V-shape respectively.

2.5. Perspective

The molecular mechanism of SMC complexes, and their function in directing the chromosomal architecture, is one of the hottest topics in cell biology today. Many open questions remain, and biophysical techniques appear to be key to answering them. Even though crystallography will continue to yield more (partial) protein structures, the flexible and open conformations of the full complexes intrinsically will escape notice. Single-molecule AFM or EM imaging, which circumvents this limitation, has already provided

new insights in the structure of SMC proteins, and we can expect many more results from emerging improved imaging techniques such as high-speed AFM and cryo- EM in the upcoming years. Looking at dynamics with high-speed AFM and FRET will be key to resolve the large conformational changes that supposedly are associated with the function of SMCs.

In vitro single-molecule experiments can provide detailed information on the molecular structure and mechanism, but it remains important to consider how their results can be extrapolated to the *in vivo* environment of the cell. *In vitro* studies with partial complexes in the absence of ATP are tricky to interpret, as partial and ATPase-deficient complexes are not often viable *in vivo*. *In vivo,* SMC complexes are regulated by many co-factors and modifications, depending on the stage in the cell cycle. As the field is progressing in understanding these factors and preparing purified proteins of increasing quality and added co-factors, they will become available for single-molecule experiments [88]. Alternatively, one can perform single-molecule experiments on proteins directly from cell extracts, which may retain their modifications and co-factors. *In vitro* single-molecule experiments can also move up in complexity by studying minimal forms of chromatin instead of naked DNA, which seems well possible since reconstitution of chromosomes requires a surprisingly low amount of factors [90].

It will be of interest to consider the differences between prokaryotic and eukaryotic SMC complexes, as they might employ different mechanisms. For example, the prokaryotic BsSMC was reported to need recruitment factors to become active [91, 92]. Such factors were not reported for eukaryotic complexes, and indeed, all *in vitro* single-molecule studies on eukaryotic condensin reported so far showed compaction activity in the absence of a loading factor. This apparent difference between eukaryotic and prokaryotic condensin is unexpected, because from an evolutionary perspective one would expect the eukaryotic SMC to exhibit a higher complexity with additional co-factors.

The differences and similarities of the various eukaryotic SMC complexes have so far largely been unresolved. For example, motor activity has only been identified for eukaryotic condensin, and not for bacterial SMC or for cohesin. It will be interesting to see if this is an intrinsic difference or related to purification details or functional co-factors. A very recent study combining Hi- C and computer simulations surprisingly found that cohesin, and not condensin, was responsible for chromosome compaction in budding yeast [93]. It may be the case that cohesin and condensin share very similar mechanisms. Or on the contrary, it may be that the same homologous complex, say condensin, functions differently in different organisms. This remains to be resolved in the forthcoming years.

Looking forward, as the field advances in protein purification and in vitro loading and more biologists are getting acquainted with biophysical tools, we can expect many more single-molecule studies on SMC proteins in the upcoming years. Critically evaluating differences between species and different SMC complexes with classical assays such as magnetic tweezers and DNA flow stretching is of interest. Such experiments should also be conducted in crowded environments, involving different co-factors known to interact with SMC proteins, as this better mimics *in vivo* conditions.

Almost all experiments discussed in this review probe a single quantity, for example the DNA extension with magnetic tweezers. Progress can also be expected from hy-

brid techniques that combine multiple single-molecule methods, for example magnetic tweezers that are combined with fluorescence imaging. Such a combination would bring the ability to monitor changes in DNA length or linking number while simultaneously following the action of fluorescently labeled SMC proteins. Similarly, the combination of FRET measurements on flow-stretched DNA could provide information on the local conformational changes within molecules while they perform their function on DNA.

Studying SMC proteins is essential for understanding the organization of the genome in all organisms. New developments in imaging and single-molecule techniques can be expected to significantly advance our understanding in the forthcoming years.

References

[1] T. Hirano, *Condensins: Universal organizers of chromosomes with diverse functions,* Genes and Development **26**, 1659 (2012).

[2] K. Nasmyth and C. H. Haering, *Cohesin: its roles and mechanisms.* Annual review of genetics **43**, 525 (2009).

[3] F. Uhlmann, *SMC complexes: from DNA to chromosomes,* Nature Reviews Molecular Cell Biology **17**, 399 (2016).

[4] C. H. Haering and S. Gruber, *SnapShot: SMC Protein Complexes Part I,* Cell **164**, 326 (2016).

[5] S. Nolivos and D. Sherratt, *The bacterial chromosome: architecture and action of bacterial SMC and SMC-like complexes,* FEMS Microbiology Reviews **38**, 380 (2014).

[6] R. A. Britton, D. C. Lin, and A. D. Grossman, *Characterization of a prokaryotic SMC protein involved in chromosome partitioning.* Genes & development **12**, 1254 (1998).

[7] O. Danilova, R. Reyes-Lamothe, M. Pinskaya, D. Sherratt, and C. Possoz, *MukB colocalizes with the oriC region and is required for organization of the two Escherichia coli chromosome arms into separate cell halves,* Molecular Microbiology **65**, 1485 (2007).

[8] S. Gruber, *Multilayer chromosome organization through DNA bending, bridging and extrusion,* Current Opinion in Microbiology **22**, 102 (2014).

[9] J. H.-C. Wang and B. P. Thampatty, *An introductory review of cell mechanobiology.* Biomechanics and modeling in mechanobiology **5**, 1 (2006).

[10] K. Nasmyth, F. Uhlmann, and F. Lottspeich, *Sister-chromatid separation at anaphase onset is promoted by cleavage of the cohesin subunit Scc1,* Nature **400**, 37 (1999).

[11] I. C. Waizenegger, S. Hauf, A. Meinke, and J. M. Peters, *Two distinct pathways remove mammalian cohesin from chromosome arms in prophase and from centromeres in anaphase.* Cell **103**, 399 (2000).

[12] M. Merkenschlager and E. P. Nora, *CTCF and Cohesin in Genome Folding and Transcriptional Gene Regulation,* Annual Review of Genomics and Human Genetics **17**, 17 (2016).

[13] T. Ono, A. Losada, M. Hirano, M. P. Myers, A. F. Neuwald, and T. Hirano, *Differential Contributions of Condensin I and Condensin II to Mitotic Chromosome Architecture in Vertebrate Cells,* Cell **115**, 109 (2003).

[14] Y. Frosi and C. H. Haering, *Control of chromosome interactions by condensin complexes.* Current opinion in cell biology **34**, 94 (2015).

[15] B. J. Meyer, *Targeting X chromosomes for repression,* Current Opinion in Genetics & Development **20**, 179 (2010).

[16] H. Betts Lindroos, L. Ström, T. Itoh, Y. Katou, K. Shirahige, and C. Sjögren, *Chromosomal Association of the Smc5/6 Complex Reveals that It Functions in Differently Regulated Pathways,* Molecular Cell **22**, 755 (2006).

[17] K. Jeppsson, K. K. Carlborg, R. Nakato, D. G. Berta, I. Lilienthal, T. Kanno, A. Lindqvist, M. C. Brink, N. P. Dantuma, Y. Katou, K. Shirahige, and C. Sj?gren, *The Chromosomal Association of the Smc5/6 Complex Depends on Cohesion and Predicts the Level of Sister Chromatid Entanglement,* PLoS Genetics **10**, e1004680 (2014).

[18] A. R. Lehmann, M. Walicka, D. J. Griffiths, J. M. Murray, F. Z. Watts, S. McCready, and A. M. Carr, *The rad18 gene of Schizosaccharomyces pombe defines a new subgroup of the SMC superfamily involved in DNA repair.* Molecular and cellular biology **15**, 7067 (1995).

[19] G. De Piccoli, F. Cortes-Ledesma, G. Ira, J. Torres-Rosell, S. Uhle, S. Farmer, J.-Y. Hwang, F. Machin, A. Ceschia, A. McAleenan, V. Cordon-Preciado, A. Clemente-Blanco, F. Vilella-Mitjana, P. Ullal, A. Jarmuz, B. Leitao, D. Bressan, F. Dotiwala, A. Papusha, X. Zhao, K. Myung, J. E. Haber, A. Aguilera, and L. Aragón, *Smc5–Smc6 mediate DNA double-strand-break repair by promoting sister-chromatid recombination,* Nature Cell Biology **8**, 1032 (2006).

[20] J. Dekker and L. Mirny, *The 3D Genome as Moderator of Chromosomal Communication,* Cell **164**, 1110 (2016).

[21] S. Cuylen, J. Metz, and C. H. Haering, *Condensin structures chromosomal DNA through topological links.* Nature structural & molecular biology **18**, 894 (2011).

[22] C. H. Haering, A.-M. Farcas, P. Arumugam, J. Metson, and K. Nasmyth, *The cohesin ring concatenates sister DNA molecules.* Nature **454**, 297 (2008).

[23] T. Kanno, D. G. Berta, and C. Sjögren, *The Smc5/6 Complex Is an ATP-Dependent Intermolecular DNA Linker,* Cell Reports **12**, 1471 (2015).

[24] L. Wilhelm, F. Bürmann, A. Minnen, H.-C. Shin, C. P. Toseland, B.-H. Oh, and S. Gruber, *SMC condensin entraps chromosomal DNA by an ATP hydrolysis dependent loading mechanism in Bacillus subtilis,*

eLife **4** (2015), 10.7554/eLife.06659.

[25] L. Baranello, F. Kouzine, and D. Levens, *CTCF and cohesin cooperate to organize the 3D structure of the mammalian genome.* Proceedings of the National Academy of Sciences of the United States of America **111**, 889 (2014).

[26] A. L. Sanborn, S. S. P. Rao, S.-C. Huang, N. C. Durand, M. H. Huntley, A. I. Jewett, I. D. Bochkov, D. Chinnappan, A. Cutkosky, J. Li, K. P. Geeting, A. Gnirke, A. Melnikov, D. McKenna, E. K. Stamenova, E. S. Lander, and E. L. Aiden, *Chromatin extrusion explains key features of loop and domain formation in wild-type and engineered genomes.* Proceedings of the National Academy of Sciences of the United States of America **112**, E6456 (2015).

[27] J. Zuin, J. R. Dixon, M. I. J. a. van der Reijden, Z. Ye, P. Kolovos, R. W. W. Brouwer, M. P. C. van de Corput, H. J. G. van de Werken, T. a. Knoch, W. F. J. van IJcken, F. G. Grosveld, B. Ren, and K. S. Wendt, *Cohesin and CTCF differentially affect chromatin architecture and gene expression in human cells.* Proceedings of the National Academy of Sciences of the United States of America **111**, 996 (2014).

[28] S. Cuylen, J. Metz, A. Hruby, and C. H. Haering, *Entrapment of chromosomes by condensin rings prevents their breakage during cytokinesis.* Developmental cell **27**, 469 (2013).

[29] R. Thadani, F. Uhlmann, and S. Heeger, *Condensin, Chromatin Crossbarring and Chromosome Condensation,* Current Biology **22**, R1012 (2012).

[30] T. M. K. Cheng, S. Heeger, R. A. G. Chaleil, N. Matthews, A. Stewart, J. Wright, C. Lim, P. A. Bates, and F. Uhlmann, *A simple biophysical model emulates budding yeast chromosome condensation.* eLife **4**, e05565 (2015).

[31] E. Alipour and J. F. Marko, *Self-organization of domain structures by DNA-loop-extruding enzymes,* Nucleic Acids Research **40**, 11202 (2012).

[32] E. Dolgin, *DNA's secret weapon against knots and tangles,* Nature **544**, 284 (2017).

[33] K. Nasmyth, *Disseminating the Genome: Joining, Resolving, and Separating Sister Chromatids During Mitosis and Meiosis,* Annual Review of Genetics **35**, 673 (2001).

[34] G. Fudenberg, M. Imakaev, C. Lu, A. Goloborodko, N. Abdennur, and L. A. Mirny Correspondence, *Formation of Chromosomal Domains by Loop Extrusion,* Cell Reports **15**, 2038 (2016).

[35] X. Wang, H. B. Brandão, T. B. K. Le, M. T. Laub, and D. Z. Rudner, *Bacillus subtilis SMC complexes juxtapose chromosome arms as they travel from origin to terminus,* Science **527**, 524 (2017).

[36] A. Goloborodko, J. F. Marko, and L. A. Mirny, *Chromosome Compaction by Active Loop Extrusion,* Biophysical Journal **110**, 2162 (2016).

[37] A. Goloborodko, M. V. Imakaev, J. F. Marko, and L. Mirny, *Compaction and segregation of sister chromatids via active loop extrusion,* eLife **5** (2016), 10.7554/eLife.14864.

[38] M.-L. Diebold-Durand, H. Lee, L. B. Ruiz Avila, H. Noh, H.-C. Shin, H. Im, F. P. Bock, F. Bürmann, A. Durand, A. Basfeld, S. Ham, J. Basquin, B.-H. Oh, and S. Gruber, *Structure of Full-Length SMC and Rearrangements Required for Chromosome Organization,* Molecular Cell **67**, 334 (2017).

[39] K. Kimura and T. Hirano, *ATP-Dependent Positive Supercoiling of DNA by 13S Condensin: A Biochemical Implication for Chromosome Condensation,* Cell **90**, 625 (1997).

[40] K. Kimura, V. V. Rybenkov, N. J. Crisona, T. Hirano, and N. R. Cozzarelli, *13S Condensin Actively Reconfigures DNA by Introducing Global Positive Writhe,* Cell **98**, 239 (1999).

[41] D. P. Bazett-Jones, K. Kimura, and T. Hirano, *Efficient Supercoiling of DNA by a Single Condensin Complex as Revealed by Electron Spectroscopic Imaging,* Molecular Cell **9**, 1183 (2002).

[42] H. Kim and J. J. Loparo, *Multistep assembly of DNA condensation clusters by SMC,* Nature Communications **7**, 10200 (2016).

[43] T. Ha, *Single-molecule methods leap ahead,* Nature Methods **11**, 1015 (2014).

[44] Y. Murayama and F. Uhlmann, *Biochemical reconstitution of topological DNA binding by the cohesin ring.* Nature **505**, 367 (2014).

[45] T. Tanaka, J. Fuchs, J. Loidl, and K. Nasmyth, *Cohesin ensures bipolar attachment of microtubules to sister centromeres and resists their precocious separation.* Nature cell biology **2**, 492 (2000).

[46] M. Ganji, S. H. Kim, J. van der Torre, E. Abbondanzieri, and C. Dekker, *Intercalation-Based Single-Molecule Fluorescence Assay To Study DNA Supercoil Dynamics,* Nano Letters **16**, 4699 (2016).

[47] E. C. Greene, S. Wind, T. Fazio, J. Gorman, and M.-L. Visnapuu, *Chapter 14 – DNA Curtains for High-Throughput Single-Molecule Optical Imaging,* in *Methods in Enzymology*, Vol. 472 (2010) pp. 293–315.

[48] M. F. Juette, D. S. Terry, M. R. Wasserman, Z. Zhou, R. B. Altman, Q. Zheng, and S. C. Blanchard, *The bright future of single-molecule fluorescence imaging,* Current Opinion in Chemical Biology **20**, 103 (2014).

[49] T. Gligoris and J. Löwe, *Structural Insights into Ring Formation of Cohesin and Related Smc Complexes,* Trends in Cell Biology **26**, 680 (2016).

[50] X.-c. Bai, G. McMullan, and S. H. Scheres, *How cryo-EM is revolutionizing structural biology,* Trends in Biochemical Sciences **40**, 49 (2015).

[51] T. Ando, N. Kodera, E. Takai, D. Maruyama, K. Saito, and a. Toda, *A high-speed atomic force microscope for studying biological macromolecules.* Proceedings of the National Academy of Sciences of the United States of America **98**, 12468 (2001).

[52] A. J. Katan and C. Dekker, *High-speed AFM reveals the dynamics of single biomolecules at the nanometer scale.* Cell **147**, 979 (2011).

[53] H. Niki, R. Imamura, M. Kitaoka, K. Yamanaka, T. Ogura, and S. Hiraga, *E.coli MukB protein involved in chromosome partition forms a homodimer with a rod-and-hinge structure having DNA binding and ATP/GTP binding activities.* The EMBO journal **11**, 5101 (1992).

[54] T. E. Melby, *The Symmetrical Structure of Structural Maintenance of Chromosomes (SMC) and MukB Proteins: Long, Antiparallel Coiled Coils, Folded at a Flexible Hinge,* The Journal of Cell Biology **142**, 1595 (1998).

[55] K. Matoba, M. Yamazoe, K. Mayanagi, K. Morikawa, and S. Hiraga, *Comparison of MukB homodimer versus MukBEF complex molecular architectures by electron microscopy reveals a higher-order multimerization.* Biochemical and biophysical research communications **333**, 694 (2005).

[56] J. Mascarenhas, A. V. Volkov, C. Rinn, J. Schiener, R. Guckenberger, and P. L. Graumann, *Dynamic assembly, localization and proteolysis of the Bacillus subtilis SMC complex.* BMC cell biology **6**, 28 (2005).

[57] Y.-m. Soh, F. Bu, H.-c. Shin, T. Oda, K. S. Jin, C. P. Toseland, C. Kim, H. Lee, S. J. Kim, M.-s. Kong, Y.-g. Kim, H. M. Kim, N. K. Lee, M. Sato, B.-h. Oh, and S. Gruber, *Molecular Basis for SMC Rod Formation and Its Dissolution upon DNA Binding,* Molecular cell **3**, 1 (2015).

[58] M. Hirano, D. E. Anderson, H. P. Erickson, and T. Hirano, *Bimodal activation of SMC ATPase by intra- and inter-molecular interactions.* The EMBO journal **20**, 3238 (2001).

[59] M. E. Fuentes-Perez, E. J. Gwynn, M. S. Dillingham, and F. Moreno-Herrero, *Using DNA as a fiducial marker to study SMC complex interactions with the atomic force microscope.* Biophysical journal **102**, 839 (2012).

[60] K. Kamada, M. Miyata, and T. Hirano, *Molecular Basis of SMC ATPase Activation: Role of Internal Structural Changes of the Regulatory Subcomplex ScpAB,* Structure **21**, 581 (2013).

[61] K. Kamada, M. Su'etsugu, H. Takada, M. Miyata, and T. Hirano, *Overall Shapes of the SMC-ScpAB Complex Are Determined by Balance between Constraint and Relaxation of Its Structural Parts,* Structure **25**, 603 (2017).

[62] S. Bahng, R. Hayama, and K. J. Marians, *MukB-mediated catenation of DNA is ATP and MukEF independent,* Journal of Biological Chemistry **291**, 23999 (2016).

[63] A. Badrinarayanan, R. Reyes-Lamothe, S. Uphoff, M. C. Leake, and D. J. Sherratt, *In Vivo Architecture and Action of Bacterial Structural Maintenance of Chromosome Proteins,* Science **338** (2012).

[64] D. E. Anderson, A. Losada, H. P. Erickson, and T. Hirano, *Condensin and cohesin display different arm conformations with characteristic hinge angles.* The Journal of cell biology **156**, 419 (2002).

[65] C. H. Haering, J. Löwe, A. Hochwagen, and K. Nasmyth, *Molecular Architecture of SMC Proteins and the Yeast Cohesin Complex,* Molecular Cell **9**, 773 (2002).

[66] A. M. Elbatsh, J. H. Haarhuis, N. Petela, C. Chapard, A. Fish, P. H. Celie, M. Stadnik, D. Ristic, C. Wyman, R. H. Medema, K. Nasmyth, and B. D. Rowland, *Cohesin Releases DNA through Asymmetric ATPase-Driven Ring Opening,* Molecular Cell **61**, 575 (2016).

[67] J. M. Eeftens, A. J. Katan, M. Kschonsak, M. Hassler, L. de Wilde, E. M. Dief, C. H. Haering, and C. Dekker, *Condensin Smc2-Smc4 Dimers Are Flexible and Dynamic,* (2016).

[68] P. J. Huis in 't Veld, F. Herzog, R. Ladurner, I. F. Davidson, S. Piric, E. Kreidl, V. Bhaskara, R. Aebersold, and J.-M. Peters, *Characterization of a DNA exit gate in the human cohesin ring.* Science (New York, N.Y.) **346**, 968 (2014).

[69] I. Kulemzina, K. Ang, X. Zhao, J. T. Teh, V. Verma, S. Suranthran, A. P. Chavda, R. G. Huber, B. Eisenhaber, F. Eisenhaber, J. Yan, and D. Ivanov, *A Reversible Association between Smc Coiled Coils Is Regulated by Lysine Acetylation and Is Required for Cohesin Association with the DNA,* Molecular Cell **63**, 1044 (2016).

[70] M. Sun, T. Nishino, and J. F. Marko, *The SMC1-SMC3 cohesin heterodimer structures DNA through supercoiling-dependent loop formation.* Nucleic acids research **41**, 6149 (2013).

[71] D. P. Bazett-Jones and M. J. Hendzel, *Electron Spectroscopic Imaging of Chromatin,* Methods **17**, 188 (1999).

[72] S. Gruber, P. Arumugam, Y. Katou, D. Kuglitsch, W. Helmhart, K. Shirahige, and K. Nasmyth, *Evidence that loading of cohesin onto chromosomes involves opening of its SMC hinge.* Cell **127**, 523 (2006).

[73] K. Nasmyth, *Cohesin: a catenase with separate entry and exit gates?* (2011).

[74] I. De Vlaminck and C. Dekker, *Recent advances in magnetic tweezers.* Annual review of biophysics **41**, 453 (2012).

[75] J. M. Eeftens, S. Bisht, J. Kerssemakers, C. Haering, and C. Dekker, *Real-time detection of condensin-driven DNA compaction reveals a multistep binding mechanism,* bioRxiv (2017).

[76] T. R. Strick, T. Kawaguchi, and T. Hirano, *Real-time detection of single-molecule DNA compaction by condensin I.* Current biology : CB **14**, 874 (2004).

[77] Y. Cui, Z. M. Petrushenko, and V. V. Rybenkov, *MukB acts as a macromolecular clamp in DNA condensation,* **15**, 411 (2008).

[78] Z. M. Petrushenko, Y. Cui, W. She, and V. V. Rybenkov, *Mechanics of DNA bridging by bacterial condensin MukBEF in vitro and in singulo.* The EMBO journal **29**, 1126 (2010).

[79] A. M. Pyle, *Translocation and Unwinding Mechanisms of RNA and DNA Helicases,* Annual Review of Biophysics **37**, 317 (2008).

[80] R. Seidel, J. G. Bloom, C. Dekker, and M. D. Szczelkun, *Motor step size and ATP coupling efficiency of the dsDNA translocase EcoR124I,* The EMBO Journal **27**, 1388 (2008).

[81] M. R. Singleton, M. S. Dillingham, and D. B. Wigley, *Structure and Mechanism of Helicases and Nucleic Acid Translocases,* Annual Review of Biochemistry **76**, 23 (2007).

[82] W. Yang, *Lessons Learned from UvrD Helicase: Mechanism for Directional Movement,* Annual Review of Biophysics **39**, 367 (2010).

[83] J. Stigler, G. Ö. Çamdere, D. E. Koshland, and E. C. Greene, *Single-Molecule Imaging Reveals a Collapsed Conformational State for DNA-Bound Cohesin,* Cell Reports **15**, 988 (2016).

[84] T. Terakawa, S. Bisht, J. M. Eeftens, C. Dekker, C. H. Haering, and E. Greene, *The condensin complex is a mechanochemical motor that translocates along DNA,* , 1 (2017).

[85] I. F. Davidson, D. Goetz, M. P. Zaczek, M. I. Molodtsov, P. J. Huis in 't Veld, F. Weissmann, G. Litos, D. A. Cisneros, M. OcampoHafalla, R. Ladurner, F. Uhlmann, A. Vaziri, and J. Peters, *Rapid movement and transcriptional relocalization of human cohesin on DNA,* The EMBO Journal **35**, e201695402 (2016).

[86] R. Ladurner, V. Bhaskara, P. J. Huis in 't Veld, I. F. Davidson, E. Kreidl, G. Petzold, and J.-M. Peters, *Cohesin's ATPase Activity Couples Cohesin Loading onto DNA with Smc3 Acetylation,* Current Biology **24**, 2228 (2014).

[87] Y. Murayama and F. Uhlmann, *Chromosome segregation: how to open cohesin without cutting the ring?* The EMBO journal **32**, 614 (2013).

[88] M. Kanke, E. Tahara, P. J. Huis In 't Veld, and T. Nishiyama, *Cohesin acetylation and Wapl-Pds5 oppositely regulate translocation of cohesin along DNA,* The EMBO Journal **35**, 2686 (2016).

[89] J. Mc Intyre, E. G. D. Muller, S. Weitzer, B. E. Snydsman, T. N. Davis, and F. Uhlmann, *In vivo analysis of cohesin architecture using FRET in the budding yeast Saccharomyces cerevisiae.* The EMBO journal **26**, 3783 (2007).

[90] K. Shintomi, T. S. Takahashi, and T. Hirano, *Reconstitution of mitotic chromatids with a minimum set of purified factors.* Nature cell biology **17**, 1014 (2015).

[91] S. Gruber, J. Errington, H. Shin, M. Suh, B. Ku, K. Lee, K. Joo, H. Robinson, J. Lee, S. Park, and et Al., *Recruitment of condensin to replication origin regions by ParB/SpoOJ promotes chromosome segregation in B. subtilis.* Cell **137**, 685 (2009).

[92] N. L. Sullivan, K. A. Marquis, D. Z. Rudner, A. Teleman, P. Silver, R. Losick, L. Shapiro, S. Moriya, P. Eichenberger, D. Rudner, and R. Losick, *Recruitment of SMC by ParB-parS organizes the origin region and promotes efficient chromosome segregation.* Cell **137**, 697 (2009).

[93] S. A. Schalbetter, A. Goloborodko, G. Fudenberg, J.-M. Belton, C. Miles, M. Yu, J. Dekker, L. Mirny, and J. Baxter, *SMC complexes differentially compact mitotic chromosomes according to genomic context,* Nat Cell Biol **advance on** (2017).

II

Structure and mechanism of the condensin complex

3

Condensin Smc2-Smc4 dimers are flexible and dynamic

Structural Maintenance of Chromosomes (SMC) protein complexes, including cohesin and condensin, play key roles in the regulation of higher-order chromosome organization. Even though SMC proteins are thought to mechanistically determine the function of the complexes, their native conformations and dynamics have remained unclear. Here, we probe the topology of Smc2-Smc4 dimers of the *S. cerevisiae* condensin complex with high-speed Atomic Force Microscopy (AFM) in liquid. We show that the Smc2-Smc4 coiled coils are highly flexible polymers with a persistence length of only ~4 nm. Moreover, we demonstrate that the SMC dimers can adopt various architectures that interconvert dynamically over time, and we uncover that the SMC head domains not only engage with each other but also with the hinge domain situated at the other end of the ~45 nm long coiled coil. Our findings reveal structural properties that shed new insights into the molecular mechanics of condensin complexes.

This chapter has been published as: J.M. Eeftens*, A.J. Katan*, M. Kschonsak, M. Hassler, L. de Wilde, E.M. Dief, C.H. Haering, C. Dekker (2016) Condensin Smc2-Smc4 dimers are flexible and dynamic. *Cell Reports*, 14(8) 1813-1818

3.1. Introduction

Cohesin and condensin protein complexes play central roles in many aspects of chromosome biology, including the segregation of sister chromatids during cell divisions, compaction of chromosomes, and regulation of gene expression during interphase (reviewed in [1, 2]. Although functionally different, cohesin and condensin have similar architectures: both complexes are composed of two different SMC subunits and a subunit of the kleisin protein family. Together, these three proteins form a ring-like structure that is conserved from bacteria to eukaryotes. The protein chain of each SMC protein folds back onto itself to form a ~45 nm long antiparallel coiled coil, which connects a globular "hinge" domain at one end to an ATPase "head" domain, created by the association of N- and C-terminal protein sequences, at the other end (Figure 3.1A). Two SMC proteins form a heterodimer by the association of their hinge domains: Smc1-Smc3 in the case of cohesin and Smc2-Smc4 in the case of condensin [3]. In addition, the head domains of the two SMC subunits can associate in the presence of ATP. The functional roles of ATP binding-mediated dimerization and hydrolysis-dependent dissociation of the two head domains have remained largely unclear. Both cohesin and condensin have been suggested to bind to chromosomes by encircling chromatin fibers topologically within their SMC-kleisin rings [4, 5].

The conformation and dynamics of SMC dimers are of great importance, since they are thought to mechanistically determine the biological function of all SMC protein complexes. Accordingly, there have been numerous efforts to gain insight into the configuration of the SMC dimers. Electron microscopy (EM) images of cohesin complexes suggest that the Smc1-Smc3 coiled coils emerge from the hinge domain in an open conformation, resulting in V- or O-shaped arrangements with the two coils separated along most of their lengths [3, 6, 7]. V-shaped conformations were also observed for condensin's Smc2-Smc4. However, in a large fraction of molecules the Smc2-Smc4 coiled coils seemed to align, resulting in rod- or I-shaped rather than V-shaped conformations [3, 8]. Support to the notion that condensin's SMC coiled coils tightly associate with each other came from a recent crystal structure of the Smc2-Smc4 hinge domains and parts of the adjacent coiled coils, as well as from chemical cross-linking experiments [9, 10]. Small Angle X-ray Scattering (SAXS) experiments implied that also the SMC subunits of cohesin and prokaryotic SMC complexes form I-shaped molecules in solution [10]. These contradicting results indicate that it is still unclear which configurations SMC dimers adopt in vivo, and under which circumstances conformational changes might occur. The major disadvantages of all methods that have so far been used to study the configuration of SMC molecules are that they either probed the protein structure in highly artificial environments (e.g. dried in vacuum or packed into a crystal lattice) or in a kinetically trapped state (e.g. by cross-linking).

Atomic Force Microscopy (AFM) has proven to be a powerful tool to visualize biomolecules and to study their mechanical properties at nanometer resolution without the need for labeling. Importantly, it can also be carried out in aqueous solution under physiological conditions. Recent technical advances have made it possible to observe single molecules in action with high-speed AFM, reaching frame rates of up to 20 frames per second and thereby allowing imaging in real-time [11, 12]. Here, we use high-speed AFM in liquid, in combination with supporting data from EM and dry AFM, to probe the structural ar-

rangement and dynamics of condensin's Smc2-Smc4 dimers under physiological conditions. We show that the coiled coils are remarkably flexible, allowing the molecules to adopt various conformations that change over time. We furthermore find that, even in the absence of ATP or DNA, the heads of the Smc2 and Smc4 subunits dynamically engage with each other and with the Smc2-Smc4 hinge. Our findings show that condensin SMC dimers are able to adopt various conformations, which suggests that condensin complexes have the structural flexibility required to engage and link the chromatin fibers of eukaryotic genomes.

3.2. Results

Smc2-Smc4 dimers display a variety of conformations

While this paper focuses on the results from liquid AFM, we first, as a point of reference and for comparison to reported data, used rotary shadowing EM to image Smc2-Smc4 dimers purified from budding yeast *Saccharomyces cerevisiae* (Figure 3.1B). Surprisingly, in only about one third of the Smc2-Smc4 dimers, the coiled coils were closely juxtaposed over part or all of their lengths, resulting in the I- or Y-shaped conformations that were predicted from previous studies [3, 8, 10]. The majority of molecules displayed instead clearly separated coiled coils, resulting in either V-shaped or O-shaped conformations (Figure S3.1A). In parallel to rotary shadowing EM, we also imaged the molecules by dry AFM (Figure 3.1C). Consistent with the EM data, the vast majority of molecules identified in the AFM images had separated coiled coils and appeared as V- or O-shaped dimers (Figure S3.1B). Notably, we never observed the coiled coils as juxtaposed stiff rods with dry AFM.

Since earlier EM and AFM studies investigated Smc2-Smc4 dimers of vertebrate and fission yeast condensin complexes, it is conceivable that the *S. cerevisiae* Smc2-Smc4 dimer represents an unusual exception to the previously reported rod-shaped architecture. We therefore purified and imaged another Smc2-Smc4 dimer, this time from the thermophilic yeast species *Chaetomium thermophilum* (Figure S3.1C). Similar to what we had observed for the *S. cerevisiae* Smc2-Smc4 dimer, we again found that the majority of the molecules were either in the V- or O-shaped conformations. We therefore conclude that the Smc2-Smc4 dimers of two yeast species, which diverged several hundred million years ago, can adopt a number of different conformations, with the majority in O- or V-shapes.

Since EM and dry AFM can only gather snapshots of protein conformations, we used high-speed AFM in liquid to create movies of *S. cerevisiae* Smc2-Smc4 dimers with a frame rate of 10 frames/second. We classified the conformations of the dimers in over 1,700 frames taken with high-speed AFM (Figure 3.1D). The V-shaped conformation accounts for a quarter of the cases (Figure 3.1D, first row), while the most abundant configuration is the O-shaped conformation (Figure 3.1D, second row). Unexpectedly, liquid AFM imaging uncovered two additional conformations, which involve interactions between the head and hinge domains. In a conformation that we refer to as 'butterfly' (B-shaped), both ATPase heads engage with the hinge and the intervening coils form two short loops that extrude from this head-hinge complex (Figure 3.1D, third row). In a conformation that we refer to as P-shaped conformation, only one of the heads en-

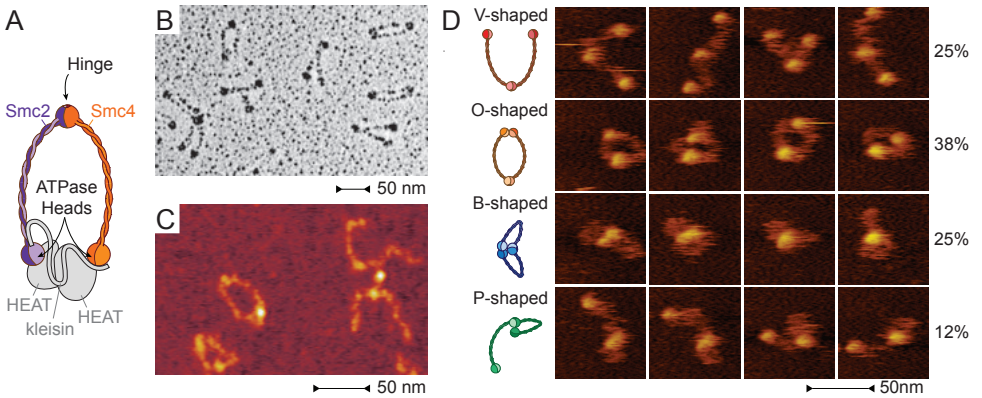

Figure 3.1: **S. cerevisiae Smc2-Smc4 dimers adopt a variety of conformations. A.** Cartoon of the eukaryotic condensin complex. Smc2 and Smc4 heterodimerize via their hingedomains. The kleisin subunit associates with the Smc2 and Smc4 ATPase head domains to create a ring-like structure and recruits two additional subunits (shown in grey, not studied here). **B.** Example image of Smc2-Smc4 dimers imaged by rotary shadowing EM. **C.** Example image of Smc2-Smc4 dimers imaged by dry AFM. **D.** Example images of different conformational classes of Smc2-Smc4 dimers from high-speed liquid AFM movies. The frequency of each conformational class (as fraction of 1795 total frames from 18 movies) is indicated. V-shaped: SMCs are only connected at the hinge while the heads are not engaged, O-shaped: additionally, the heads are engaged with each other, B-shaped ('butterfly'): both heads are engaging with the hinge, P-shaped: one of the heads is engaged with the hinge.

gages with the hinge and the other head is moving freely (Figure 3.1D, fourth row). We conclude that, in addition to the conformations also found with dry imaging techniques, high-speed AFM in liquid uncovered that Smc2-Smc4 dimers can adopt two additional conformations that had escaped prior notice.

Smc2-Smc4 dimers undergo frequent conformational changes

Analysis of an individual Smc2-Smc4 dimer recorded in real-time revealed that the dimer did not remain in one static configuration during the course of the experiment (Figure 3.2). At the start of the movie, the molecule was O-shaped (first frame in Figure 3.2A), then the heads approached the hinge to form a 'butterfly' structure (second frame in Figure 3.2A). The molecule switched between O- and B-shaped conformations multiple times before converting to a V-shaped 'open' conformation towards the end of the movie (last four frames in Figure 3.2A). Remarkably, all Smc2-Smc4 dimers that we studied underwent conformational changes during the imaging time (Figure S3.2).

Head-head and head-hinge engagements are dynamic

To more carefully analyze the dynamics by which the Smc2-Smc4 ATPase heads engage with each other and with the hinge, we determined the distances between the centers of the two heads and the distances between the centers of each head to the center of the hinge. The distance between the heads (Figure 3.3A, top histogram) showed a clear peak, which can be fit by a Gaussian profile at 2.5 ± 1.3 nm (error denotes standard deviation). This peak corresponds to all conformations with associated head domains, i.e.

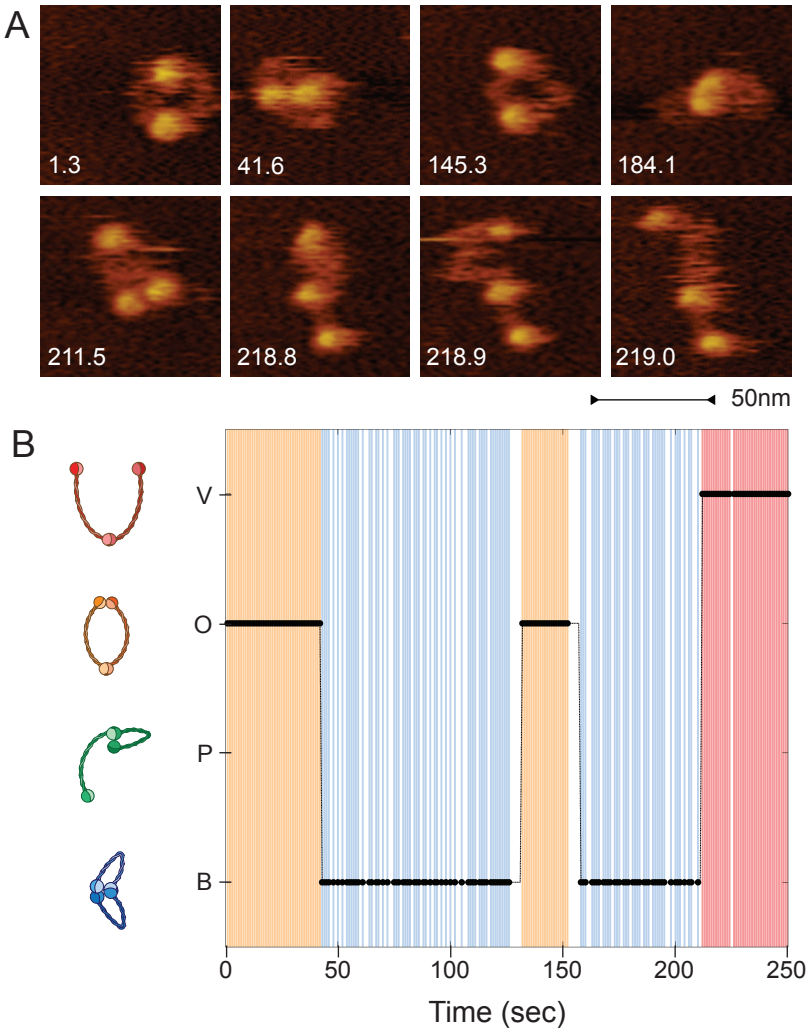

Figure 3.2: **Smc2-Smc4 dimers change conformations dynamically. A.** Snapshots of an Smc2-Smc4 dimer followed over time with high-speed AFM at a rate of 10 frames per second. Snapshots are taken at various time points in the movie (shown in seconds). **B.** Annotation of conformational classes for each frame of Movie S1. O- shaped conformations are indicated in orange, B-shaped conformations in blue, V-shaped conformations in red. White gaps indicate that the conformation could not be confidently classified for a particular frame.

all O- and B-shaped conformations, which group on the left side of the red line in the scatter plot (Figure 3.3A, main panel). The head-head distance distribution also contained a second population at much larger distances of 20-60 nm (right of the red line), which corresponds to V- and P-shaped conformations. The distances between head and hinge domains (Figure 3.3A, right histogram) showed a large peak at 2.4 ± 1.9 nm. This peak corresponds to conformations in which at least one of the two heads engages with the hinge, i.e. all B- and P-shaped conformations in the group below the blue line in the scatter plot. The second broad peak at 23.8 ± 9.1 nm signals the large head-hinge distance in open V- and P-shaped conformations.

To quantify the degree of openness of the Smc2-Smc4 dimers, we measured the angle between the two coiled coils at the hinge. For all conformations combined (Figure 3.3B, black histogram), we find that the frequency of occurrence increases approximately linearly up to ~70 degrees and then levels off for higher angles. Low angles are strikingly absent, which reflects the fact that we never observed a conformation in which the coiled coils are clamped together into a rod. Furthermore, the angle distribution depends on the conformation of the dimer. In the O-shaped conformation, the frequency of occurrence has a broad asymmetric peak with a maximum near 70 degrees. In all other conformations, we observed almost exclusively large-angle conformations.

For comparison, we also measured the hinge angles of *S. cerevisiae* Smc2-Smc4 dimers in electron micrographs (Figure S3.3A). We again observed a wide distribution of angles between the two coils, with a peak at around 40 degrees and a lower occurrence of smaller angles. The quantitative difference between peak values measured by EM and liquid AFM implies that vacuum drying SMC dimers on mica surfaces, an unavoidable protocol for EM, may impact the coiled coil arrangement. To exclude the possibility that the attachment of the head domains to the surface artificially biases the coiled coils into an open conformation during preparation for EM, we also measured the hinge angles of 'head-less' *C. thermophilum* Smc2-Smc4 dimers in electron micrographs (Figures S3.3B and D) and compared them to the angles measured for full-length *C. thermophilum* Smc2-Smc4 dimers (Figures S3.1C and S3.3C). In both cases, we again observed a wide distribution of angles with a peak around 40 degrees. These measurements confirm that the coiled coils emanate from the Smc2-Smc4 hinge domains in an open conformation, rather than in a juxtaposed closed conformation, independent of the presence of the ATPase head domains or species origin.

The SMC coiled coils are highly flexible

A corollary of the finding that Smc2-Smc4 dimers can adopt a large number of conformations is that the coiled coil structure of the SMC proteins must be very flexible and thereby allow the free movement of the head domains in relation to the hinge domain. In fact, the flexibility of the coils can be directly observed in the time-lapse recordings of the SMC dimers in liquid (Figure 3.2A). Even when the molecule remains in the same conformational class, the coiled coils are highly mobile. For example, in the last three panels of the time lapse shown in Figure 3.2A, the Smc2-Smc4 dimer remains in the V-shaped conformation, but the coiled coils change their position between every frame (taken at 0.1 seconds intervals). The coils are even able to sharply bend into the B- and P-shaped conformations to enable head-hinge interactions (Figure 3.1D, third and forth

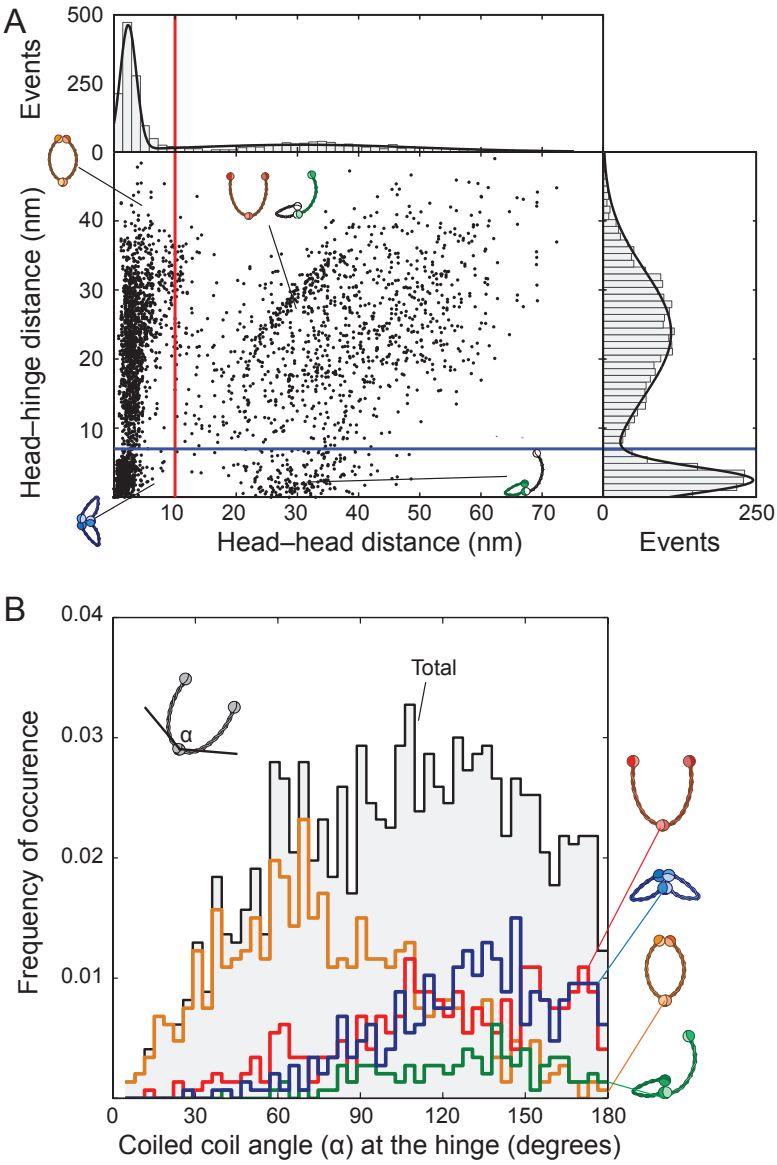

Figure 3.3: **Structural analysis of Smc2-Smc4 conformations. A.** Scatter plot of head-head distances versus head-hinge distances for each subunit of an Smc2-Smc4 dimer imaged by high-speed liquid AFM (total 1795 frames of 18 independent molecules). Each dot represents a measurement of one SMC subunit. Frequencies of data points for head-head distances or head-hinge distances are plotted as histograms at the top and right side of the plot, respectively. Data points left of the vertical red line and below the horizontal blue line: B-shaped conformations, points left of the red and above the blue line: O-shaped conformations, points right of the red and above the blue line: V-shaped conformations and the head-hinge disengaged arm of P-shaped conformations, points right of the red line and below the blue line: the head-hinge engaged arm of P-shaped conformations. **B.** Histogram plot of the angles between the Smc2-Smc4 coiled coils, measured at the hinge. The black histogram shows the frequency of occurrence for all conformations. Histograms for individual conformational classes are shown in red (V-shaped), orange (O-shaped), green (P-shaped) or blue (B-shaped).

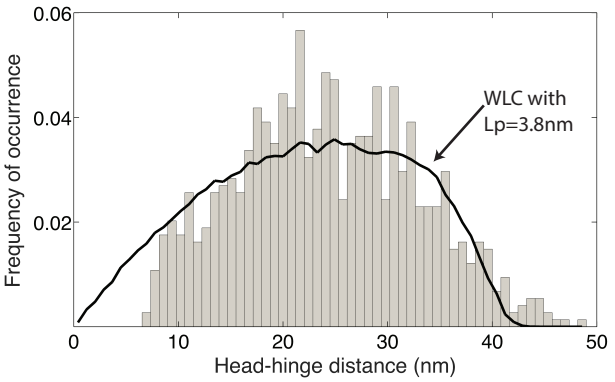

Figure 3.4: **The Smc2-Smc4 coiled coils can be characterized by a worm-like-chain model with a persistence length of about 4nm.** The measured end-to-end length histogram (head-hinge distance) of open configurations (grey bars) has a broad peak around 25 nm. This shape is well reproduced by the end-to-end distribution of 10^5 simulated worm-like-chain polymers with a persistence length of 3.8 nm (black line).

rows), a motion that could not be achieved if the coiled coils were stiff.

We quantified this flexible behavior of the coiled coils by comparison to theoretical models developed for flexible polymers. The worm-like-chain (WLC) model is often used to describe the behavior of homogeneous semi-flexible polymers such as DNA or proteins [13–15]. In the WLC model, the stiffness of a polymer is expressed as the persistence length L_p. It can be estimated from AFM images through the mean squared end-to-end distance of the coiled coil (i.e. head-hinge distance, [16]. We took only V-shaped conformations into account (to exclude the effect of the head-hinge and head-head interactions) and fitted WLC model predictions to the histogram of end-to-end lengths of the coiled coils (Figure S3.4A). Because there was no closed form available to describe this distribution analytically and approximations were only published for a limited set of persistence lengths [17], we generated the distributions through Monte-Carlo simulations. These simulations reproduced the histogram of head-hinge distances for V-shaped conformations quite well. We found that our data is best described by a WLCmodel with an L_p of 3.8 ± 0.2 nm and a contourlength of 46 ± 2 nm (Figure 3.4). As a visual control, we used the same simulation algorithm and parameters to generate example shapes of dimers. The simulations strikingly resemble our observations in high-speed AFM (Figure S3.4B), hereby confirming our method. We conclude that the coiled coils of Smc2-Smc4 dimers can be described as flexible polymers with a persistence length of only about 4 nm.

3.3. Discussion

Using high-speed AFM under liquid conditions, we have examined the structure and dynamics of condensin's Smc2-Smc4 dimers in real-time and under physiological conditions. Contrary to the suggestion from a crystal structure of the Smc2-Smc4 hinge domain, cross-linking experiments [10], and from images of Smc2-Smc4 dimers taken after drying them on a solid surface (Figure S3.1; [3, 8], we never observed rod-shaped

molecules with their coiled coils juxtaposed under liquid conditions. We conclude that the coiled coils are not stiff rods, but are instead highly flexible.

Coiled coils serve a broad range of functions in many different proteins. It is hence useful to put our finding of the highly flexible nature of the Smc2-Smc4 coiled coils (L_p 4 nm) into perspective. While a single alpha helix is very flexible (L_p 1 nm; [18], coiled coils are in general significantly more stiff. Theoretically, the persistence length of a coiled coil formed by two alpha helixes has been predicted to be as high as 200 nm [19]. In reality, the global stiffness of a coiled coil structure depends on its sequence and on local interruptions by non-coiled sequences. Measured values of L_p of coiled coil proteins range from 25 nm for myosin II [20] to up to 100 nm for tropomyosin [21–23]. All hitherto reported L_p values are larger than the value that we deduced for the Smc2-Smc4 dimers, emphasizing the remarkably flexible nature of these condensin subunits.

We find that Smc2-Smc4 dimers characteristically display an open structure. The discrepancy to previously reported structures can be due to several factors. Firstly, to accurately assess the behavior of the coiled coils, it is important to take the full-length SMC proteins into account, since the engagement of the heads with each other and the hinge has an influence on the behavior of the coils. Our results indeed indicate that the heads have a certain attractive force towards each other and to the hinge. Measurements on truncated proteins that lack the heads or parts of the coiled coil could therefore yield skewed results. Secondly, sample preparation conditions for EM and dry AFM can result in experimental artifacts, such that certain conformations are missed. Measuring in liquid at near-physiological conditions is closer to the in vivo situation. Thirdly, our liquid AFM data shows that the configuration of the SMC dimers is dynamic over time. Consequently, results from bulk crosslinking experiments should be treated with caution, as transient interactions can be kinetically trapped with this method. Moreover, the open conformations would be missed and cross-linking interactions might occur between adjacent molecules.

We find that the ATPase heads of the Smc2-Smc4 dimers engage and disengage with each other in a dynamic manner. Excitingly, we find that the heads also interact dynamically with the hinge, resulting in a hitherto undiscovered structure. The dip in the head-hinge distance probability density at 7 nm (Figure 3.3A, right panel) suggests that this interaction takes place despite a considerable entropic penalty. In the P-shaped form, only one head interacts with the hinge, which indicates that the two ATPase heads interact with the hinge independently of each other. It has previously been suggested that the head and hinge domains of cohesin?s Smc1-Smc3 dimer might need to associate to enable an ATP hydrolysis-driven disengagement of the hinge for DNA entry into the cohesin ring, a feat that can only be achieved by the folding of the intervening coiled coils [24, 25]. If DNA enters condensin rings in an analogous manner to what has been proposed for cohesin, then the newly identified 'butterfly' structure reveals a conformation that is important in condensin?s DNA loading mechanism.

Here, we demonstrated that high-speed AFM in liquid is able to provide a quantitative analysis of the dynamics of SMC dimers under physiological conditions. We showed that even in the absence of ATP or DNA, Smc2-Smc4 dimers adopt highly dynamic and flexible conformations. The biophysical properties of the SMC coiled coils revealed by our study provide the fundamental basis for the mechanics of DNA entrapment by the

SMC protein machinery and set the stage for further in-depth biochemical and structural studies of condensin and cohesin.

3.4. Experimental procedures

Purification of Smc2-Smc4 dimers

S. cerevisiae Smc2 fused to a C-terminal His_6 epitope tag and Smc4 fused to a C-terminal StrepII tag were co-expressed from an episomal plasmid under the control of the galactose-inducible GAL1 or GAL10 promoters in protease-deficient budding yeast cells (strain C2598) and purified via Ni-NTA, StrepTactin and gel filtration steps as described [26].

EM and rotary shadowing

Smc2-Smc4 protein preparations were dialyzed for 45 min against 200 mM NH_4HCO_3, 30% glycerol, 2 mM DTT (pH 7.6). 3 µl of 0.1 mg/ml dialyzed Smc2-Smc4 dimers were sprayed onto freshly cleaved mica, immediately dried in vacuum and rotary shadowed with Pt-C at an angle of 7°C. Images were recorded in a Morgagni FEI microscope at 56,000x magnification.

Dry AFM

SMC dimers were diluted to a concentration of 7.1 µg/ml in 200 mM NaCl, 10 mM TRIS-HCl pH 7.0, 30 mM $MgCl_2$, 5 mM DTT and 10% glycerol. Samples were incubated on mica for 10 seconds before rinsing with MilliQ water and drying with a nitrogen gun. Imaging was performed on a Bruker Multimode AFM, using BudgetSensors SHR150 ultrasharp probes.

High-speed AFM in liquid

Purified Smc2-Smc4 dimers at a concentration of 2.2 mg/ml were 20x diluted with imaging buffer (20 mM TRIS-HCl pH 7.0, 200 mM NaCl, 10 mM $MgCl_2$, 5 mM DTT, 10% glycerol) and immediately snap-frozen in aliquots and stored at ?80°C. Prior to imaging, samples were thawed, diluted another 40x with imaging buffer and a droplet of protein solution was applied to freshly cleaved mica. After 10 seconds, the surface was rinsed with imaging buffer and placed - without drying - into the imaging bath of the AFM (HS-AFM 1.0, RIBM, Tsukuba, Japan). Procedures for imaging were largely according to those described in published protocols [27]. Nanoworld USC-f1.2-k0.15 and USC-f1.5-k-0.6 cantilevers were used. AFM movies of selected areas with single molecules, typically 70x80 nm in size, were acquired at frame rates of 2-10 Hz. The tip forces are controlled through a system that stabilizes the oscillation via a feedback mechanism on the second harmonic amplitude [28, 29].

Image analysis

A user-guided semi-automatic image analysis was performed. Because of the large data volume, only every fifth frame of the AFM movies was analyzed. This resulted in a total of more than 1,700 data points.

Stiffness analysis and Monte Carlo simulations

We simulated two-dimensional worm-like chains by dividing each chain into N segments of length L_s=0.2nm, and assigning angles αbetween the segments that are drawn from a normal distribution with a variance L_p/L_s. This definition of the persistence length L_p follows the analysis of Rivetti et al. [16]. From the angles between segments, x and y coordinates are calculated for the entire chain. For each value of the persistence length and contour length, 10^6 chains are simulated (See Figure S3.4B for examples), and histograms are calculated of the end-to-end distances. Using the sum of the least squares between the Monte Carlo results and the experimental data as a goodness-of-fit estimator, the values of L_p and L_c are iterated to obtain the best fits and confidence intervals. The errors of the fits are one standard deviation confidence intervals, obtained through the graphical Monte Carlo method [30]. We note that this procedure significantly extends beyond the traditional approach first described by Rivetti et al., which yields an estimate for the persistence length using only the mean square end-to-end distance. In our case, that approach yields a value of 4.6 nm. The difference can be ascribed to the fact that data for end-to-end distances near zero are missing from the distribution due to the head-hinge interactions. Finally, it should be noted that in our experimental data, the centers of the heads and hinges are taken as markers for the ends of the coiled coils, i.e., we do not take the finite size of the hinge and head domains into account, nor the (unknown) position of the attachment points.

3.5. Supplementary Information

Supplemental Figures

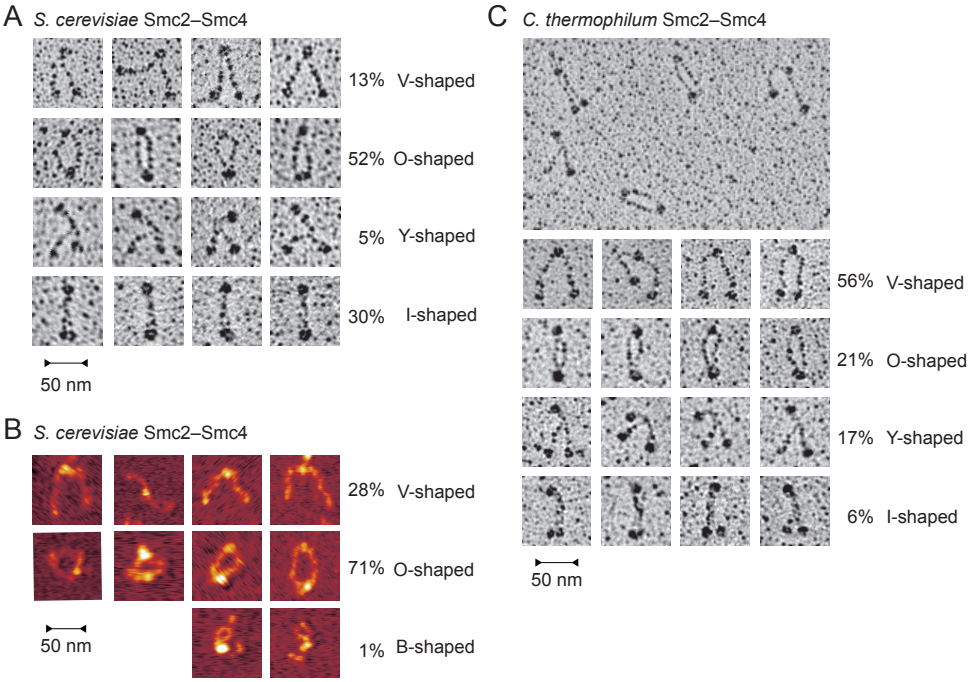

Figure S3.1: **Smc2-Smc4 dimer conformations in EM and dry AFM. A.** Examples of different conformation classes of *S. cerevisiae* Smc2-Smc4 dimers observed by rotary shadowing EM. Frequencies of occurrence are listed on the right as a fraction of 500 molecules classified. Molecules were categorized as O-shaped if a space of at least the width of a coiled coil was visible between the SMC coiled coils. **B.** Examples of different conformations of *S. cerevisiae* Smc2-Smc4 dimers observed by dry AFM. Frequencies of occurrence are listed on the right as a fraction of 400 molecules classified. **C.** Examples of different conformations of *Ch. thermophilum* Smc2-Smc4 dimers observed by rotary shadowing EM. Frequencies of occurrence are listed on the right as a fraction of 400 molecules classified.

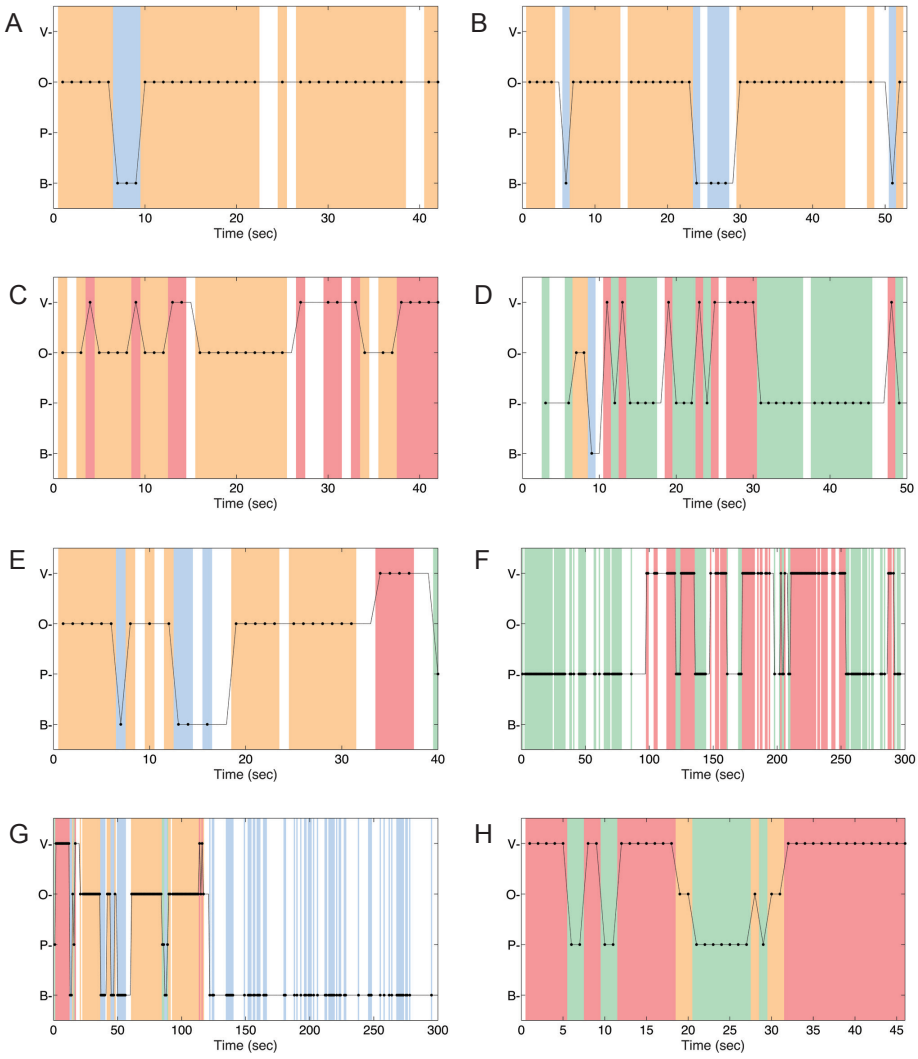

Figure S3.2: **Conformational changes of different Smc2-Smc4 dimers followed by high- speed AFM.** Conformations of individual frames of eight movies of different Smc2-Smc4 molecules were classified. V-shaped in red, O-shaped in orange, P-shaped in green, B-shaped in blue. White gaps indicate that the conformation could not be confidently classified for a particular frame.

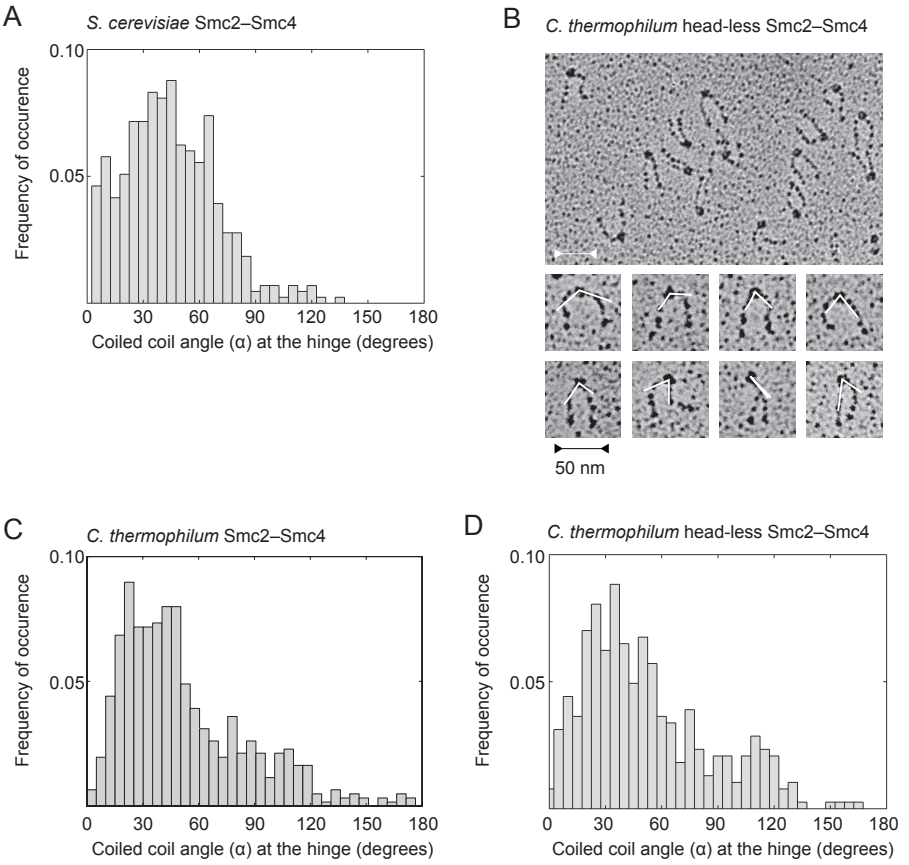

Figure S3.3: **Coiled coil angle measured in electron micrographs. A.** Histogram frequency plot of coiled-coil angles measured at the hinge of full-length *S. cerevisiae* Smc2-Smc4 dimers (displayed as fraction of a total 430 individual molecules). **B.** Example image of ?head-less *Ch. thermophilum* Smc2-Smc4 dimers imaged by rotary shadowing EM. **C.** Histogram frequency plot of the coiled coil angles at the hinge of head-less *Ch. Thermophilum* Smc2-Smc4 dimers (displayed as fraction of a total 385 individual molecules). **D.** Histogram frequency plot of the coiled coil angles at the hinge *Ch. Thermophilum* Smc2-Smc4 dimers (displayed as fraction of a total 613 individual molecules).

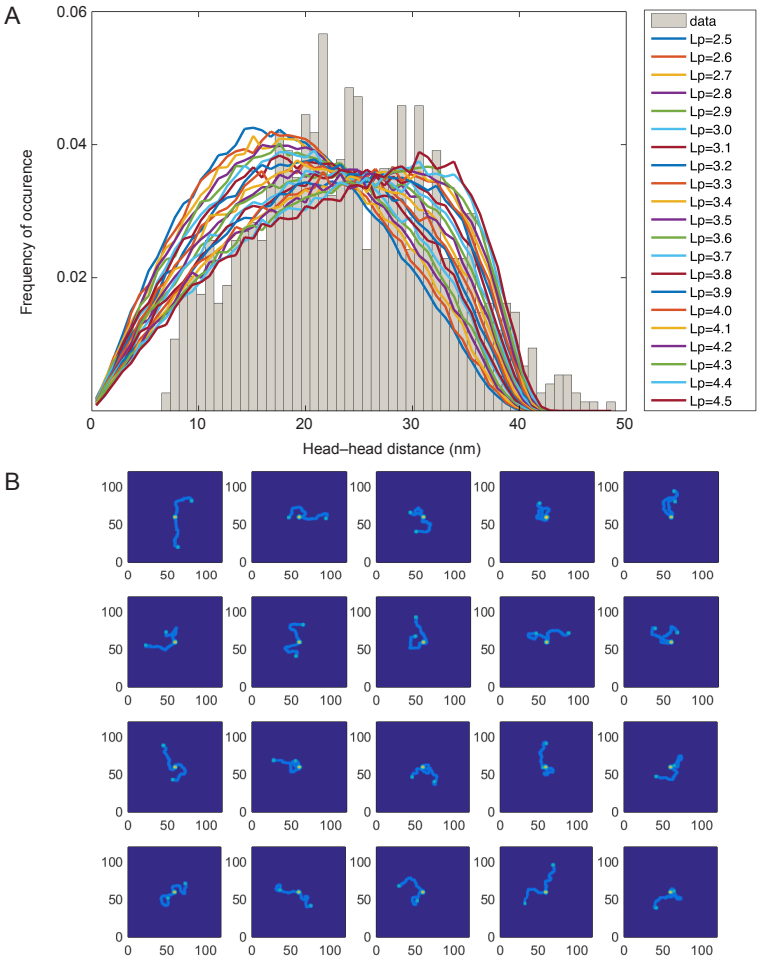

Figure S3.4: **A worm-like chain model to describe the behavior of Smc2-Smc4 dimers. A.** We simulated worm-like chains with varying persistence length and a set contour length of 46 nm. A persistence length of 3.8 nm fits our data measured for *S. cerevisiae* Smc2-Smc4 dimers in the V-shaped (grey histogram) best, as judged from minimizing for the least squared residues. **B.** We used the found persistence length of 3.8 nm to simulate the behavior of the coiled-coils. The results of these simulations resemble our AFM images.

Table S1

Persistence lengths of coiled coils and other biological polymers, ranged from stiff to flexible.

Polymer	Persistence length	Reference
Coiled coil (theoretical)	200nm	Yogurtcu et al., 2010[19]
Tropomyosin coiled coil	40-100nm	Li et al., 2010, 2012; Loong et al., 2012[21–23]
Vimentin coiled coil	63nm	Ackbarow and Buehler, 2007[31]
Double stranded RNA	62nm	Abels et al., 2005[32]
Double stranded DNA	50nm	Bustamante et al., 1994[13]
Rad50 coiled coil	35nm	de Jager et al., 2001[33]
Myosin II coiled coil	25nm	Schwaiger et al., 2002[20]
Smc2-Smc4 coiled coil	*4nm*	*this manuscript*
Protein alpha helix	1nm	Papadopoulos et al., 2006[18]
Single strand DNA	0.8nm	Smith et al., 1996[34]
Unstructured amino acid chain	0.4nm	Carrion-Vazquez et al., 1999[35]

Supplemental experimental procedures

Force control in AFM imaging and the possible influence of the scanning motion on SMC dynamics

We operate the AFM in intermittent contact ('tapping') mode. The tapping amplitude A during imaging is approximately 4 nm, and the 'amplitude ratio' (imaging amplitude divided by free amplitude) is typically 85-95%. The imaging feedback keeps the amplitude A constant, but because the drive efficiency of the tapping piezo is subject to temporal fluctuations, the amplitude ratio can fluctuate substantially outside the user's control. To have more control over the applied forces, A_2, the second harmonic of the cantilever's sinusoidal motion is monitored using a Signal Recovery model 7280 lock-in amplifier and kept constant by a homebuilt feedback unit, that modulates the drive amplitude. In the range of imaging parameters that we use, A_2 is monotonic in the strength of the tip-sample interaction, and therefore it is a good proxy for the imaging force. However, the exact relation between A_2 and force depends on several unknown parameters and is therefore not quantifiable.

The bandwidth of the AFM imaging system depends on the force that is applied to the sample. At the lowest imaging forces, the image quality is poor and only the location, but not the conformation of the dimers can be seen. Evaluation of these images indicates that the mobility of the dimers is not reduced under these imaging conditions compared to the higher forces used to obtain quantitative results, suggesting that the tip influence on these results is minimal. To obtain images that are sharp enough to distinguish all four configurations from each other while maintaining an image speed of 2 frames/s, we find that an A_2 value of 20 pm or more is required. Values of 50-70 pm are sufficient to obtain high-quality images up to 10 frames/s, and hence we did not go beyond this. Notably, within the range of forces that yields movies of sufficient quality, we find no effect of the imaging on the dynamics of the SMC dimers. In addition, we see no correlation between the head positions and the fast scanning direction. We therefore conclude that there is no indication that the AFM scanning induces changes to the molecular configuration of the SMC dimers or the dynamic behavior of the heads through energy input from the tip.

Purification of full-length *Chaetomium thermophilum* Smc2-Smc4 dimers

C. thermophilum Smc2 fused to a C-terminal StrepII tag and Smc4 (residues 1-1,542) fused to a C-terminal His_8 tag were co-expressed in Sf21 cells cultured in Sf-900 III SFM serum-free medium (Invitrogen) from a single baculovirus. About 0.5-0.8x10^8 Sf21 cells were lysed by sonication in lysis buffer (50mM TRIS-HCl pH 7.5, 300mM NaCl, 20mM imidazole, 5mM β-mercaptoethanol) supplemented with 1x Complete EDTA-free protease inhibitor cocktail (Roche) at 4°C. The lysate was cleared by centrifugation at 45,000xg for 50min at 4°C and incubated with NiNTA Sepharose (GE Healthcare) for 2h at 4°C. The resin was washed with ~100 column volumes (CV) lysis buffer before elution with 4 CV elution buffer (50mM TRIS-HCl pH 7.5, 300mM NaCl, 320mM imidazole, 5mM β-mercaptoethanol). Eluted protein fractions were combined and dialyzed over night at 4°C in dialysis buffer (25mM TRIS-HCl pH 7.5, 300mM NaCl, 1mM DTT), diluted with 10 volumes of low-salt buffer (25mM TRIS-HCl pH 7.5, 100mM NaCl, 1mM DTT), and loaded onto a 6ml-RESOURCE Q anion-exchange column (GE Healthcare). The resin was washed with 5 CV low-salt buffer and eluted in a 60ml linear gradient to high-salt buffer (25mM TRIS-HCl pH 7.5, 1 M NaCl, 1mM DTT). Peak fractions were collected and concentrated by ultrafiltration with a 100,000 MWCO cut-off Vivaspin concentrator (Sartorius).

Purification of head-less *Chaetomium Thermophilum* Smc2-Smc4 dimers

N-terminally His_6-tagged Smc2 (residues 224-982) and Smc4 (residues 509-1,258) from *C. thermophilum* were co-expressed in E. coli strain BL21(DE3)Rosetta2 pLysS (Novagen) grown in 2xTY medium and induced with 200µM IPTG at 18°C for 16h. Cell pellets were resuspended in lysis buffer (50mM TRIS-HCl pH 7.5, 500mM NaCl, 25 mM imidazole, 5mM β-mercaptoethanol) supplemented with 1x Complete EDTA-free protease inhibitors and lysed using a sonicator (Branson). Cell debris were pelleted for 1h at 40,000xg and the supernatant was incubated with NiNTA Sepharose (GE Healthcare) pre-equilibrated in lysis buffer. The resin was extensively washed with lysis buffer and eluted with 250mM imidazole. Eluted protein was dialyzed to 50mM TRIS-HCl pH 7.5, 100mM NaCl, 1mm DTT and then loaded onto a RESOURCE Q anion-exchange column equilibrated in the same buffer. Proteins were eluted with a linear gradient to 1M NaCl. The single peak fraction was concentrated and passed over a Superdex S200 26/60 gel filtration column (GE Healthcare) in 25mM TRIS pH 7.5, 200mM NaCl, 1mM DTT, where the proteins eluted in a single peak. Peak fractions were concentrated using a Vivaspin concentrator, flash frozen in liquid nitrogen, and stored at -80°C.

References

[1] L. Aragon, E. Martinez-Perez, and M. Merkenschlager, *Condensin, cohesin and the control of chromatin states,* Current Opinion in Genetics and Development **23**, 204 (2013).

[2] T. Hirano, *At the heart of the chromosome: SMC proteins in action.* Nature reviews. Molecular cell biology **7**, 311 (2006).

[3] D. E. Anderson, A. Losada, H. P. Erickson, and T. Hirano, *Condensin and cohesin display different arm conformations with characteristic hinge angles.* The Journal of cell biology **156**, 419 (2002).

[4] S. Cuylen, J. Metz, and C. H. Haering, *Condensin structures chromosomal DNA through topological links.* Nature structural & molecular biology **18**, 894 (2011).

[5] C. H. Haering, A.-M. Farcas, P. Arumugam, J. Metson, and K. Nasmyth, *The cohesin ring concatenates sister DNA molecules.* Nature **454**, 297 (2008).

[6] C. H. Haering, J. Löwe, A. Hochwagen, and K. Nasmyth, *Molecular Architecture of SMC Proteins and the Yeast Cohesin Complex,* Molecular Cell **9**, 773 (2002).

[7] P. J. Huis in 't Veld, F. Herzog, R. Ladurner, I. F. Davidson, S. Piric, E. Kreidl, V. Bhaskara, R. Aebersold, and J.-M. Peters, *Characterization of a DNA exit gate in the human cohesin ring.* Science (New York, N.Y.) **346**, 968 (2014).

[8] S. H. Yoshimura, K. Hizume, A. Murakami, T. Sutani, K. Takeyasu, and M. Yanagida, *Condensin Architecture and Interaction with DNA,* Current Biology **12**, 508 (2002).

[9] H. Barysz, J. H. Kim, Z. A. Chen, D. F. Hudson, J. Rappsilber, D. L. Gerloff, W. C. Earnshaw, and W. C. Earnshaw, *Three-dimensional topology of the SMC2 / SMC4 subcomplex from chicken condensin I revealed by cross-linking and molecular modelling,* Open Biology (2015).

[10] Y.-M. Soh, F. Bürmann, H.-C. Shin, T. Oda, K. S. Jin, C. P. Toseland, C. Kim, H. Lee, S. J. Kim, M.-S. Kong, M.-L. Durand-Diebold, Y.-G. Kim, H. M. Kim, N. K. Lee, M. Sato, B.-H. Oh, and S. Gruber, *Molecular basis for SMC rod formation and its dissolution upon DNA binding.* Molecular cell **57**, 290 (2015).

[11] T. Ando, N. Kodera, E. Takai, D. Maruyama, K. Saito, and a. Toda, *A high-speed atomic force microscope for studying biological macromolecules.* Proceedings of the National Academy of Sciences of the United States of America **98**, 12468 (2001).

[12] A. J. Katan and C. Dekker, *High-speed AFM reveals the dynamics of single biomolecules at the nanometer scale.* Cell **147**, 979 (2011).

[13] C. Bustamante, J. F. Marko, E. D. Siggia, and S. Smith, *Entropic elasticity of lambda-phage DNA.* Science (New York, N.Y.) **265**, 1599 (1994).

[14] M. S. Kellermayer, *Folding-Unfolding Transitions in Single Titin Molecules Characterized with Laser Tweezers,* Science **276**, 1112 (1997).

[15] J. van Noort, T. van der Heijden, M. de Jager, C. Wyman, R. Kanaar, and C. Dekker, *The coiled-coil of the human Rad50 DNA repair protein contains specific segments of increased flexibility,* Proceedings of the National Academy of Sciences **100**, 7581 (2003).

[16] C. Rivetti, M. Guthold, and C. Bustamante, *Scanning force microscopy of DNA deposited onto mica: equilibration versus kinetic trapping studied by statistical polymer chain analysis.* Journal of molecular biology **264**, 919 (1996).

[17] B. Hamprecht, W. Janke, and H. Kleinert, *End-to-end distribution function of two-dimensional stiff polymers for all persistence lengths,* Physics Letters A **330**, 254 (2004).

[18] P. Papadopoulos, G. Floudas, I. Schnell, I. Lieberwirth, T. Q. Nguyen, and H.-A. Klok, *Thermodynamic confinement and alpha-helix persistence length in poly(gamma-benzyl-L-glutamate)-b-poly(dimethyl siloxane)-b-poly(gamma-benzyl-L-glutamate) triblock copolymers.* Biomacromolecules **7**, 618 (2006).

[19] O. N. Yogurtcu, C. W. Wolgemuth, and S. X. Sun, *Mechanical response and conformational amplification in α-helical coiled coils.* Biophysical journal **99**, 3895 (2010).

[20] I. Schwaiger, C. Sattler, D. R. Hostetter, and M. Rief, *The myosin coiled-coil is a truly elastic protein structure.* Nature materials **1**, 232 (2002).

[21] X. E. Li, K. C. Holmes, W. Lehman, H. Jung, and S. Fischer, *The shape and flexibility of tropomyosin coiled coils: implications for actin filament assembly and regulation.* Journal of molecular biology **395**, 327 (2010).

[22] X. E. Li, W. Suphamungmee, M. Janco, M. A. Geeves, S. B. Marston, S. Fischer, and W. Lehman, *The flexibility of two tropomyosin mutants, D175N and E180G, that cause hypertrophic cardiomyopathy.* Biochemical and biophysical research communications **424**, 493 (2012).

[23] C. K. P. Loong, H.-X. Zhou, and P. B. Chase, *Persistence length of human cardiac α-tropomyosin measured by single molecule direct probe microscopy.* PloS one **7**, e39676 (2012).

[24] S. Gruber, P. Arumugam, Y. Katou, D. Kuglitsch, W. Helmhart, K. Shirahige, and K. Nasmyth, *Evidence that loading of cohesin onto chromosomes involves opening of its SMC hinge.* Cell **127**, 523 (2006).
[25] K. Nasmyth, *Cohesin: a catenase with separate entry and exit gates?* (2011).
[26] I. Piazza, A. Rutkowska, A. Ori, M. Walczak, J. Metz, V. Pelechano, M. Beck, and C. H. Haering, *Association of condensin with chromosomes depends on DNA binding by its HEAT-repeat subunits.* Nature structural & molecular biology **21**, 560 (2014).
[27] T. Uchihashi, N. Kodera, and T. Ando, *Guide to video recording of structure dynamics and dynamic processes of proteins by high-speed atomic force microscopy.* Nature protocols **7**, 1193 (2012).
[28] N. Kodera, M. Sakashita, and T. Ando, *Dynamic proportional-integral-differential controller for high-speed atomic force microscopy,* Review of Scientific Instruments **77**, 083704 (2006).
[29] J. Schiener, S. Witt, M. Stark, and R. Guckenberger, *Stabilized atomic force microscopy imaging in liquids using second harmonic of cantilever motion for setpoint control,* Review of Scientific Instruments **75**, 2564 (2004).
[30] G. Cowan, *Statistical data analysis* (Oxford University Press, 1998).
[31] T. Ackbarow and M. J. Buehler, *Superelasticity, energy dissipation and strain hardening of vimentin coiled-coil intermediate filaments: atomistic and continuum studies,* Journal of Materials Science **42**, 8771 (2007).
[32] J. A. Abels, F. Moreno-Herrero, T. van der Heijden, C. Dekker, and N. H. Dekker, *Single-molecule measurements of the persistence length of double-stranded RNA.* Biophysical journal **88**, 2737 (2005).
[33] M. de Jager, J. van Noort, D. C. van Gent, C. Dekker, R. Kanaar, and C. Wyman, *Human Rad50/Mre11 Is a Flexible Complex that Can Tether DNA Ends,* Molecular Cell **8**, 1129 (2001).
[34] S. B. Smith, Y. Cui, and C. Bustamante, *Overstretching B-DNA: The Elastic Response of Individual Double-Stranded and Single-Stranded DNA Molecules,* Science **271**, 795 (1996).
[35] M. Carrion-Vazquez, A. F. Oberhauser, S. B. Fowler, P. E. Marszalek, S. E. Broedel, J. Clarke, and J. M. Fernandez, *Mechanical and chemical unfolding of a single protein: A comparison,* Proceedings of the National Academy of Sciences **96**, 3694 (1999).

4

The condensin complex is a mechanochemical motor that translocates along DNA

Condensin plays crucial roles in chromosome organization and compaction, but the mechanistic basis for its functions remains obscure. Here, we use single-molecule imaging to demonstrate that *Saccharomyces cerevisiae* condensin is a molecular motor capable of ATP hydrolysis-dependent translocation along double-stranded DNA. Condensin's translocation activity is rapid and highly processive, with individual complexes traveling an average distance of ≥10 kilobases at a velocity of ~ 60 base pairs per second. Our results suggest that condensin may take steps comparable in length to its ~50-nanometer coiled-coil subunits, suggestive of a translocation mechanism that is distinct from any reported DNA motor protein. The finding that condensin is a mechanochemical motor has important implications for understanding the mechanisms of chromosome organization and condensation.

This chapter has been published as: T. Terakawa*, S. Bisht*, J.M. Eeftens*, C. Dekker, C.H. Haering, E. Greene, *Science* (2017)

Structural maintenance of chromosomes (SMC) complexes are the major organizers of chromosomes in all living organisms [1, 2]. These protein complexes play essential roles in sister chromatid cohesion, chromosome condensation and segregation, DNA replication, DNA damage repair, and gene expression. A distinguishing feature of SMC complexes is their large ring-like architecture, the circumference of which is made up of two SMC protein coiled-coil proteins and a single kleisin subunit (Fig.4.1A) [1–4]. The ~50-nm long antiparallel coiled-coils are connected at one end by a stable dimerization interface, referred to as the hinge domain, and at the other end by globular ATP-binding cassette (ABC) family ATPase domains [5]. The ATPase domains are bound by a protein of the kleisin family, along with additional accessory subunits, which vary for different types of SMC complexes (Fig. 4.1A). The relationship between SMC structures and their functions in chromosome organization is not completely understood [6], but many models envision that the coiled-coil domains allow the complexes to topologically embrace DNA [1–4]. Given the general resemblance to myosin and kinesin, some early models postulated that SMC proteins might be mechanochemical motors [7–10].

SMC complexes are thought to regulate genome architecture by physically linking distal chromosomal loci, but how these bridging interactions might be formed remains unknown [1, 2, 11]. An early model suggested that many three-dimensional (3D) features of eukaryotic chromosomes might be explained by DNA loop extrusion (Fig. 4.1B) [12, 13], and recent polymer dynamics simulations have shown that loop extrusion can recapitulate the formation of topologically associating domains (TADs), chromatin compaction, and sister chromatid segregation [14–18]. This loop extrusion model assumes a central role for SMC complexes in actively creating the DNA loops [11, 12]. Similarly, it has been proposed that prokaryotic SMC proteins may structure bacterial chromosomes through an active loop extrusion mechanism [19–21]. Yet, the loop extrusion model remains hypothetical, in large part because the motor activity that is necessary for driving loop extrusion could not be identified [11]. Indeed, the absence of an identifiable motor activity in SMC complexes instead has lent support to alternative models in which DNA loops are not actively extruded, but instead are captured and stabilized by stochastic pairwise SMC binding interactions to bridge distal loci [22].

To help distinguish between possible mechanisms of SMC protein-mediated chromosomal organization, we examined the DNA-binding properties of condensin [23]. We overexpressed the five subunits of the condensin complex in budding yeast and purified the complex to homogeneity (Fig. 4.1C and fig. S4.1). Electron microscopy images confirmed that the complexes were monodisperse (Fig. 4.1D). As previously described for electron micrographs of immunopurified *Xenopus laevis* or human condensin [24], we observed electron density that presumably corresponds to the two HEAT-repeat subunits in close vicinity of the Smc2-Smc4 ATPase head domains. We confirmed that the *S. cerevisiae* condensin holocomplex binds double-stranded (ds) DNA and hydrolyzes ATP in vitro (Fig. 4.1E and F). Addition of dsDNA stimulated the condensin ATPase activity ~3-fold, which is consistent with previous measurements with *X. laevis* condensin I complexes [25], and revealed K_M and k_{cat} values of 0.4 ± 0.07 mM and 2.0 ± 0.1 s^{-1}, respectively, for ATP hydrolysis in the presence of linear dsDNA (Fig. 4.1G). Furthermore, condensin could promote extensive ATP hydrolysis-dependent DNA compaction of single-tethered DNA curtains, which was reversible by increasing the salt concentra-

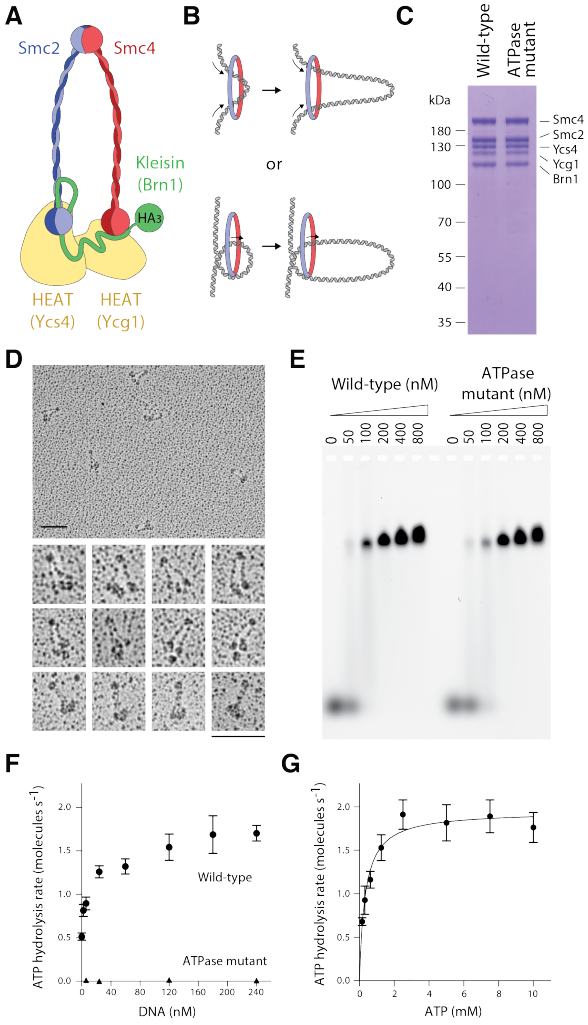

Figure 4.1: **Biochemistry of budding yeast condensin holocomplexes. A.** Schematic of the *S. cerevisiae* condensin complex. The Brn1 kleisin subunits connects the ATPase head domains of the Smc2-Smc4 heterodimer and recruits the HEAT-repeat subunits Ycs4 and Ycg1. The cartoon highlights the position of the HA3-tag used for labeling. **B.** Conceptual schematic of loop extrusion for models with either two (top panel) of one (bottom panel) DNA strand(s) passing through the centre of the SMC ring. **C.** Wild-type and ATPase-deficient Smc2(Q147L)-Smc4(Q302L) condensin complexes analyzed by SDS PAGE and Coomassie staining. **D.** Electron micrographs of wild-type condensin holocomplexes rotary shadowed with Pt/C. Scale bar: 100 nm. **E.** Electrophoretic mobility shift assays with 6-FAM labelled 45-bp dsDNA substrate (100 nM) and the indicated protein concentrations. **F.** ATP hydrolysis by wild-type and ATPase mutant condensin complexes (0.5 μM) upon addition of increasing concentrations of a 6.4-kb linear DNA at saturated ATP concentrations (5 mM). The plot shows mean ± S.D. of n = 3 (wild-type) or 2 (ATPase mutant) independent experiments. **G.** Michaelis-Menten kinetics for the rate of ATP hydrolysis by wild-type condensin complexes (0.5 μM) at increasing ATP concentrations in the presence of 240 nM 6.4-kb linear DNA. The plot shows mean ± S.D. of N = 3 independent experiments. The fit corresponds to a K_m of 0.4 ± 0.07 mM for ATP and k_{cat} of 2.0 ± 0.1 s^{-1} per molecule of condensin (mean ± standard error).

tion to 0.5M NaCl (Fig. S4.2A-C). An ATPase-deficient version of condensin with mutations in the γ-phosphate switch loops (Q-loops) of Smc2 and Smc4 still bound DNA (Fig. 4.1E), but exhibited no ATP hydrolysis activity (Fig. 4.1F) or DNA compaction activity (Fig. S4.2D).

We then used total internal reflection fluorescence microscopy (TIRFM) to visualize binding of single fluorescently-tagged condensin holocomplexes to double-tethered DNA substrates [26]. Initial experiments using single-tethered DNA curtains demonstrated that condensin could promote extensive ATP hydrolysis-dependent DNA compaction, which was reversible by increasing the salt concentration to 0.5 M NaCl (Fig. S4.2). We next asked whether we could directly visualize the binding of single fluorescently-tagged condensin holocomplexes to double-tethered DNA substrates. We fluorescently labeled condensin with quantum dots (Qdots) conjugated to antibodies against the HA3-tag fused to the Brn1 kleisin subunit (Fig. 4.1A). Electrophoretic mobility shift assays confirmed that condensin was quantitatively labeled (Fig. S4.3A). Importantly, binding to the Qdots inhibited neither condensin's ATP hydrolysis activity nor its ability to alter DNA topology (Fig. S4.3B and C). We prepared double-tethered curtains by attaching the DNA substrates (~48.5-kb λ-DNA) to a supported lipid bilayer through a biotin-streptavidin linkage, and aligned one end of the DNA molecules at nanofabricated chromium (Cr) barriers and anchored the other end of the DNA to Cr pedestals located 12 μm downstream (Fig. 4.2A) [26].

Using double-tethered curtains, we were able to detect binding of condensin complexes to individual DNA molecules (Fig. 4.2B). Kymographs revealed that, remarkably, ~85% of all bound condensin complexes (N = 671) underwent linear motion along the DNA (Fig. 4.2C). The up/down direction of movement was random, but once a complex started translocation, it generally proceeded unilaterally without a reversal of direction (reversals were observed occasionally, in 6% of the traces). Condensin has not been previously shown to act as a molecular motor, but the observed movement is fully consistent with expectations for an ATP- dependent DNA-translocating motor protein. Unlike the wild-type condensin, the ATPase-deficient Q-loop mutant of condensin only exhibited motion consistent with random 1-dimensional (1D) diffusion (Fig. 4.2D). Wild-type condensin in the presence of the non-hydrolyzable ATP analog ATPγS also displayed only 1D-diffusion (Fig. S4.4A). Analysis of the initial binding positions for wild-type condensin revealed a preferential binding to A/T-rich regions (Pearson's r = 0.66, P = $5x10^{-6}$; Fig. 4.2E), similar to values reported for *Schizosaccharomyces pombe* cohesin [27]. In contrast, the condensin dissociation positions were not correlated with A/T content (Pearson's r = -0.05, P = 0.77), nor were there any other preferred regions for dissociation within the DNA, with the exception of the Cr barriers and pedestals (Fig. 4.2F). These findings are consistent with a model where condensin loads at A/T-rich sequences and then translocates away. Interestingly, previous single-molecule experiments demonstrated rapid 1D diffusion of cohesin on DNA, but found no evidence for ATP-dependent translocation, suggesting that there may be differences between how the two SMC complexes process DNA [27, 28].

We used particle tracking to quantitatively analyze the movement of condensin on DNA (Fig. 4.3A and B, and fig. S4.4B). Wild-type condensin did not travel in a preferred direction: 52% (N=255/491) of the complexes went one direction, and 48% went the op-

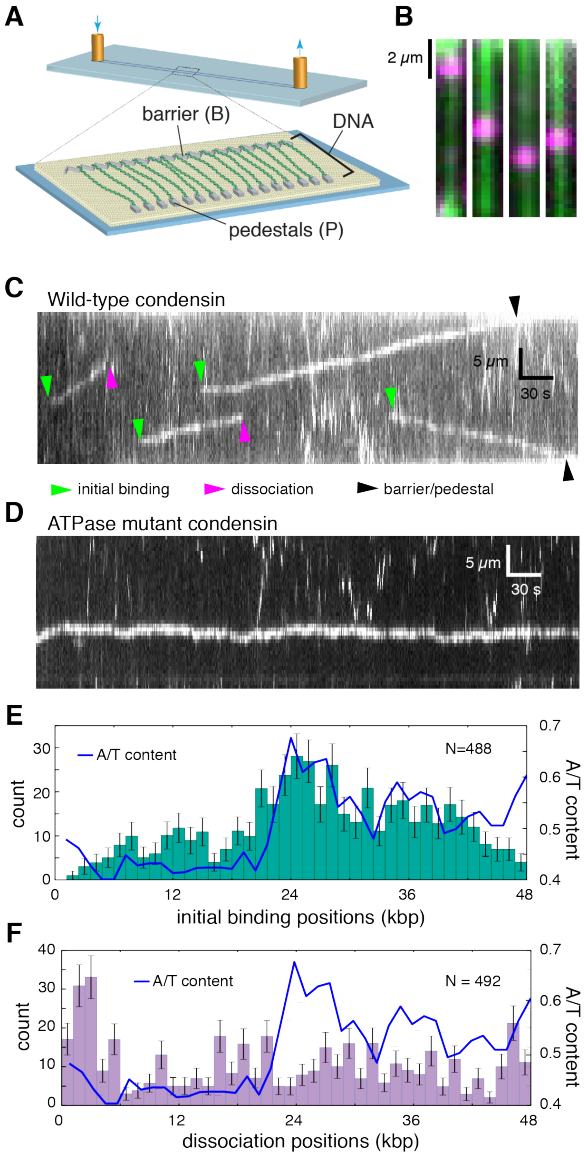

Figure 4.2: **DNA curtain assay for condensin DNA-binding activity. A.** Schematic of the double- tethered DNA curtain assay. **B.** Still images showing Qdot-tagged condensin (magenta) bound to YoYo1-stained DNA (green). **C.** Kymograph showing examples of Qdot-tagged condensin translocating on a single DNA molecule (unlabeled); the initial condensin binding sites, dissociation positions, and collisions with the barriers/pedestals are highlighted with color-coded arrowheads. **D.** Kymograph showing Qdot-tagged ATPase-deficient mutant Smc2(Q147L)- Smc4(Q302L) condensin undergoing 1D diffusion on DNA (unlabeled). **E.** Initial binding sites and **F.** dissociation site distributions of condensin superimposed on the AT content of the λ-DNA substrate. All reactions contained 4 mM ATP. Error bars in (E) and (F) represent standard deviations calculated by boot strap analysis.

posite direction (N=236/491). The condensin ATPase mutant did not exhibit any evidence of unidirectional translocation. Linear MSD plots were characteristic of random diffusive motion [29], yielding diffusion coefficients ($D_{1,obs}$) of (1.7 ± 1.4)x10^{-3} and (0.8 ± 1.0)x10^{-3} μm^2/s (mean± S.D.) for ATPase-deficient condensin and wild-type condensin plus ATPγS, respectively.

We used the tracking data to determine the velocity and processivity for wild-type condensin. A plot of the velocity distributions for data collected in the presence of saturated concentrations of ATP (4 mM; Fig. 4.1G) was well described by a log-normal distribution, revealing a mean apparent translocation velocity of 63 ± 36 bp/s (16 ± 9 nm/s, N=491) (mean±S.D.) (Fig. 4.3E). Interestingly, upon initial binding, condensin paused for a brief period (τ =13.3 ± 1.5 s) before beginning to move along the DNA, which suggests the existence of a rate-limiting step prior to becoming active for translocation (Fig. 4.2C and fig. S4.5). Each translocating condensin complex remained bound to the DNA for an average total time of 4.7 ± 0.2 min and traveled on average 10.3 ± 0.4 kb (2.6 ± 0.1 μm) before dissociating (Figs. 4.3F and fig. S4.6A). This value provides merely a lower limit of the processivity of condensin, because a significant fraction (42%) of the complexes traveled all the way to the ends of the 48.5-kb DNA, where they collided with the Cr barriers or pedestals (see, for example, Fig. 4.2C). There was no correlation between translocation velocity and processivity at a given ATP concentration (Pearson's r = 0.035, P = 0.43 at 4 mM ATP) (Fig. S4.6B). However, velocity and processivity both varied with revealed increasing slopes, which is only consistent with directed motion [29]. In contrast, MSD plots were linear for the ATPase-deficient condensin mutant and for wild-type condensin in the presence of ATP concentrations. Michaelis-Menten analysis revealed a v_{max} of 62 ± 2 bp/s and a K_{cat} of 0.2 ± 0.04 mM ATP (Fig. S4.7A and B). The initial pause time (τ) also varied with ATP concentration, from a mean value of 3.9 ± 0.8 min at 50 μM ATP to 13.3 ± 1.5 s at 4 mM ATP, suggesting that this delay reflects a transition from a translocation-inactive to translocation- active state that is dependent upon ATP binding, ATP hydrolysis, or both (Fig. S4.7C).

Our finding that condensin is an ATP hydrolysis-dependent molecular motor lends support to models invoking SMC protein-mediated loop extrusion as a means for 3D genome organization. An important prediction of the loop extrusion model is that condensin must simultaneously interact with two distal regions of the same chromosome, and at least one (or possibly both) of the interaction sites must translocate away from the other site, allowing for movement of the two contact points relative to one another (Fig. 4.4A) [12, 14–17]. Such "*cis*" loop geometry is inaccessible in our double-tethered assays because the DNA is held in an extended configuration (Fig. 4.2B), which likely decouples loop extrusion from translocation. However, a *cis* loop configuration can be mimicked experimentally by providing a second DNA molecule in *trans* (Fig. 4.4B). To test the possible relationship between the observed linear translocation of condensin along the double- tethered DNA and the loop extrusion model, we asked whether condensin could move a second DNA substrate provided in *trans* relative to the tethered DNA. Indeed, fluorescently labeled (not extended) λ-DNA molecules added in *trans* to wild-type condensin moved at an apparent velocity of 76 ± 19 bp/s (19 ± 5 nm/s, N=102) (Fig. 4.4C and D) while traveling an average distance of 11 ± 0.9 kb (2.7 ± 0.2 μm, N=102) (Fig. 4.4E) - numbers that match well with the condensin motor properties measured above. These

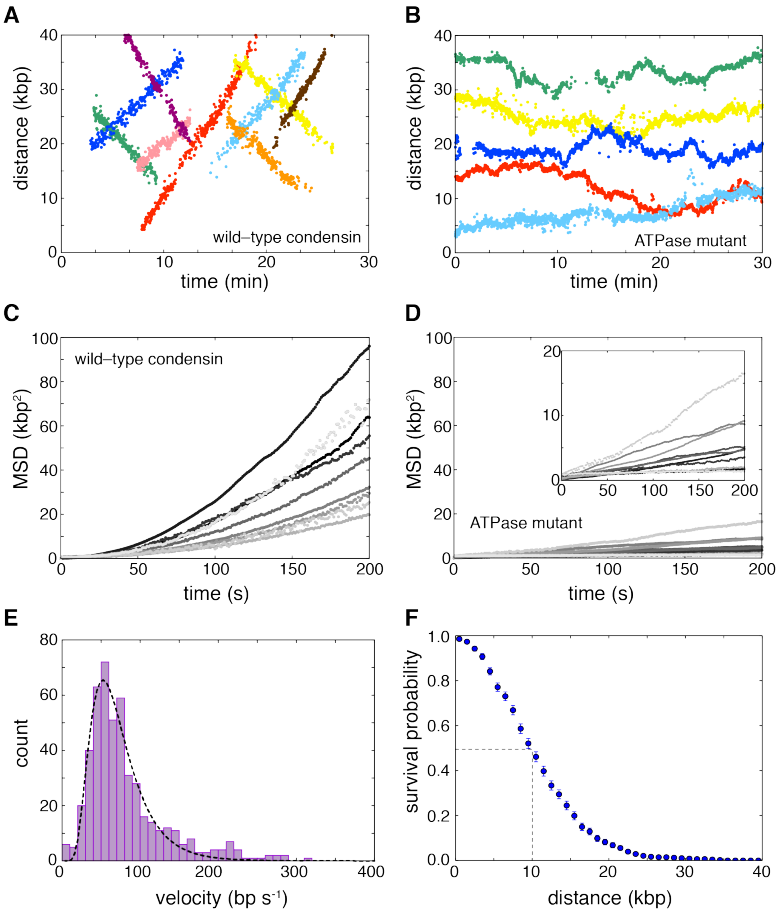

Figure 4.3: **Condensin is an ATP-dependent mechanochemical molecular motor. A.** Examples of tracked translocation trajectories for Qdot-tagged wild-type condensin and **B.** the ATPase- deficient Smc2(Q147L)-Smc4(Q302L) condensin mutant. Mean squared displacement (MSD) plots for **C.** wild-type condensin and **D.** the ATPase deficient mutant obtained from the tracked trajectories; the inset in **D** is a magnification of the main curves. **E.** Velocity distributions for condensin translocation activity; the dashed line is a log-normal fit to the translocation rate data. **F.** Processivity measurements of condensin motor activity. The dashed line highlights the translocation distance corresponding to dissociation of one half of the bound condensin complexes. Error bars represent standard deviations calculated by boot strap analysis.

experiments strongly indicate that translocating condensin complexes were able to interact simultaneously with the tethered DNA and a second DNA. Also, condensin could translocate while bound to both DNA substrates, since one piece of DNA was observed to move with respect to the other piece of DNA. Thus, we conclude that condensin is capable of moving two DNA substrates relative to one another, fulfilling a key expectation of the loop extrusion model.

Heretofore, a common argument against SMC proteins acting as molecular motors was their low rates of ATP hydrolysis when compared to other known nucleic acid motor proteins, which implied that they would not move fast enough to function as efficient motors on biologically relevant time scales. However, this discrepancy can be readily reconciled if condensin were able to take large steps, which is conceptually possible given its large 50-nm size. The available data in fact suggests a large step size: Comparison of the single complex translocation rate (~60 bp/s, or ~14.9 nm/s) to the bulk rate of ATP hydrolysis (k_{cat} = 2.0 s^{-1} in the presence of linear DNA) suggest that condensin may take steps on the order of ~30 bp per molecule of ATP hydrolyzed. Even larger steps are inferred if each step is coupled to the hydrolysis of more than one molecule of ATP. These estimates assume that all of the proteins are ATPase active (one would deduce a smaller step size if a fraction of the protein were inactive), and also assume perfect coupling between ATP hydrolysis and translocation (while a more inefficient coupling would necessitate even larger step sizes). The idea that condensin takes very large steps is also consistent with the step sizes reported from magnetic tweezers experiments of DNA compaction induced by *X. leavis* condensin (80 ± 40 nm, [30] or *S. cerevisiae* condensin [31]. Such large step sizes would seem to rule out models for condensin movement similar to common DNA motor proteins such as helicases, translocases or polymerases, which are typically found to move in 1-bp increments [32–35]. Higher-resolution measurements may prove informative for further defining the fundamental step size for translocating condensin.

To explain our novel results, we searched for possible models for condensin motor activity that (i) can explain the relationship between a slow ATP hydrolysis rate relative to the rate of translocation; (ii) can accommodate a very large step size; and (iii) are consistent with the physical dimensions of the SMC complex. Based on these criteria, we can think of two theoretical possibilities, both of which use the SMC coiled-coils as the means of motility. Condensin might translocate along DNA through reiterative extension and retraction of the long Smc2-Smc4 coiled-coil domains, allowing for movement through a "scrunching" mechanism involving rod- to butterfly-like structural transitions (Fig. 4.4F); or condensin may perhaps use a myosin- or kinesin-like "walking" mechanism (Fig. 4.4G). The maximum single step size for each model is defined by the physical dimensions of the SMC coiled-coils, corresponding to ≤50 nm and ≤100 nm for the scrunching and walking mechanisms, respectively (Fig. 4.4F and G). Both models are consistent with the range of condensin architectures observed by electron microscopy and atomic force microscopy [24, 36]. Movements might be powered by similar ATPase- dependent transitions between different structural states as reported for prokaryotic SMC complexes [21, 37, 38], though it remains to be determined how conformational changes could be translated into the directed movement depicted in our models. Further refinement of the translocation mechanism will depend upon fully defining

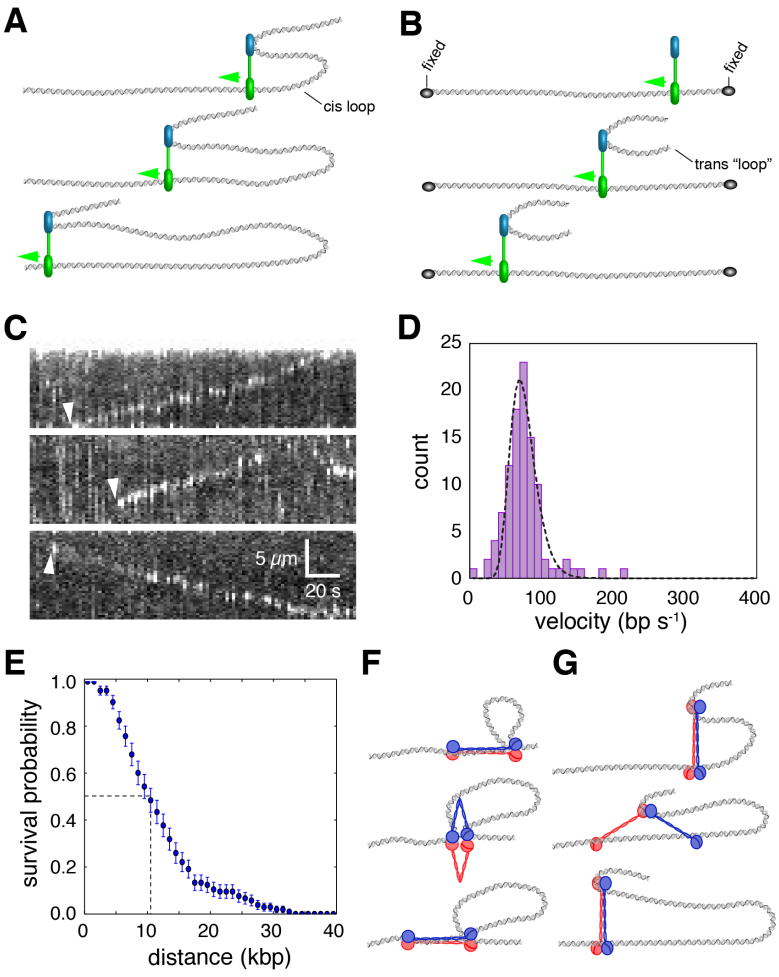

Figure 4.4: **Coupling condensin motor activity to DNA loop extrusion. A.** Minimal mechanistic framework necessary for coupling ATP-dependent translocation to the extrusion of a *cis* DNA loop. In this generic model, a motor domain (green) must move away from a second DNA- binding domain (blue), and this secondary domain can either remain stationary (as depicted) or it may also act as a motor domain and move in the opposite direction (not depicted). **B.** Detection of *cis* loop extrusion is not possible when the DNA is held in a fixed configuration as in the double-tethered curtains that allows for direct detection of condensin motor activity in the absence of condensation (top panel). The middle and bottom panels show a schematic of an assay to mimic *cis* DNA loop extrusion by providing a second λ-DNA substrate in *trans*. **C.** Examples of kymographs showing translocation of a second l-DNA substrate (stained with YoYo1) provided in *trans* in the presence of unlabeled condensin. The presence of the *trans* DNA substrate is revealed as regions of locally high YoYo1 signal intensity, as highlighted by arrowheads. The regions of higher signal intensity are not detected when the trans DNA is omitted from the reaction. **D.** Velocity distribution histogram and **E.** survival probability plot for condensin bound to the trans DNA substrate. The dashed line in (E) highlights the translocation distance corresponding to dissociation of one half of the bound condesin complexes. Error bars represent standard deviations calculated by boot strap analysis. Cartoons of generalized models for condensin motor activity through a **F.** "scrunching" or **G.** "walking" mechanisms, both of which can be based upon ATP hydrolysis-dependent changes in the geometry of the SMC coiled-coil domains. Models are discussed in the text.

the structural transitions that take place during the ATP hydrolysis cycle and establishing a better understanding of whether and if so, how different domains in the condensin complex engage DNA.

Recent Hi-C studies have revealed that condensin-dependent DNA juxtaposition occurs at an apparent rate of ~900bp/s in *B. subtilis* [19]. This rate is ~15-times faster than the rates we observed for single *S. cerevisiae* condensin complexes. However, the apparent rate of *in vivo* DNA juxtaposition may reflect the cumulative action of multiple condensin complexes acting in concert. Assuming there are ~30 condensins per replication origin, and that mechanism of DNA juxtaposition allows for a linear relationship between the number of condensin complexes present and the rate of DNA juxtaposition, then each *B. subtilis* condensin might be expected to translocate DNA at a rate of ~30 bp/s. But, these comparisons should be made with extreme caution, as it is currently quite unclear if the biophysical properties of the molecular machinery of the prokaryotic system are similar to the eukaryotic counterpart, and recent single molecule analysis of the *B. subtilis* SMC complex on flow-stretched DNA did not report evidence for DNA translocation [39].

The finding that *S. cerevisiae* condensin is a mechanochemical motor capable of translocating along DNA has important implications for understanding fundamental mechanisms of chromosome organization across all domains of life. We propose that the ATP hydrolysis-dependent motor activity of condensin may be intimately linked to its role in promoting chromosome condensation, suggesting that condensin, and perhaps other SMC proteins, may provide the driving forces necessary to support 3D chromosome organization and compaction through a loop extrusion mechanism. Our findings raise the question of whether other types of SMC complexes also exhibit intrinsic motor activity, and what molecular or regulatory features distinguish SMC motor proteins from those SMC complexes that seemingly lack motor activity.

4.1. Supplementary Information

Materials and Methods

Condensin holocomplex overexpression and purification

The five subunits of the condensin complex were co-overexpressed in *Saccharomyces cerevisiae* from galactose-inducible promoters on 2μ high-copy plasmids (URA3 leu2-d pGAL7-SMC4(wild-type or Q302L)-StrepII3 pGAL10-SMC2(wild-type or Q147L) pGAL1-BRN1-HA3-His12 and TRP1 leu2-d pGAL10-YCS4 pGAL1-YCG1; yeast strains C4491 and C4724) as described [40], with the following modifications. Cultures were grown at 30°C in -URA-TRP dropout media containing 2% raffinose to OD600 of 1. Expression was induced with 2% galactose for 8 hours. Since expression of the Q-loop mutant complex affected the growth rate of the cultures, cells were initially grown at 30°C URA TRP dropout media containing glucose to OD600 of 1, transferred to media containing 2% raffinose for one hour and then induced by addition of galactose to 2%.

Cells were harvested by centrifugation, re-suspended in buffer A (50 mM TRIS-HCl pH 7.5, 200 mM NaCl, 5% (v/v) glycerol, 5 mM β-mercaptoethanol, and 20 mM imidazole) containing 1x cOmplete EDTA-free protease-inhibitor mix (Roche) and lysed in a FreezerMill (Spex). The lysate was cleared by two rounds of 20 min centrifugation at 45,000 xg at 4°C and loaded onto a 5 ml HisTrap column (GE Healthcare) pre-equilibrated with buffer A. The resin was washed with five column volumes buffer A containing 500 mM NaCl; buffer A containing 1 mM ATP, 10 mM KCl and 1 mM $MgCl_2$; and then buffer A containing 40 mM imidazole to remove non- specifically bound proteins. Protein was eluted in buffer A containing 200 mM imidazole and transferred to buffer B (50 mM TRIS-HCl pH 7.5, 200 mM NaCl, 5% (v/v) glycerol, 1 mM DTT) using a desalting column. After addition of EDTA to 1 mM, PMSF to 0.2 mM and Tween20 to 0.01%, the protein was incubated overnight with 2 ml (bed volume) of pre-equilibrated Strep-Tactin high-capacity Superflow resin (IBA).

The Strep-Tactin resin was packed into a column and washed with 15 resin volumes buffer B by gravity flow. Protein was eluted with buffer B containing 5 mM desthiobiotin. The eluate was concentrated by ultrafiltration and loaded onto a Superose 6 size exclusion chromatography column (GE Healthcare) pre-equilibrated in buffer B containing 1 mM $MgCl_2$. Peak fractions were pooled and concentrated to 4 μM by ultrafiltration. Purified proteins were analyzed by SDS PAGE (NuPAGE 4-12% Bis-Tris protein gels, ThermoFisher Scientific) and protein bands were identified by in-gel digestion and mass spectrometric analysis.

Nick ligation assays

Nick ligation assays were performed as described earlier [41] with the following modifications. A 6.4-kb plasmid containing a single BbvCI nicking site was used as a substrate and relaxed by incubation with Nb.BbvCI (NEB). The nicking enzyme was heat- inactivated once the reaction was complete (as confirmed by agarose gel electrophoresis). For assessing supercoiling, reactions were set up in a volume of 20 μl containing 1 nM nicked plasmid DNA and varying amounts of condensin (7.8-500 nM) in 50 mM TRIS-HCl pH 7.5, 100mM NaCl, 2.5% (v/v) glycerol, 10 mM MgCl2, 1 mM ATP, and 10 mM DTT. Reactions were incubated at room temperature for 30 min before addition of 0.2 μl T4 ligase

(5 Weiss U/μl, ThermoFisher Scientific) and fresh 1 mM ATP, followed by an additional 30 min incubation at room temperature to allow the ligation reaction to complete. Reactions were quenched by the addition of 60 μl stop buffer (50 mM TRIS-HCl pH 7.5, 10 mM EDTA, 1% SDS, 100 μg/ml proteinase K) and incubation at 37°C for 30 min. DNA was purified by phenol-chloroform extraction and ethanol precipitation. The DNA pellet was re-suspended in TE buffer and topoisomers were resolved at 4 V/cm for 9 h on a 0.7% TAE agarose gel containing 0.2 μg/ml chloroquine. The gel running buffer was also supplemented with chloroquine at the same concentration. Gels were stained with ethidium bromide and scanned on a Typhoon (GE Healthcare).

Pt/C rotary shadowing electron microscopy

Samples for platinum/carbon (Pt/C) shadowing were prepared following the glycerol spray method [42]. Condensin samples were diluted to a concentration of 0.05 μM in freshly prepared 200 mM NH_4HCO_3 pH 7.5, 30% (v/v) glycerol and 1 mM DTT, immediately sprayed onto freshly cleaved mica and dried under vacuum. Pt/C was shadowed at an angle of 7° followed by deposition of a stabilizing layer of carbon. The Pt/C layers were then floated off and placed onto 100 mesh copper grids. The grids were dried and imaged on a Morgagni TEM (FEI).

Electrophoretic mobility assay

6-carboxyfluorescein (6-FAM) labelled 45 bp dsDNA was prepared by annealing two complementary HPLC-purified DNA oligonucleotides (IDT, 5'-6- FAM-CCA GCT CCA ATT CGC CCT ATA GTG AGT CGT ATT ACA ATT CAC TGG-3'; 5'- CCA GTG AAT TGT AAT ACG ACT CAC TAT AGG GCG AAT TGG AGC TGG-3') in annealing buffer (10 mM TRIS-HCl pH 7.5, 50 mM NaCl, 1 mM EDTA) at a concentration of 10 μM in a temperature gradient of 0.1°C/s from 95°C to 4°C. 10 μl reactions were prepared with 100 nM 6-FAM-dsDNA and protein concentrations ranging from 50 to 800 nM in reaction buffer (40 mM TRIS-HCl pH 7.5, 125 mM NaCl, 5 mM $MgCl_2$, 10% glycerol, and 1 mM DTT). After 10 min incubation at room temperature (~25°C), free DNA and DNA-protein complexes were resolved by electrophoresis for 10 h at 2 V/cm on 0.8% (w/v) TAE-agarose gels at 4°C. 6-FAM labelled DNA was detected on a Typhoon FLA 9500 scanner (GE Healthcare) with excitation at 473 nm and detection using a 510-nm long pass filter.

Native gel electrophoresis

Protein samples (100 nM) were incubated with 1x and 2x molar ratio of anti-HA Qdots for 10 min at room temperature and the loaded onto a composite agarose- acrylamide gel (0.5% agarose and 2% acrylamide) [43]. Electrophoresis was performed in TBE buffer at 30V for 10 h at 4°C. The gels were analyzed by silver staining.

ATP hydrolysis assays

ATPase reactions were set up in a volume of 5 μl containing 0.1 μM or 0.5 μM condensin and the indicated concentrations of DNA in 40 mM TRIS-HCl pH 7.5, 125 mM NaCl, 5 mM $MgCl_2$, 0.5 mg/ml BSA and 1 mM DTT. 6.4-kb plasmid DNA had been linearized by NheI restriction digest and purified by phenol-chloroform extraction and ethanol precipitation. Reactions were initiated by the addition of ATP at the indicated concentra-

tions (containing 6.7 nM[α-^{32}P]ATP) and incubated at room temperature. At consecutive time intervals, 1 μl of the reaction mix was spotted onto PEI cellulose F TLC plates (Merck). TLC plates were developed in 0.5 M LiCl, and 1 M formic acid, exposed to imaging plates and analyzed on a Typhoon FLA 9500 scanner (GE Healthcare). ATP hydrolysis rates were calculated from the change of ATP/ADP ratios between time points in the linear range of the reaction. Non-linear regression analysis (GraphPad Prism 7.0) was used to estimate the Michaelis-Menten parameters.

Single molecule assays

Double-tethered DNA curtains were prepared as described previously [26, 27]. Unless otherwise stated, all single molecule measurements were performed in condensin buffer (40 mM TRIS-HCl pH 7.5, 125 mM NaCl, 10 mM $MgCl_2$, 1 mM DTT, 0.5 mg/mL BSA, and 4 mM ATP) and all assays were conducted at room temperature (~25°C). Quantum dots were labeled with anti-HA antibodies as per the manufacturer's instructions using a SiteClickTM Qdot 705 Antibody Labeling Kit (ThermoFisher, Cat No. S10454). Purified condensin (1 μl of 1 μM stock) was labeled by mixing with 2 μl anti-HA quantum dots (1 μM) in 7 μl of condensin buffer and incubated on ice for 10 minutes. The labeling reactions were diluted to 100 μl with condensin buffer and then injected into the sample chambers at a flow rate 0.1 ml/min. Flow was then terminated, and the samples were incubated for an additional 20 minutes. Samples were visualized with a custom modified inverted Nikon microscope equipped with a Nikon 60x CFI Plan Apo VC water immersion objective, as described [26, 27]. Image acquisition was initiated immediately before injecting condensin and continued throughout the 20-minute incubation. All images were acquired with an iXon EMCCD camera (Andor) at a 1 Hz frame acquisition rate. In the absence of nucleotide co-factor, condensin adhered non-specifically to the surfaces of the sample chambers, so all single molecule measurements contained either ATP or ATPγS, as specified. Note that although we observed single quantum dot tagged condensin complexes in the double-tethered DNA curtain assays, we do not yet know to oligomeric state(s) of these complexes. Future work will be necessary to determine whether the observed complexes represent single condensin molecules, or condensin oligomers.

Particle tracking

The positions *(z(t))* of each condensin complex were tracked using an in-house Python script. In this script, the intensity profile along DNA was fit with a one- dimensional Gaussian function, taking the mean of the Gaussian fits as the position *(z(t))* in sub-pixel resolution [44]. The total length of the l-DNA substrate used in these experiments is 48,502 base pairs, or 16.49 μm. The DNA is extended to a mean length of ~12 μm in the double- tethered DNA curtains, corresponding to ~72% mean extension, and spans a distance of 48 pixels at 60x magnification. Were indicated, the measured length pixels was converted to base pairs by assuming that each pixel contains 1,010 base pairs of DNA, corresponding to a conversion factor of 4.04 base pairs per nanometer. All particle tracking data are measured in nanometers, and then converted to base pairs for comparison, and both sets of distances are reported. The mean square displacement (MSD) of each trajectory was calculated as $MSD\ (\Delta t) = (z(t + t\Delta t) - z(t))$.

Translocation of each condensin complex showed a characteristic linear relationship between time and position (Fig. 4.3A). Thus, data points were fitted with a linear function to calculate slope, which corresponds to the translocation velocity. The resulting translocation velocity data were plotted as histograms, as shown in Fig. 4.3E and Fig. 4.4D, which were well described by log-normal distributions. The functional form of the fits is:

$$f(x) = \frac{A*exp[-\frac{1}{2}(\frac{ln(x)-\mu}{\sigma})^2]}{\sqrt{2\pi}\sigma x}$$

where A is amplitude, $e^{\mu+\frac{\sigma^2}{2}}$ is mean, and $e^{2\mu+\sigma^2}(e^{\sigma^2}-1)$ is variance. Also, we calculated the reduced chi square values represented by:

$$\chi^2 = \frac{1}{v}\sum_i \frac{n_i - n^2_{expected,i}}{n_i}$$

where n_i is the number of data in the i-th bin form the experiments, $n_{expected,i}$ is that from the fitting function. v is represented by:

$$v = n_{all} - p - 1$$

where n_{all} is the number of all the observations, and p is the number of parameters in the fitting function (p=3 in the current work). The goodness of fit for the log-normal distributions was determined by calculating χ^2 values, which were 0.09 and 0.20 for Fig. 4.3E and Fig. 4.4D, respectively.

The translocation start (t_s) and end (t_e) times were manually obtained by visual inspection of the data, where the starting time was taken after the brief ~13 s pausing time at the start of the linear trace. A small fraction (6%) of the condensin trajectories displayed a sudden change in direction, and in these instances the translocation end time (t_e) was specified as the time when the molecules changed direction. The distance of translocation was defined as $|z(t_e\text{-}z(t_s)|$, and these values were used to calculate the survival probability plot (i.e. processivity) presented in Fig. 4.3F. The reported processivity values reflect the translocation distance at which one half of the condensin complexes dissociate from the DNA based upon the survival probability plots.

Single molecule trans loop assays

Assays were conducted using double-tethered DNA curtains, as described above. A 100 μL reaction mix was prepared in condensin buffer containing 1 nM condensin, 18 pM free l-DNA (untagged), and 20 nM YoYo1 (ThermoFisher, Cat. No. Y3601). This reaction mix was then injected at a flow rate of 0.1 ml min^{-}1 into a sample chamber that already contained double-tethered λ-DNA molecules. Note that the tethered λ-DNA was labeled at one end with biotin and at the other end with digoxigenin, as previously described [26, 27], whereas the free λ-DNA was not labeled. Buffer flow was then terminated, and the reactions were incubated for an additional 20 minutes at room temperature while capturing 100-millisecond images at 0.2 Hz frame acquisition rate. The laser was shuttered between each 100- millisecond exposure to minimize YoYo1-induced

photo-damage. The resulting data were analyzed by particle tracking as describe above.

Supplementary figures

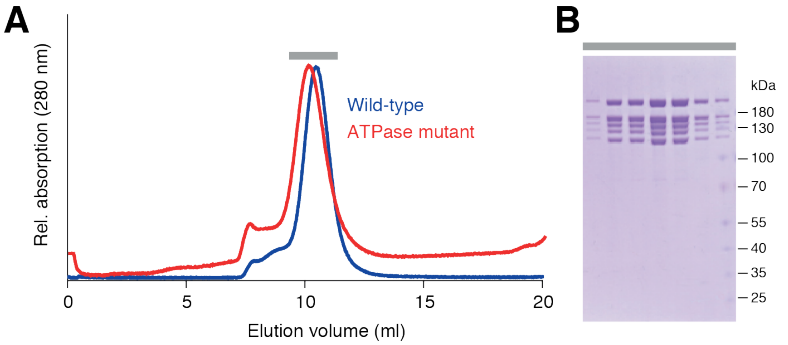

Figure S4.1: **Purification of budding yeast condensin holocomplexes. A.** Size exclusion chromatograms of wild-type and ATPase-deficient Smc2(Q147L)-Smc4(Q302L) condensin complexes. **B.** Analysis of peak fractions (grey bar) of the wild-type condensin purification by SDS PAGE and Coomassie staining.

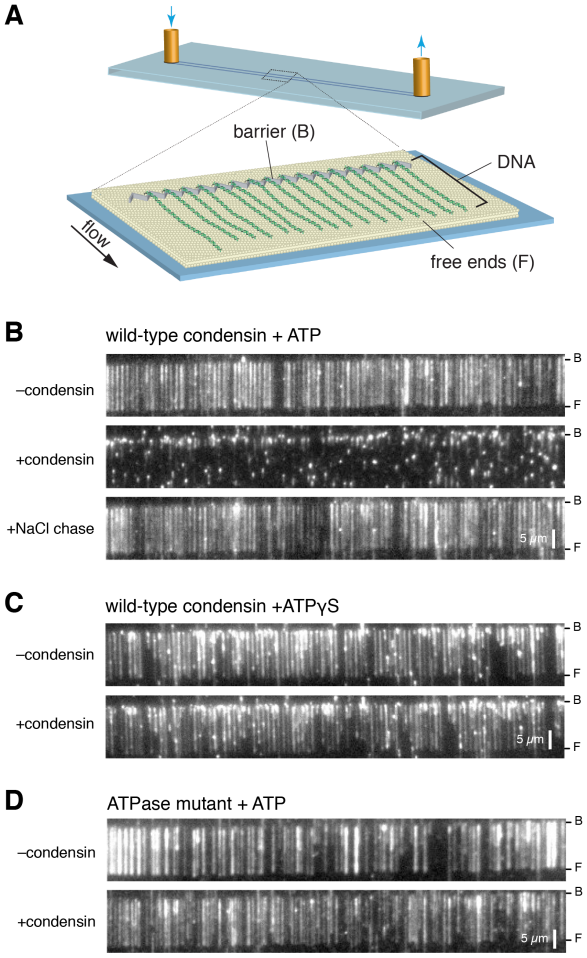

Figure S4.2: **Condensin can reversibly compact single-tethered DNA curtains. A.** Schematic of the single-tethered DNA curtain assay used to test for DNA compaction by unlabeled condensin. **B.** Still images showing the YoYo1-stained DNA before addition of wild-type condensin, after a 20-minute incubation with 10 nM condensin and 4 mM ATP, and still images after chasing the reactions with 500 mM NaCl. Note that the integrated signal intensity of the extended and compacted DNA molecules should not be compared to one another due to the change in the location of the DNA with respect to the penetration depth of the evanescent field. **C.** Still images showing the YoYo1-stained DNA before addition of wild-type condensin, after a 20-minute incubation with 10 nM condensin (in the absence of buffer flow) and 4 mM ATPγS. **D.** Still images showing the YoYo1-stained DNA before addition of ATPase deficient condensin, after a 20-minute incubation (in the absence of buffer flow) with 10 nM ATPase deficient condensin mutant and 4 mM ATPγS.

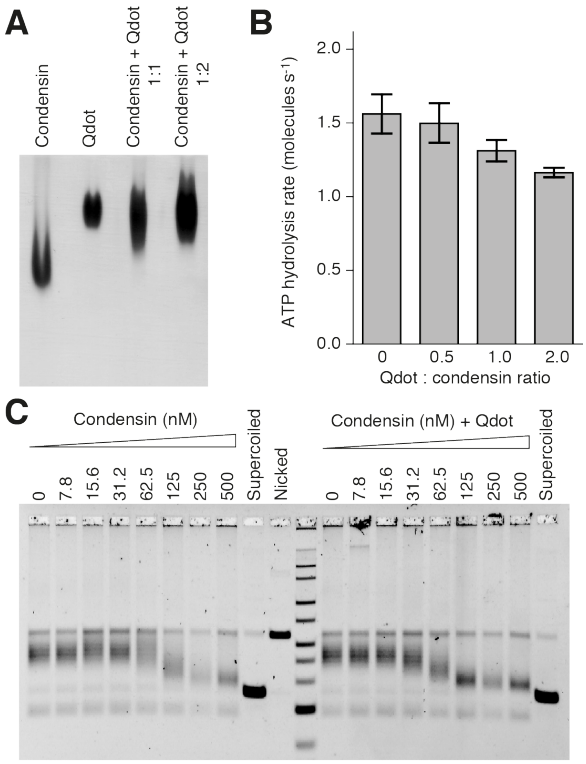

Figure S4.3: **Condensin labeling with quantum dots.** **A.** Native composite agarose-acrylamide gel electrophoresis of wild-type condensin complexes upon addition of Qdots coupled to antibodies directed against the HA3 epitope tag at the C terminus of the Brn1 kleisin condensin subunit. **B.** Effect of increasing ratios of anti-HA Qdot on the ATPase hydrolysis rate by wild-type condensin complexes (0.1 μM) in the presence of 6.4-kb linear DNA (240 nM) at saturated ATP concentrations (5 mM). **C.** Nick ligation assay of a 6.4-kb circular DNA (1 nM) with wild-type condensin complexes alone and in the presence of an equimolar amount of anti-HA Qdot.

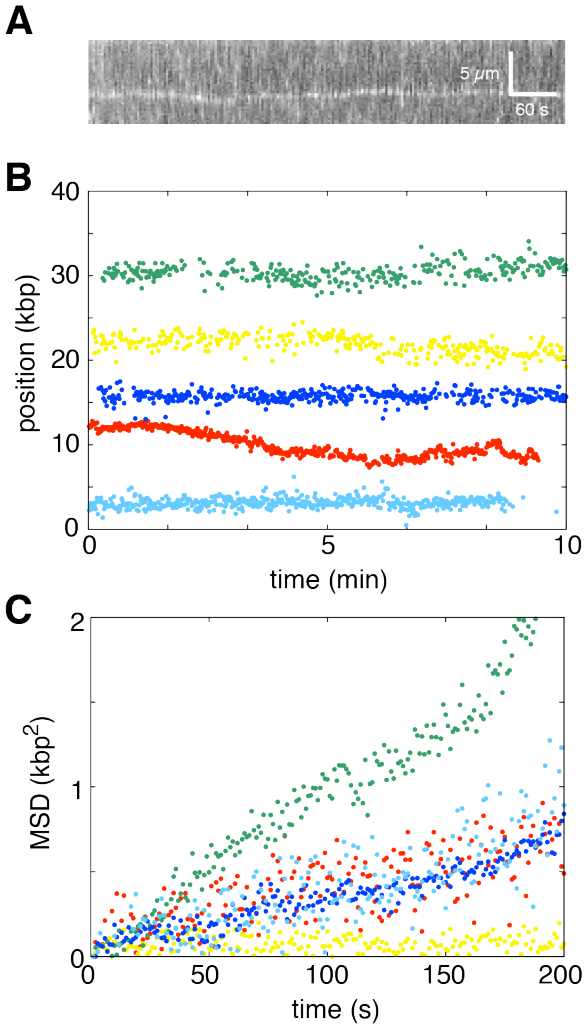

Figure S4.4: **Condensin exhibits no motor activity in reactions with ATPγS. A** Kymograph showing condensin bound to DNA in the presence of 4 mM ATPγS. **B.** Examples of particle tracking data, and **C.** MSD plots for data collected with wild-type condensin in reactions with 4 mM ATPγS.

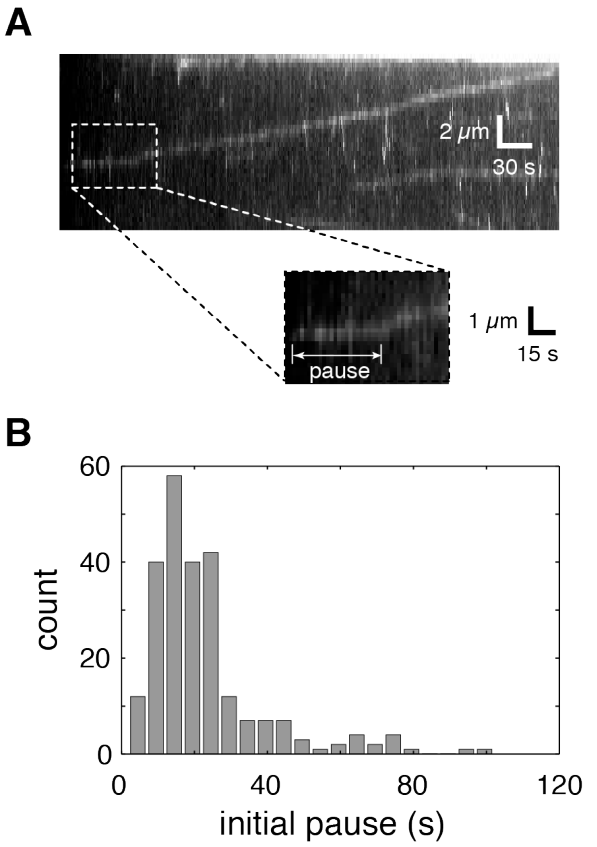

Figure S4.5: **Condensin pauses prior to initiating translocation. A.** Kymograph highlighting the initial pause τ_{pause} prior to the initiation of translocation (also see Fig. 2C).**B.** Histogram showing the distribution of initial pause times prior to initiating translocation for reactions containing 4 mM ATP.

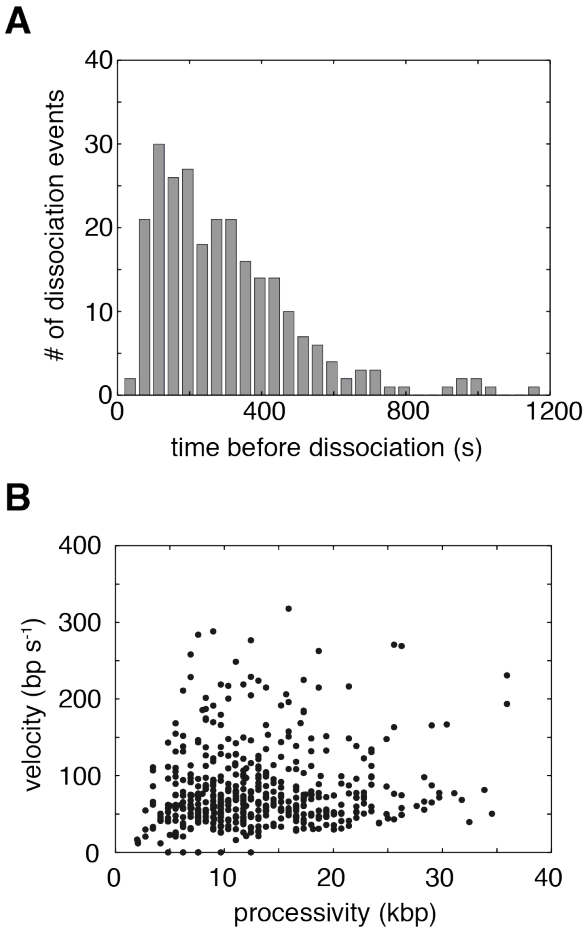

Figure S4.6: **Condensin's DNA-binding properties. A.** Distribution of binding lifetimes for translocating condensin complexes. **B.** Scatter plot showing that there is no apparent correlation between condensin translocation velocity and processivity. All data shown in this figure reflect results from experiments conducted in the presence of 4 mM ATP.

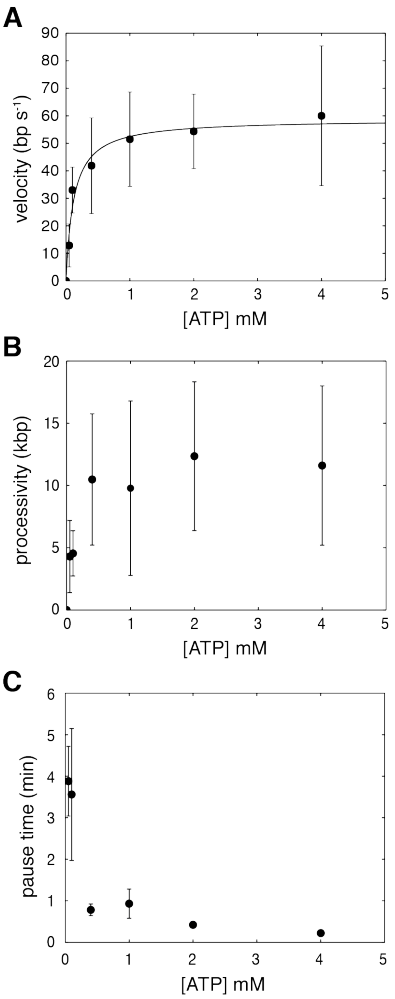

Figure S4.7: **ATP concentration dependence of condensin translocation characteristics. A.** Condensin translocation velocity versus ATP concentration for data collected at room temperature (~25ř **C.** The data are fit to the Michaelis-Menten equation to extract the kinetic parameters K_M and v_{max} **B.** Condensin processivity at different ATP concentrations, as indicated. **C.** Initial condensin pause times τ_{pause} prior to initiating translocation at different ATP concentrations. For each graph, error bars represent standard deviations calculated by boot strap analysis.

References

[1] T. Hirano, *Condensin-Based Chromosome Organization from Bacteria to Vertebrates,* Cell **164**, 847 (2016).

[2] F. Uhlmann, *SMC complexes: from DNA to chromosomes,* Nature Reviews Molecular Cell Biology **17**, 399 (2016).

[3] D. K. C. E. Huang, M. Milutinovich, *Rings, bracelet or snaps: fashionable alternatives for Smc complexes,* Philosophical transactions of the Royal Society of London. Series B, Biological sciences **360**, 537 (2005).

[4] K. Nasmyth and C. H. Haering, *Cohesin: its roles and mechanisms.* Annual review of genetics **43**, 525 (2009).

[5] C. H. Haering and S. Gruber, *SnapShot: SMC Protein Complexes Part I,* Cell **164**, 326 (2016).

[6] G. Hauk and J. M. Berger, *The role of ATP-dependent machines in regulating genome topology,* Current Opinion in Structural Biology **36**, 85 (2016).

[7] V. Guacci, A. Yamamoto, A. Strunnikov, J. Kingsbury, E. Hogan, P. Meluh, and D. Koshland, *Structure and function of chromosomes in mitosis of budding yeast.* Cold Spring Harbor symposia on quantitative biology **58**, 677 (1993).

[8] T. Hirano, T. J. Mitchison, and J. R. Swedlow, *The SMC family: from chromosome condensation to dosage compensation,* Current Opinion in Cell Biology **7**, 329 (1995).

[9] C. L. Peterson, M. Sheetz, T. Chi, B. Fletcher, H. Herschman, M. Yanagida, and M. Yanagida, *The SMC family: novel motor proteins for chromosome condensation?* Cell **79**, 389 (1994).

[10] H. Niki, R. Imamura, M. Kitaoka, K. Yamanaka, T. Ogura, and S. Hiraga, *E.coli MukB protein involved in chromosome partition forms a homodimer with a rod-and-hinge structure having DNA binding and ATP/GTP binding activities.* The EMBO journal **11**, 5101 (1992).

[11] J. Dekker and L. Mirny, *The 3D Genome as Moderator of Chromosomal Communication,* Cell **164**, 1110 (2016).

[12] K. Nasmyth, *Disseminating the Genome: Joining, Resolving, and Separating Sister Chromatids During Mitosis and Meiosis,* Annual Review of Genetics **35**, 673 (2001).

[13] *Dna methylation and gene regulation - dna methylation and late replication probably aid cell memory, and type i dna reeling could aid chromosome folding and enhancer function,* Philosophical Transactions of the Royal Society of London B: Biological Sciences **326**, 285 (1990), http://rstb.royalsocietypublishing.org/content/326/1235/285.full.pdf .

[14] E. Alipour and J. F. Marko, *Self-organization of domain structures by DNA-loop-extruding enzymes,* Nucleic Acids Research **40**, 11202 (2012).

[15] A. Goloborodko, M. V. Imakaev, J. F. Marko, and L. Mirny, *Compaction and segregation of sister chromatids via active loop extrusion,* eLife **5** (2016), 10.7554/eLife.14864.

[16] A. Goloborodko, J. F. Marko, and L. A. Mirny, *Chromosome Compaction by Active Loop Extrusion,* Biophysical Journal **110**, 2162 (2016).

[17] G. Fudenberg, M. Imakaev, C. Lu, A. Goloborodko, N. Abdennur, and L. A. Mirny Correspondence, *Formation of Chromosomal Domains by Loop Extrusion,* Cell Reports **15**, 2038 (2016).

[18] N. Naumova, M. Imakaev, G. Fudenberg, Y. Zhan, B. R. Lajoie, L. A. Mirny, and J. Dekker, *Organization of the Mitotic Chromosome,* Science **342** (2013).

[19] X. Wang, H. B. Brandão, T. B. K. Le, M. T. Laub, and D. Z. Rudner, *Bacillus subtilis SMC complexes juxtapose chromosome arms as they travel from origin to terminus,* Science **527**, 524 (2017).

[20] A. Badrinarayanan, R. Reyes-Lamothe, S. Uphoff, M. C. Leake, and D. J. Sherratt, *In Vivo Architecture and Action of Bacterial Structural Maintenance of Chromosome Proteins,* Science **338** (2012).

[21] A. Minnen, F. Bürmann, L. Wilhelm, A. Anchimiuk, M.-L. Diebold-Durand, and S. Gruber, *Control of Smc Coiled Coil Architecture by the ATPase Heads Facilitates Targeting to Chromosomal ParB/parS and Release onto Flanking DNA,* Cell Reports **14**, 2003 (2016).

[22] T. M. K. Cheng, S. Heeger, R. A. G. Chaleil, N. Matthews, A. Stewart, J. Wright, C. Lim, P. A. Bates, and F. Uhlmann, *A simple biophysical model emulates budding yeast chromosome condensation.* eLife **4**, e05565 (2015).

[23] I. Piazza, A. Rutkowska, A. Ori, M. Walczak, J. Metz, V. Pelechano, M. Beck, and C. H. Haering, *Association of condensin with chromosomes depends on DNA binding by its HEAT-repeat subunits.* Nature structural & molecular biology **21**, 560 (2014).

[24] D. E. Anderson, A. Losada, H. P. Erickson, and T. Hirano, *Condensin and cohesin display different arm conformations with characteristic hinge angles.* The Journal of cell biology **156**, 419 (2002).

[25] K. Kimura and T. Hirano, *Dual roles of the 11S regulatory subcomplex in condensin functions.* Proceedings of the National Academy of Sciences of the United States of America **97**, 11972 (2000).

[26] E. C. Greene, S. Wind, T. Fazio, J. Gorman, and M.-L. Visnapuu, *Chapter 14 – DNA Curtains for High-Throughput Single-Molecule Optical Imaging,* in *Methods in Enzymology*, Vol. 472 (2010) pp. 293–315.
[27] J. Stigler, G. Ö. Çamdere, D. E. Koshland, and E. C. Greene, *Single-Molecule Imaging Reveals a Collapsed Conformational State for DNA-Bound Cohesin,* Cell Reports **15**, 988 (2016).
[28] I. F. Davidson, D. Goetz, M. P. Zaczek, M. I. Molodtsov, P. J. Huis in 't Veld, F. Weissmann, G. Litos, D. A. Cisneros, M. Ocampo-Hafalla, R. Ladurner, F. Uhlmann, A. Vaziri, and J. Peters, *Rapid movement and transcriptional re-localization of human cohesin on DNA,* The EMBO Journal **35**, e201695402 (2016).
[29] H. Qian, M. Sheetz, and E. Elson, *Single particle tracking. Analysis of diffusion and flow in two-dimensional systems,* Biophysical Journal **60**, 910 (1991).
[30] T. R. Strick, T. Kawaguchi, and T. Hirano, *Real-time detection of single-molecule DNA compaction by condensin I.* Current biology : CB **14**, 874 (2004).
[31] J. M. Eeftens, S. Bisht, J. Kerssemakers, C. Haering, and C. Dekker, *Real-time detection of condensin-driven DNA compaction reveals a multistep binding mechanism,* bioRxiv (2017).
[32] A. M. Pyle, *Translocation and Unwinding Mechanisms of RNA and DNA Helicases,* Annual Review of Biophysics **37**, 317 (2008).
[33] M. R. Singleton, M. S. Dillingham, and D. B. Wigley, *Structure and Mechanism of Helicases and Nucleic Acid Translocases,* Annual Review of Biochemistry **76**, 23 (2007).
[34] W. Yang, *Lessons Learned from UvrD Helicase: Mechanism for Directional Movement,* Annual Review of Biophysics **39**, 367 (2010).
[35] R. Seidel, J. G. Bloom, C. Dekker, and M. D. Szczelkun, *Motor step size and ATP coupling efficiency of the dsDNA translocase EcoR124I,* The EMBO Journal **27**, 1388 (2008).
[36] J. M. Eeftens, A. J. Katan, M. Kschonsak, M. Hassler, L. de Wilde, E. M. Dief, C. H. Haering, and C. Dekker, *Condensin Smc2-Smc4 Dimers Are Flexible and Dynamic,* (2016).
[37] Y.-m. Soh, F. Bu, H.-c. Shin, T. Oda, K. S. Jin, C. P. Toseland, C. Kim, H. Lee, S. J. Kim, M.-s. Kong, Y.-g. Kim, H. M. Kim, N. K. Lee, M. Sato, B.-h. Oh, and S. Gruber, *Molecular Basis for SMC Rod Formation and Its Dissolution upon DNA Binding,* Molecular cell **3**, 1 (2015).
[38] F. Bürmann, A. Basfeld, R. Vazquez Nunez, M.-L. Diebold-Durand, L. Wilhelm, and S. Gruber, *Tuned SMC Arms Drive Chromosomal Loading of Prokaryotic Condensin,* Molecular Cell , 861 (2017).
[39] H. Kim and J. J. Loparo, *Multistep assembly of DNA condensation clusters by SMC,* Nature Communications **7**, 10200 (2016).
[40] J. St-Pierre, M. Douziech, F. Bazile, M. Pascariu, É. Bonneil, V. Sauvé, H. Ratsima, and D. D'Amours, *Polo Kinase Regulates Mitotic Chromosome Condensation by Hyperactivation of Condensin DNA Supercoiling Activity,* Molecular Cell **34**, 416 (2009).
[41] J. Stray, N. Crisona, and B. Belotserkovskii, *The Saccharomyces cerevisiae Smc2/4 condensin compacts DNA into (+) chiral structures without net supercoiling,* Journal of Biological (2005).
[42] J. M. Tyler and D. Branton, *Rotary shadowing of extended molecules dried from glycerol,* Journal of Ultrastructure Research **71**, 95 (1980).
[43] M.-H. Suh, P. Ye, A. B. Datta, M. Zhang, and J. Fu, *An agarose?acrylamide composite native gel system suitable for separating ultra-large protein complexes,* Analytical Biochemistry **343**, 166 (2005).
[44] A. Yildiz, J. N. Forkey, S. A. McKinney, T. Ha, Y. E. Goldman, and P. R. Selvin, *Myosin V Walks Hand-Over-Hand: Single Fluorophore Imaging with 1.5-nm Localization,* Science **300**, 2061 (2003).

5

Real-time detection of condensin-driven DNA compaction reveals a multistep binding mechanism

Condensin, a conserved member of the SMC protein family of ring-shaped multi- subunit protein complexes, is essential for structuring and compacting chromosomes. Despite its key role, its molecular mechanism has remained largely unknown. Here, we employ single-molecule magnetic tweezers to measure, in real-time, the compaction of individual DNA molecules by the budding yeast condensin complex. We show that compaction can proceed in large steps, driving DNA molecules into a fully condensed state against forces of up to 2pN. Compaction can be reversed by applying high forces or adding buffer of high ionic strength. While condensin can stably bind DNA in the absence of ATP, ATP hydrolysis by the SMC subunits is required for rendering the association salt-insensitive and for the subsequent compaction process. Our results indicate that the condensin reaction cycle involves two distinct steps, where condensin first binds DNA through electrostatic interactions before using ATP hydrolysis to encircle the DNA topologically within its ring structure, which initiates DNA compaction. The finding that both binding modes are essential for its DNA compaction activity has important implications for understanding the mechanism of chromosome compaction.

J.M. Eeftens, S. Bisht, J. Kerssemakers, M. Kschonsak, M. Kschonsak, C.H. Haering, C. Dekker, *submitted* (2017)

5.1. Introduction

The Structural Maintenance of Chromosome (SMC) complexes cohesin and condensin play central roles in many aspects of chromosome biology, including the successful segregation of mitotic chromosomes, chromatin compaction, and regulation of gene expression (reviewed in refs [1–3]). SMC protein complexes are characterized by their unique ring-like structure (Fig. 5.1a). The architecture of condensin is formed by a heterodimer of Smc2 and Smc4 subunits, which each fold back onto themselves to form ~45-nm long flexible coiled coils [4], with an ATPase "head" domain at one end and a globular "hinge" hetero-dimerization domain at the other end [5]. The role of ATP binding and hydrolysis by the head domains has remained largely unclear. The head domains of the Smc2 and Smc4 subunits are connected by a protein of the kleisin family, completing the ring-like structure (Fig. 5.1a). The condensin kleisin subunit furthermore recruits two additional subunits that consist mainly of HEAT-repeat motifs. Most metazoan cells express two condensin complexes, condensin I and II, which contain different non-SMC subunits and make distinct contributions to the formation of mitotic chromosomes [6]. The budding yeast *Saccharomyces cerevisiae*, however, has only a single condensin complex, which contains the kleisin subunit Brn1 and the HEAT-repeat subunits Ycg1 and Ycs4 (Fig. 5.1a).

How condensin complexes associate with chromosomes has remained incompletely understood. Biochemical experiments have provided evidence that condensin, similar to cohesin, embraces DNA topologically within the ring formed by the Smc2, Smc4 and kleisin subunits [7]. In addition, the HEAT-repeat subunits were found to contribute to condensin's loading onto chromosomes and the formation of properly structured chromosomes [8, 9]. In contrast, ATP hydrolysis by the Smc2-Smc4 ATPase heads does not seem to be absolutely required for the association of condensin with chromosomes *in vivo* [10] and condensin binds DNA in vitro even in the absence of ATP [11]. DNA, however, can stimulate ATP hydrolysis by the Smc2-Smc4 ATPase heads [8, 12]. These findings have led to the speculation that condensin might initially bind to the DNA double helix by a direct interaction with its HEAT-repeat and kleisin subunits and that this binding might subsequently trigger an ATP hydrolysis- dependent transport of DNA into the condensin ring [7]. Such a hypothesis has not yet been confirmed, however. The condensin-DNA interaction is presumably the key to the mechanism by which condensin drives DNA compaction, a subject of keen interest that is intensely debated (reviewed in refs [13, 14]). Models for the condensin-driven compaction of DNA include random crosslinking, condensin multimerization, and/or DNA loop extrusion[15–20]. The loop extrusion model has recently gained support, but a consensus has not yet been reached [21]. Finally, condensin has also been suggested to alter the supercoiled state of DNA to promote DNA compaction [12, 22–24].

One caveat of most biochemical experiments is that they can only probe the final geometry of the DNA, but cannot address the interaction of condensin molecules with DNA during the compaction cycle. To truly resolve the compaction mechanism, an understanding of the binding properties of individual condensin complexes to DNA will be essential. Single-molecule techniques are especially suitable for investigating the mechanical properties, structure, and molecular mechanism of SMC proteins. For example, single-molecule imaging methods proved to be crucial for revealing the sliding and

motor action of individual SMC complexes on DNA [25–28]. Likewise, magnetic tweezers experiments have been successfully used to describe the compaction of DNA by the Escherichia coli SMC protein MukB [29] and by condensin I complexes immunoprecipitated from mitotic *Xenopus laevis* egg extracts [11].

To obtain insights into the DNA compaction mechanism of condensin complexes, we here employ magnetic tweezers to study DNA compaction induced by the *S. cerevisiae* condensin holocomplex at the single-molecule level. Magnetic tweezers are exquisitely fit to study the end-to-end length and supercoiling state of DNA at the single-molecule level. We show real-time compaction of DNA molecules upon addition of condensin and ATP. The compaction rate depends on the applied force and the availability of protein and hydrolysable ATP. Through rigorous systematic testing of experimental conditions, we provide evidence that condensin makes a direct electrostatic interaction with DNA that is ATP-independent. We further show that ATP hydrolysis is then required to to render the association with DNA into a salt-resistant, most likely topological binding mode, where the DNA is fully encircled by the condensin ring. Our findings are inconsistent with a "pseudo-topological" binding mode, in which a DNA molecule is sharply bent and pushed through the condensin ring without the need to open the SMC-kleisin ring. Our results show that condensin uses its two DNA-binding modes to successfully compact the DNA, thus setting clear boundary conditions that must be considered in any DNA organization model. We present a critical discussion of the implications of our results on the various models for the mechanics of condensin-mediated DNA compaction and conclude that our findings are compatible with a loop-extrusion model.

5.2. Results

Condensin compacts DNA molecules against low physical forces

To measure the real-time compaction of individual linear DNA molecules by the *S. cerevisiae* condensin holocomplex in a magnetic tweezers set-up, we tethered individual DNA molecules between a magnetic bead and a glass surface in a buffer condition that reflects physiological salt concentrations (Fig. 5.1b). We then used a pair of magnets to apply force and thereby stretch the tethered DNA molecules. We routinely performed a pre-measurement to determine the end-to-end length of the bare DNA at the force applied (Fig. 5.1c, left of the black vertical line at time point zero). We then simultaneously added condensin (8.6nM) and ATP (1mM) to the flow cell (time point zero, Fig. 5.1c). Following a short lag time, the end-to-end length of the DNA started to decrease until, in the vast majority of cases, the bead had moved all the way to the surface. We thus observe condensin-driven DNA compaction in real-time at the single-molecule level.

As different DNA tethers in the same experiment typically displayed a sizeable variation between individual compaction traces (Fig. 5.1d), we quantitatively characterized the compaction traces using two clearly defined parameters. First, we measured the lag time, i.e. the time it took for compaction to initiate after adding condensin at time zero (Fig. 5.1c). Second, starting from the decrease in the end-to-end length of the DNA, we measured the compaction rate in nanometers per second (Fig.5.1c). To avoid a bias at either end of the curve, we extracted the average compaction rate from the decrease between the 90% and 10% levels of the initial end-to-end length. Different DNA teth-

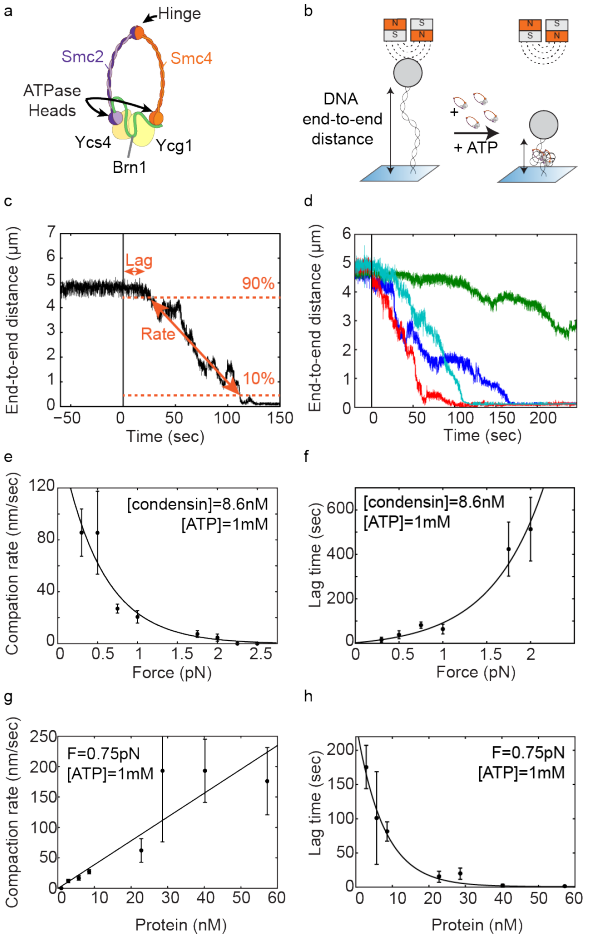

Figure 5.1: **Condensin compacts DNA in the presence of ATP. a.** Cartoon of the yeast condensin complex. Smc2 and Smc4 dimerize via their hinge domains. The kleisin Brn1 associates with the head domains to create a ring-like structure. HEAT-repeat subunits Ycs4 and Ycg1 bind to Brn1. **b.** Schematic representation of the compaction experiment. A DNA molecule is tethered between a glass slide and a magnetic bead. When condensin and ATP are added, the end-to-end length of the DNA decreases. **c.** Characterization of the compaction process with two parameters. The lag time is defined as the time it takes for the compaction to initiate. The compaction rate is set by the compaction speed between 90% and 10% of the original end-to-end length. **d.** Examples of compaction traces. Each color represents a different individual DNA tether measured in the same experiment. Condensin (8.6nM) and ATP (1mM) are added at time point zero. **e.** The average compaction rate decreases as force increases. At forces higher than 2pN, condensin does not compact DNA. At 2pN, 2 out of 9 tethers did not condense. At 1.75pN, 2 out of 8 tethers did not condense. Error bars represent SEM. For all these experiments, condensin concentration was 8.6nM and ATP concentration was 1mM ATP. An exponential curve (line) is added as a guide to the eye. **f.** The lag time increases as force increases. An exponential curve (line) is added as a guide to the eye. **g.** The average compaction rate increases linearly as protein concentration increases. Asterisk indicates that not all DNA tethers showed compaction at that protein concentration. At 2.86nM, 5 out of 15 tethers in the experiment did not compact. **h.** The lag time decreases as protein concentration increases. An exponential curve (line) is added as guide to the eye.

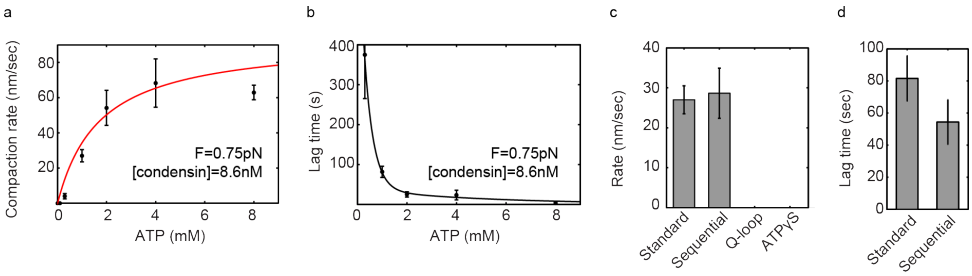

Figure 5.2: **Compaction depends on ATP hydrolysis. a.** Average compaction rate increases according to a Michaelis-Menten relation with ATP concentration. For this protein concentration, the rate saturates at ATP concentrations higher than 2mM. **b.** Lag time decreases as ATP concentration increases. Line is added as guide to the eye. **c.** Average compaction rate for the standard experiment (0.75pN, 8.6nM protein, 1mM ATP) and the sequential addition experiment (first 8.6nM protein/no ATP, wash with buffer, and only then add 1mM ATP). Rate is similar for standard and sequential addition. The ATPase mutant and wild-type in the presence of ATPγS do not show compaction. **d.** The lag time for the standard experiment and the sequential addition experiment. The lag time decreases for sequential addition.

ers in the same experiment typically displayed a sizeable variation between individual compaction traces (Fig. 5.1d).

While keeping protein and ATP concentrations constant, we first determined compaction rates at different applied forces. We found that condensin was able to compact DNA against applied forces of up to 2pN, albeit with rates that strongly decreased with increasing force (Fig. 5.1e). This is surprising, since many biological motor proteins can work against forces much higher than 2pN. On average, the rate was in the same range as measured for the *Xenopus* complex previously [11] and remained constant over the course of the experiment for each tether, only slowing down slightly towards the end (Supplementary Fig. S5.1). Concurrent with the decrease in compaction rate, lag times increased with increasing force (Fig. 5.1f). We conclude that compaction is slower and takes longer to initiate when condensin complexes are acting against a higher applied force.

The compaction rate increased approximately linearly with the concentration of the budding yeast condensin complex (Fig. 5.1g). Higher amounts of protein were able to condense DNA much faster, at rates of up to 200nm/sec. Similarly, the lag times decreased at higher protein concentrations (Fig. 5.1h). These findings suggest that, at higher concentrations, multiple condensin complexes might work in parallel on the same DNA molecule, resulting in faster compaction.

DNA compaction requires DNA binding and subsequent ATP hydrolysis by condensin

We found that the compaction rate increased with increasing ATP concentrations and saturated at concentrations above a few mM (Fig. 5.2a). A Michaelis-Menten fit to the data resulted in a maximum compaction rate v_{max} of 85 ± 28nm/s (95% confidence interval) and a K_M of 1.4 ± 1.5mM. Lag times were much longer at lower ATP concentrations (Fig. 5.2b).

We test whether *S. cerevisiae* condensin could, like the *Xenopus* condensin I com-

plex [23], bind DNA in the absence of ATP, we incubated condensin with DNA substrates for 20 minutes in the absence of ATP and, as expected, observed no DNA compaction during this time period (Supplementary Fig. S5.2a). We then washed the flow cell with buffer without ATP to remove all unbound condensin, before flowing in buffer containing 1mM ATP but no additional protein (hereafter called "sequential addition"). After ATP addition, we observed robust compaction (Supplementary Fig. S5.2a, N=11) with a rate that was similar to the rate measured when adding protein and ATP simultaneously (Fig. 5.2c). These experiments indicate that condensin binds in the absence of ATP, remains attached during washing steps, and can start DNA compaction when ATP is subsequently added [11]. Interestingly, the lag time was shorter for the sequential addition, although the difference is not statistically different (Fig. 5.2d). A shorter lag time could suggest that part of the delay that we had observed after protein addition in the standard reaction setup is due to the time it takes for condensin to bind to the DNA.

To verify that the compaction that we observed was due to the interaction of the condensin complex with DNA in a manner that reflects the physiological properties of condensin function *in vivo*, we tested a tetrameric condensin complex that lacked the Ycg1 HEAT-repeat subunit. Together with the kleisin subunit Brn1, Ycg1 creates a DNA binding groove in the condensin complex that is essential for the loading of condensin onto chromosomes [8, 30]. Indeed, this tetrameric version of condensin showed no DNA compaction activity whatsoever (Fig S5.3A). To specifically test the requirement for the Ycg1?Brn1 DNA-binding groove, we repeated the experiment with a version of the condensin holocomplex that contains charge-reversal mutations in the DNA-binding groove [30]. Consistent with the result for the tetrameric complex, this complex was also unable to induce DNA compaction in our assay (Fig S5.3B).

To further test whether compaction is due to ATP binding and hydrolysis by the Smc2 and Smc4 subunits of the condensin complex, we purified a version of the condensin complex with point mutations in the Q-loop motifs of the Smc2 and Smc4 ATPase sites (Smc2Q147L-Smc4Q302L). As expected, the mutant complex was unable to induce DNA compaction in our assay (Fig 2C and S5.3C). We then replaced ATP by the only slowly hydrolyzable analog ATPγS to distinguish whether the reaction depends on ATP hydrolysis or merely on ATP binding to condensin. Also in this experiment, we observed no DNA compaction (Fig 2C and S5.3D), which demonstrates that compaction requires ATP hydrolysis. Finally, we tested whether ATP hydrolysis is required only to initiate compaction or continuously during the active compaction process by exchanging ATP by ATPγS once the DNA had been compacted half-way. In this experiment, compaction did not proceed any further (Fig S5.3E). We conclude that both, ATP binding and ATP hydrolysis, are essential for the DNA compaction activity that we observe.

Condensin remains bound to DNA after force-induced de-compaction

We next tested whether the condensin-DNA interaction could be disrupted by applying a high force once the compaction reaction had taken place. First, we quantified the end-to-end extension of the bare DNA at 10pN and 0.75pN forces (Fig. 5.3a). After adding condensin and ATP we observed compaction, as before (Fig. 5.3b). As soon as the DNA molecule had been compacted to about half of its original length, we abruptly increased the force to 10pN (Fig. 5.3c). Upon this sudden force increase, the end-to-end length

did not immediately recover to the fully extended level, in contrast to the response of a bare DNA molecule. Instead, it took a few seconds (here 5sec) until the DNA had extended all the way to the end-to-end length we had measured for the bare DNA at 10pN (Fig. 5.3a). When we subsequently lowered the force to 0.75pN, the DNA started to compact again from the same level it had started at the beginning of the experiment (Fig. 5.3d). We conclude that condensin-dependent DNA compaction can be fully reversed by stretching the DNA with high forces, consistent with a previous report for the *Xenopus* condensin I complex [11]. This, however, does not hinder subsequent compaction at low force.

In the same experiment, we repeated the 10pN pulling step, and this time it took even longer (~25 sec) until the DNA recovered the full end-to-end length (Fig. 5.3e). While keeping the force at 10pN, we then washed the flow cell with buffer without ATP or protein to remove all nucleotide and unbound condensin. When we then lowered the force to 0.75pN, the DNA did not compact (Fig. 5.3f). Strikingly, however, as soon as we added ATP (but no additional protein), we again observed compaction (Fig. 5.3g). This result demonstrates that, first, condensin can stay bound to DNA even when stretching the DNA at high forces and washing with physiological buffers and, second, that condensin that had remained bound to DNA requires ATP to initiate a new round of DNA compaction. We confirmed the findings such as those outlined in Figure 5.3a-g in many independent experiments (N=28).

Condensin uses two distinct modes to bind DNA

Condensin might mediate DNA compaction through direct electrostatic interactions with the DNA helix, through topologically encircling DNA within its ring structure, through pseudo-topologically entrapping DNA by inserting a DNA loop into its ring, or through a combination of these modes (see Discussion). Whereas electrostatic interactions are sensitive to high salt concentrations, bulk biochemistry experiments have shown that condensin's topological interaction is resistant to salt concentrations of 500-1000mM NaCl [7]. We therefore assayed whether compaction remained stable after washing with buffer containing 500mM NaCl after compaction had been achieved by condensin and ATP. We found that DNA compaction was fully reversed by the high salt conditions (Fig. 5.3h, t=450sec, N=7). This indicates that electrostatic interactions with DNA are required for maintaining the condensin- mediated compaction state of DNA. Strikingly, when we subsequently lowered salt concentrations to physiological levels (125mM NaCl) in the presence of ATP (but without adding more protein), we again observed compaction (Fig. 5.3i, t=1050sec). This demonstrates that condensin, once it had been loaded onto DNA by use of ATP, remained associated with the DNA during the high salt wash and was capable of again compacting DNA in an ATP-dependent reaction once salt concentrations had been lowered.

We next tested whether ATP was required to allow condensin to bind DNA in a salt-resistant manner. We first incubated condensin with DNA in physiological buffer conditions without ATP (as in the sequential addition experiment). As expected, we observed no compaction in the absence of nucleotide (Fig. 5.3j, t=0-1300sec). We then washed with high salt buffer (500mM NaCl) before lowering salt concentrations again to 125mM and adding ATP (Fig. 5.3k). In contrast to the previous experiment where condensin had

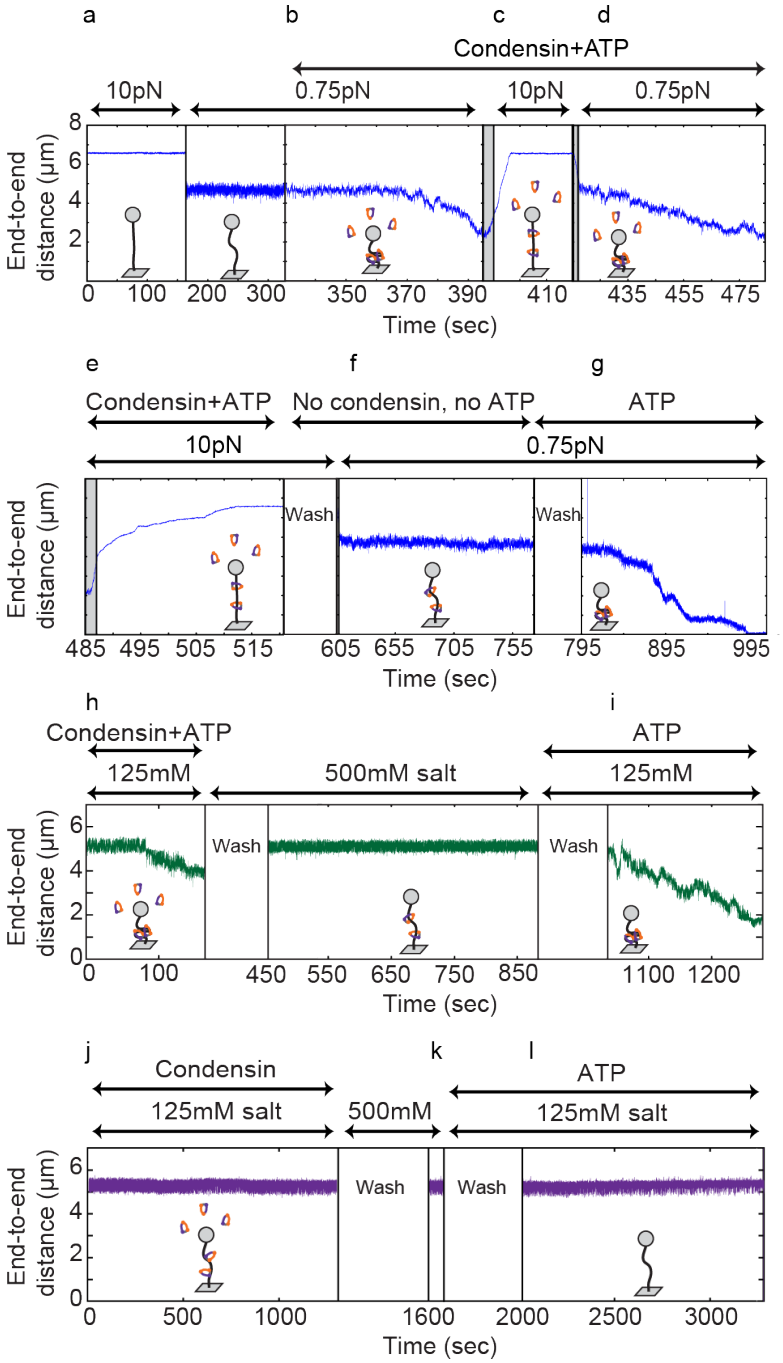
a
b
c
d
Condensin+ATP
10pN
0.75pN
10pN
0.75pN
End-to-end distance (μm)
Time (sec)
e
f
g
Condensin+ATP
No condensin, no ATP
ATP
10pN
0.75pN
Wash
Wash
h
i
Condensin+ATP
ATP
125mM
500mM salt
125mM
Wash
Wash
j
k
l
Condensin
ATP
125mM salt
500mM
125mM salt
Wash
Wash

Figure 5.3: **De-compaction by switching to high force or high salt. a.** Pre-measurements of the DNA tether length before addition of condensin. The average end-to-length was recorded at 10pN (left) and 0.75pN (right). This trace is an example taken from N=28 independent experiments. Although different tethers showed different rates of compaction and de-compaction, the qualitative result was identical for all. **b.** With the force at 0.75pN, condensin (8.6nM) and ATP (1mM) were added and the DNA was compacted. **c.** After about 50% compaction, the force was suddenly increased to 10pN. The grey area indicates where the time that the magnet was moving and the black vertical line indicates the point the magnet arrived at the 10pN position. DNA end-to-end length increased, reversing compaction and eventually recovering the full end-to-end length. d) The force was subsequently lowered to 0.75pN again. Condensin and ATP were still present and the DNA condensed again. **e.** The force was increased to 10pN again. The DNA end-to-end length again increased and eventually recovered to the premeasured full length of bare DNA at 10 pN. Next, the flow cell was washed with buffer without any ATP or protein. **f.** The force was then lowered to 0.75pN, and the DNA was observed to not compact in the absence of ATP. Next, the flow cell was washed with buffer with 1mM ATP but no protein. **g.** After thus adding ATP but no extra protein, the DNA was able to condense again, indicating that the protein remained bound after pulling and washing. **h.** The green trace shows a different experiment. At time=0s, 8.6nM condensin and 1mM ATP were added as normal. After compaction, the flow cell was washed with high salt (500mM), and the compacted structure was extended again. **i.** At time=900s, the flow cell was washed with physiological salt and 1mM ATP but no additional protein, and the DNA compacted again. **j.** The purple trace shows a different experiment. At time=0s, 8.6nM condensin but no ATP was added, and no compaction was observed. **k.** The flow cell was then washed with high salt (500mM), and no change in end-to- end length was detected. **l.** The flow cell was washed with physiological salt and 1mM ATP was added. No compaction was observed.

been allowed to bind DNA in the presence of ATP before the high salt wash (Fig. 5.3l, N=9). Similarly, when we incubated condensin with DNA in the presence of ATPγS instead of ATP, we did not observe compaction we did not observe any compaction once we lowered the salt conditions and added ATP (Fig. S5.3B, N=14). These experiments demonstrate that ATP hydrolysis is required to convert condensin from a salt-sensitive to a salt-resistant binding mode, which is indicative of topological binding.

We finally examined whether continued ATP hydrolysis was necessary to maintain DNA in the compacted form, since it had been reported that continuous ATP hydrolysis is necessary to maintain the structure of mitotic chromosomes [9]. When we interrupted ongoing DNA compaction by flushing with buffer without ATP, compaction did neither continue nor reverse. Instead, the DNA end-to-end length remained stable (Supplementary Fig. S5.3C, N=9). When we added ATP again, compaction proceeded. These data demonstrate that the presence of ATP is required to initiate and continue compaction, but is neither necessary for maintaining condensin's association with DNA nor essential for preserving already compacted DNA structures.

Condensin compacts DNA in a stepwise manner

Many compaction traces showed sudden distinct decreases in the DNA end-to-end length, which we will refer to as "steps". We used a very conservative user-bias-independent step-finding algorithm to extract the size of these compaction steps (see Methods and Appendix for details). In brief, this algorithm objectively evaluates if a trace displays steps without prior knowledge of step size or location, based on chi-squared minimization. Figure 5.4A shows a typical example of a DNA compaction trace with fitted steps. We used this hands-off algorithm to analyze all traces we had collected and to determine step sizes.

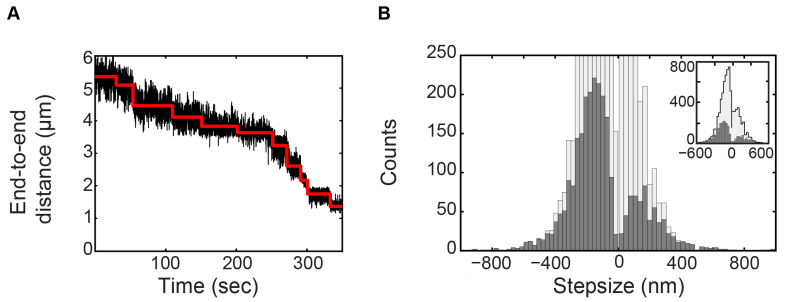

Figure 5.4: **Condensin compacts DNA in a stepwise manner. a.** Compaction occurs with discrete steps. Black trace depicts the raw data; red is the fitted step trace. **b.** Histogram of detected step sizes (dark grey) and corrected distribution (light grey, see Appendix for details about the correction of the step size distribution). Inset shows the same histograms displayed to higher counts.

This analysis revealed that condensin can induce steps of hundreds of nm size (Fig 5.4B, dark grey). Note that these are remarkably high values, which are clearly larger than the size of the ~50-nm long condensin molecule itself. The step distribution is very broad, indicating that there is a range of possible outcomes for individual compaction steps. A critical evaluation of the step-size analysis, including crosschecks where we detected simulated steps (for details see Appendix), revealed that the experimentally determined that the distribution analysis is biased towards the observation of larger steps. Small steps in the range of the dimensions of the condensin complex are, in contrast, difficult to detect and are likely to have been missed in the step detection shown in Figure 5.4B. Indeed, our validation analysis suggests that the real step distribution contains more small steps (Fig 5.4B, light grey histogram). The fact that we miss these steps in the step-size detection algorithm is mainly due to the noise that is intrinsically large for magnetic tweezers under the low-force conditions required for the compaction experiments. The same limitation holds for previously published magnetic tweezer data, although details will depend on data processing, filtering, and averaging. Notably, traces resulting from force-induced de-compaction (Fig 5.3, 10pN) were smooth and did not show any discernable steps (and were accordingly rejected by our step-finding algorithm).

Condensin does not compact DNA by inducing DNA supercoiling

As condensin was reported to influence the supercoiled state of plasmid DNA in the presence of topoisomerases [12, 22–24], it has been proposed that condensin might actively introduce (positive) supercoiling into DNA helices to promote their compaction. We therefore examined the compaction activity as a function of the DNA supercoiling state, an assay for which magnetic tweezers are especially suitable. An example of a rotation curve for a torsionally constrained DNA molecule is shown in Figure 5.5a. On average, half of the DNA tethers in each experiment were torsionally constrained (and hence can be used to test possible effects of supercoiling on the compaction), while the other half did not show a decrease in end-to-end length upon rotation due to a nicked tether. When we compared compaction rates between nicked and torsionally constrained DNA molecules, we found no differences (Fig. 5.5b). This finding is fully consistent with the

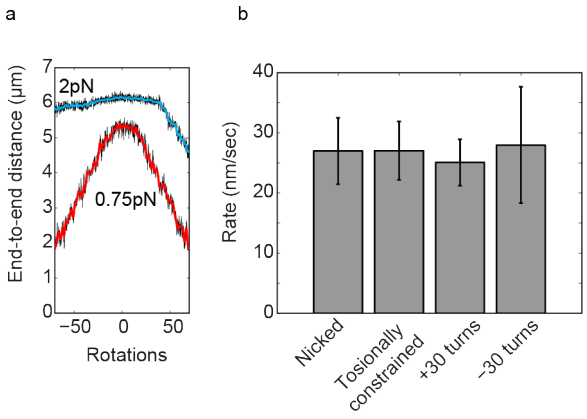

Figure 5.5: **DNA supercoiling does not influence compaction. a.** Rotation curves of a bare DNA molecule at constant forces (2pN in blue, 0.75pN in red), showing that this molecule is torsionally constrained and supercoils are introduced by applying positive or negative rotations to the magnets. **b.** Compaction rates for different supercoiling states. All measurements are for the standard experiment: 0.75pN, 1mM ATP, 8.6nM condensin. There is no difference between nicked DNA and coilable DNA. Also there is no difference between relaxed DNA, and DNA with applied turns in either direction.

results of an earlier study using *Xenopus* condensin I [11]. In addition, we tested whether the initial topological state of the DNA would affect the compaction process by introducing +30 or -30 turns into the DNA molecules before adding protein and ATP. Again, we did not find a measurable effect on the compaction rate (Fig. 5.5b).

If the decrease in the end-to-end length during compaction were due to condensin introducing supercoils, we should be able to actually extend DNA that previously was compacted by condensin, as condensin would remove some of the applied supercoils [31]. We therefore applied +50 or -50 turns to a DNA molecule that was halfway compacted (Supplementary Fig. S5.5a). Upon starting the rotation curve to either direction, we never observed that the DNA end-to-end length increased, but instead measured a decrease in compaction in both cases (Supplementary Fig. S5.5b). These findings show that the condensin-induced decrease in compaction was not a result of DNA supercoiling.

However, when we rotated the magnet back to the starting position (0 turns) after applying 50 turns to compacted tethers, we found that the end-to-end length did not fully recover. In fact, the end-to-end length started to decrease further already before the "relaxed" point at 0 turns. This behavior occurred regardless of the direction in which the DNA had initially been rotated (N=8, both directions). We speculate that instead of actively introducing supercoils, condensin is able to "lock" DNA plectonemes by embracing their stem (see Supplementary Fig. S5.4c).

5.3. Discussion

DNA binding and compaction are distinct steps in the condensin reaction cycle

We used single-molecule magnetic tweezers to demonstrate that condensin holocomplexes purified from *S. cerevisiae* are able to compact DNA, similar to a previous study of condensin I complexes immunopurified from *X. laevis* egg extracts [11]. In contrast to this previous report, DNA compaction clearly dominated any de-compaction in our assays.

Our data show that association of condensin with DNA can take place in the absence of ATP (Supplementary Fig. S5.2a). This ATP-independent interaction is able to survive washing steps with physiological salt concentrations, but it does not survive in buffer conditions of high ionic strength (Fig. 5.3j, k), indicative that this interaction of condensin with DNA might be electrostatic. We propose that this binding step occurs through the direct interaction with the DNA double helix of the condensin HEAT- repeat and kleisin subunits [8] and/or possibly through another yet unidentified DNA binding site in the complex (Fig. 5.6). Notably, condensin apparently does not require any loading factor(s) to associate with and to compact DNA. This contrasts cohesin, which commonly uses specific loading factors to increase the efficiency of its binding to chromosomes [25, 27, 32, 33].

When condensin is added to DNA in the presence of ATP, however, it is able to survive high salt conditions (Fig. 5.3h, i). This suggests that the ATP-dependent mode of DNA binding must be exceptionally stable, e.g. such as provided by a topological binding mode where the Smc2-Smc4-kleisin ring encircles the DNA. The subsequent compaction step essentially depends on ATP hydrolysis by the Smc2-Smc4 subunits of the condensin complex, since neither a Q-loop ATPase mutant version of the condensin in the presence of ATP nor a wild-type version of condensin in the presence of ATPγS are able to compact the tethered DNA substrates in our assay. It thus appears logical to conclude that the electrostatic interaction is converted into a topological interaction by an ATP-dependent temporary ring opening and entry of the bound DNA into the ring (Fig. 5.6). It is conceivable that the initial electrostatic interaction releases upon ATP hydrolysis, which frees this binding site to be available to grab another piece of the same DNA and thereby create a DNA loop. In summary, our results reveal that at least one electrostatic interaction and a topological interaction must function as the principle binding modes that condensin employs to compact DNA. It is furthermore possible that a third interaction and binding mode is involved in the actual compaction process. Following a short lag time after addition of ATP, condensin induces a fast compaction of the DNA tethers. We interpret the lag time before compaction starts after addition of condensin and ATP as the sum of the time necessary for condensin to bind to DNA and to become active for compaction. The latter step likely involves the conversion of an electrostatic into a topological binding mode (Fig 5.6C). This interpretation is consistent with the findings that the lag time depends on the concentration of ATP and is reduced when condensin has been pre-bound to DNA in the sequential addition setup. The observation of a lag time is furthermore consistent with recent measurements of condensin movements on DNA curtains, where condensin binds and pauses before becoming ac-

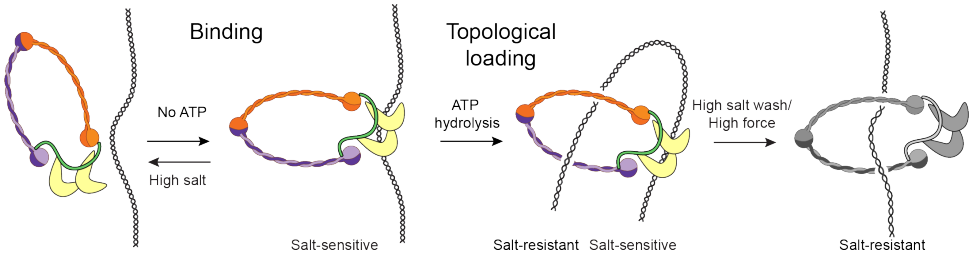

Figure 5.6: **Condensin compacts DNA using a multistep binding mechanism.** We propose a multistep model for condensin's binding mechanism, represented by the colored panels. First, condensin binds to DNA electrostatically, presumably through the HEAT-repeat subunits. Next, upon ATP hydrolysis, condensin embraces the DNA topologically. This initiates the compaction of DNA. Finally (most right panel in gray), in our experiments, we disrupted the electrostatic interactions in some of our assays with high salt or high force.

tive for translocation [28].

Once the compaction reaction had been initiated, it frequently proceeded to the maximally compacted state that we can measure in our setup. Dominance of DNA compaction over any de-compaction in our assays contrasts previous findings with *Xenopus* condensin I complexes, where DNA compaction reverted spontaneously in many instances [11]. Another difference to this previous report is our finding that compaction rates by the *S. cerevisiae* condensin complex scaled approximately linearly with protein concentration. Whereas these data cannot rule out that multiple condensin complexes cooperate in the compaction reaction, they are consistent with a model in which multiple complexes act as individual motors on DNA.

Whereas our experiments strongly suggest that the required energy for compaction must stem from ATP hydrolysis by the Smc2-Smc4 subunits (see above), we find that condensed DNA remains compacted even after washing with buffer that does not contain ATP (Fig S5.2C) or buffer that contains ATPγS (Fig S5.3E). This shows that continuous ATP hydrolysis by condensin is not required to maintain the compact state of the DNA. The compact state can, however, be disrupted by applying very high physical forces or high salt conditions, which presumably disrupt non-topological condensin?DNA contacts (Fig 5.6C).

The amount of work needed for compaction can be calculated as the product of the displacement against the applied force. Taking into account that k_BT=4.1pN*nm and that the free energy resulting from hydrolysis of one DNA molecule of ATP is ~20k_BT, we can calculate the amount of ATP molecules that would minimally be required to drive compaction against a certain force. Assuming for the sake of argument that condensin converts the energy from ATP hydrolysis with 100% efficiency, we estimate that full compaction (from 5 to 0μm length) against a force of 0.75pN requires the hydrolysis of 46 ATP molecules, or equivalently, the hydrolysis of each ATP molecule would correspond to a 110-nm step. While this clearly provides an order-of-magnitude estimate only, the result is consistent with previous estimate of large steps as observed for condensin translocation [28]. As the force increases, more ATP needs to be hydrolyzed to provide the necessary energy in order to achieve compaction.

A surprising finding from our experiments is the broad distribution of compaction

step sizes, which includes very large step sizes, larger than the condensin complex itself. One explanation for this conundrum might be that condensin could be taking smaller individual compaction steps and that the steps that we are detecting are in fact bursts of smaller steps that cannot be resolved within the temporal resolution and noise of the magnetic tweezer assay (0.1-0.4sec, see Appendix and [34]. Our step-finding validation demonstrates that, while large steps are confidently detected, the assay is unable to detect very small steps (see Appendix). Our conservative method revealed that one should be cautious with step fitting at high compaction activity of condensin and the low forces applied in the magnetic tweezers. For this reason, we refrain from reporting a typical step size for a single condensin-driven compaction cycle.

Consequences for geometric models for condensin-induced DNA compaction

Which of the various geometric models for condensin?s mechanism are compatible with our findings? Generation of DNA supercoiling has been proposed as a mechanism to condense DNA [22]. Our data are not consistent with this model, since we could never observe unwinding of induced supercoils after compaction (Fig S4). We also did not find any difference in rates between relaxed DNA, torsionally constrained DNA, and DNA molecules with pre-applied turns [11]. Instead, our results indicate that condensin might stabilize or ?lock? plectonemes, for example by binding specifically to crossed DNA segments at the stem of DNA plectonemes (Fig S5.4C). However, while such a mechanism would allow condensin to stabilize an already compacted DNA state, it is unable to induce compaction on its own and hence cannot explain the observed compaction activity.

The random crosslinking model proposes that condensin compacts DNA by randomly connecting different pieces of the same DNA molecule [35] (Fig 5.5A). Such a scenario fits well with a broad distribution of step sizes as well as with step sizes that are considerably larger than the dimensions of the condensin complex itself. This model requires, however, that distant DNA regions come into close proximity for crosslinking in the first place, without the action of condensin. Since, at a force of 1pN, the DNA tethers in our assay are already stretched to 85% of their contour lengths, it is difficult to imagine how, under these forces, large loops could be generated through random crosslinking. Furthermore, since this model does not involve a catalytic compaction activity, it does not explain how halfway compacted DNA molecules can compact further after any free protein has been washed away, as it is quite unlikely that this would happen by condensin letting go of one piece of DNA to grab another piece of DNA further away in order to create a larger loop. Theoretical modeling of the biophysics of a crosslinked DNA polymer under an applied force would be helpful to estimate these notions quantitatively. A variation of the random crosslinking model might involve individual condensin complexes that mutually interact to generate a DNA loop, i.e., in a variation of the handcuff-like model that has been proposed for the cohesin complex [36]. Yet, this model also faces the same challenge of explaining how halfway compacted DNA molecules can continue to compact after any free protein has been washed away.

A model that recently gained much attention is loop extrusion [37]. Here, condensin binds to DNA and moves it through its ring to extrude a loop of DNA, which thereby con-

tinuously increases in size (Fig 5.5B). Simulations have shown that loop extrusion can indeed achieve efficient chromosome condensation [17]. Requirements for this model are that condensin has DNA motor activity, which was demonstrated recently [28], and that the extrusion machine can interact with at least two points along the DNA simultaneously. If the interaction of condensin with DNA would only be topological, loop extrusion would not work, as DNA can slip out of the ring, which certainly will happen under an applied force. Our finding that a direct (electrostatic) contact between condensin and DNA is required to maintain the compacted state of DNA suggests that such a contact might serve as an anchor site at the base of a forming loop [30]. The finding that halfway compacted DNA molecules can eventually compact fully without the addition of extra protein is furthermore easy to imagine for a motor extruding a loop of ever-larger size.

Cartoons of the loop extrusion mechanism often depict a pseudo-topological embrace of the DNA (Fig S5.5C). For such pseudo-topological loading, the condensin ring does not necessarily have to open, in contrast to real topological loading. Importantly, we find that a pseudo-topological embrace is inconsistent with our data, as such a conformation would not survive high salt washes and high force. Instead, our data indicate that the ATP-hydrolysis-assisted DNA loading is truly topological. This is an important distinction that changes the way one should think about loop extrusion, and we accordingly suggest that one should take the topologically loaded state as the basis for future modeling of the loop extrusion process (Fig. 5.6).

In conclusion, systematic evaluation of DNA compaction by condensin complexes allowed us to resolve the binding mode conditions that must be met in any geometric model. Our data demonstrate a two-step model: first ATP-independent direct interaction of condensin with DNA, followed by ATP-hydrolysis-dependent topological loading and DNA compaction. This model provides an important stride forward in unraveling the mechanism of chromosome compaction by condensin complexes.

5.4. Methods

Protein purification

Wild-type (Smc2?Smc4?Brn1?Ycs4?Ycg1), tetrameric (Smc2?Smc4?Brn1?Ycs4), ATPase mutant (Smc2Q147L?Smc4Q302L?Brn1?Ycs4?Ycg1) and DNA binding mutant (Smc2?Smc4?Brn1K409D, R411D, K414D, K451D, K452D, K456D, K457D?Ycs4?Ycg1) versions of the *S. cerevisiae* condensin holocomplex were overexpressed from galactose-inducible promoters in budding yeast. The complexes were purified from interphase cell extracts via a tandem affinity chromatography strategy, using a His12 tag fused to the Brn1 subunit and a triple StrepII tag fused to the Smc4 subunit, followed by a gelfiltration step. Expression and purification of the complexes are described in detail in ref. [28]. Purified proteins were aliquoted, snap frozen in liquid nitrogen, and stored at -80°C.

Magnetic Tweezers

We used a multiplexed magnetic tweezers as described in refs [38] and [39]. We used a 20kb DNA construct with digoxygenin- and biotin-handles and nitrocellulose coated flow cells (volume 30μl) as described in ref [38]. In brief, nitrocellulose-coated flow cells

were incubated with 100mM anti-digoxygenin antibodies (Fab-fragment, Roche). Then, the flow cell was washed with washing buffer (20mM TRIS-HCl pH7.4, 5mM EDTA). Next, the surface was passivated with 10mg/ml BSA for 1 hour and washed again. Streptavidin-coated beads (MyOne, Life Technologies) were incubated with biotin-functionalized DNA for 20 minutes. After incubation, the beads were washed three times with washing buffer plus 0.05%Tween. An excess amount of beads with digoxygenin-functionalized DNA was then incubated in the flow cell for 10 minutes. Finally, the flow cell was washed extensively with compaction buffer (10mM HEPES-NaOH pH7.9, 125mM NaCl, 5mM MgCl2, 1mM DTT) to flush out all unbound beads and provide near-physiological reaction conditions. Compaction was only observed at conditions around physiological salt concentrations (50-250mM NaCl, data not shown). Different forces were applied by linear translation of the magnets, while rotation of the magnets was used to apply supercoils. A force calibration curve was generated to correlate the magnet height to the force. Before all experiments, all tethers were routinely checked for coilability and for their end-to-end length before starting the compaction reaction (pre-measurement).

Determination of the compaction-rate and lag-time

All compaction experiments were carried out in compaction buffer (10mM HEPES- NaOH pH 7.9, 125mM NaCl, 5mM MgCl2, 1mM DTT). Different concentrations of ATP and of the *S. cerevisiae* condensin holocomplex (nanomolar range) were dissolved in 50μl of compaction buffer and flushed in, which typically took 15 seconds. Tracking of the beads was started immediately after flushing in the protein and the force was kept constant throughout the experiment. The lag-time was defined as the time it took for the compaction to start. The time points at which the DNA reached 90%, 80%, 70%, etc. of their original end-to-end length (taken from the pre-measurement) were automatically recorded by our custom-made software. The compaction rate was determined by calculating the difference in end-to-end length between the 90% and 10% time points. In the case that compaction did not reach the 10% point, we determined the rate from the initial part of the compaction curve. The standard duration of an experiment was 20 minutes.

Step analysis

We used a well-defined step-fitting algorithm that was previously described [39]. This algorithm objectively evaluates if a trace shows steps, without prior knowledge of step size or location, based on chi-squared minimization. To evaluate the variation of step sizes in an objective manner, we improved the implementation of this algorithm to allow for hands-off, batch style analysis. For details, see Supplementary Methods.

5.5. Supplementary Information

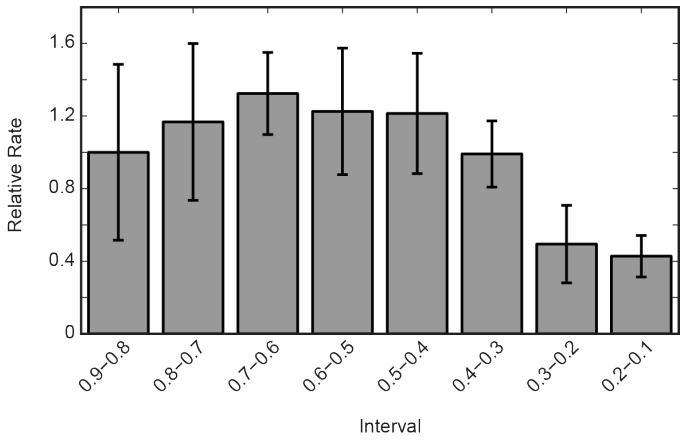

Figure S5.1: **Relative average rate as compaction progresses.** The compaction rate is relatively steady over the course of a condensation experiment, but slows down towards the end. Rate depicted relative to the rate in the interval of 0.9 to 0.8 of the original end-to-end distance as measured in the pre-measurement.

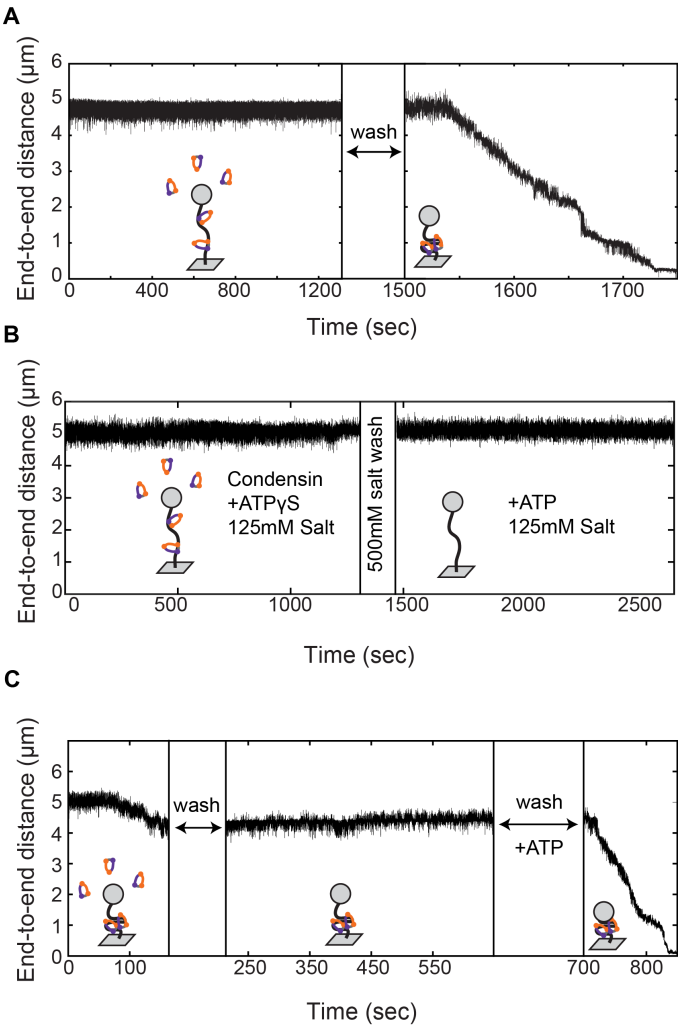

Figure S5.2: **Condensin does not compact DNA in the absence of hydrolysable ATP or at high salt. a.** Example trace of DNA when condensin is added in the absence of ATP. After a 20-minute incubation, no condensation is observed. After washing the flow cell with buffer with no additional protein (t=1300), ATP is added (t=1500) and compaction is observed, indicating protein was bound in the absence of ATP. **b.** At t=0, condensin and ATPγS are added, no compaction is observed. The flowcell is then washed with high salt (500mM). Next, ATP and physiological salt are added, and no compaction is observed. This indicates that ATP hydrolysis is necessary to achieve salt resistant binding. **c.** At t=0, condensin and ATP are added and compaction is initiated. We interrupt ongoing DNA compaction by flushing with buffer without ATP (t=150). The compacted DNA remains compacted after washing with buffer without extra protein or ATP. Addition of ATP is necessary for compaction to proceed (t=700).

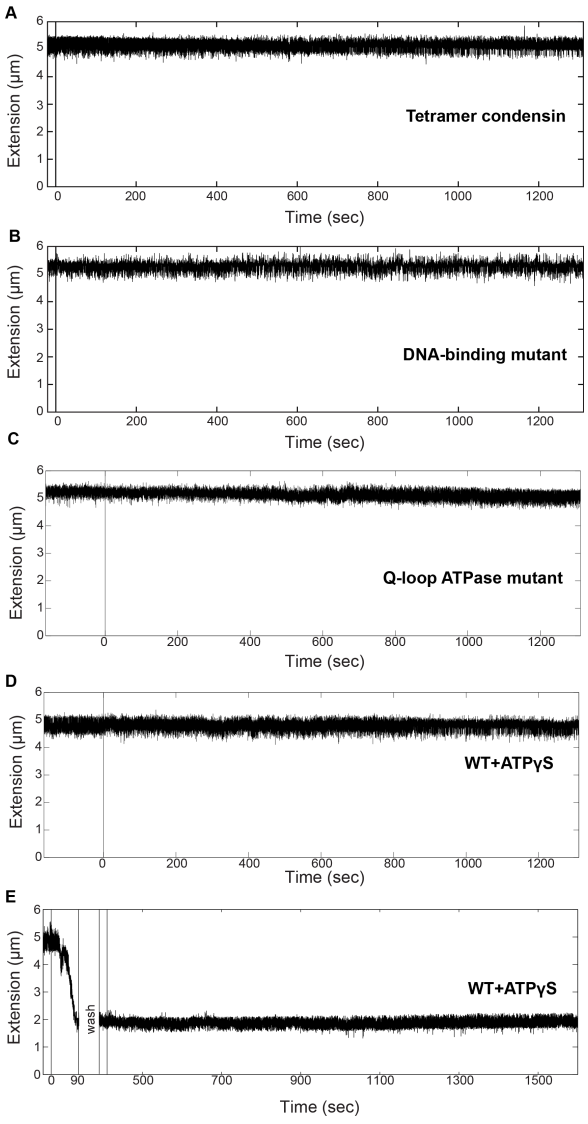

Figure S5.3: **Condensin tetramer, DNA binding mutant condensin, ATPase mutant condensin, and wiltype protein+ATPγS do not compact DNA. a.** Example trace showing that tetramer (lacking Ycg1) condensin does not compact DNA. **b.** Example trace showing condensin with mutations in the DNA binding domain does not compact DNA. **c.** Representative trace showing that the Q-loop condensin mutant does not compact DNA (N=12). Protein is added at t=0. **d.** Representative trace showing that the wildtype condensin protein does not compact in the presence of ATPγS (N=11). Protein+ATPγS is added at t=0. **e.** Representative trace showing that ATP hydrolysis is necessary for compaction (N=6). At t=0, protein and ATP are added as normal. After half compaction (t=90), the flow cell is washed. ATPγS is added at t=400. Compaction is unable to continue in the presence of ATPγS.

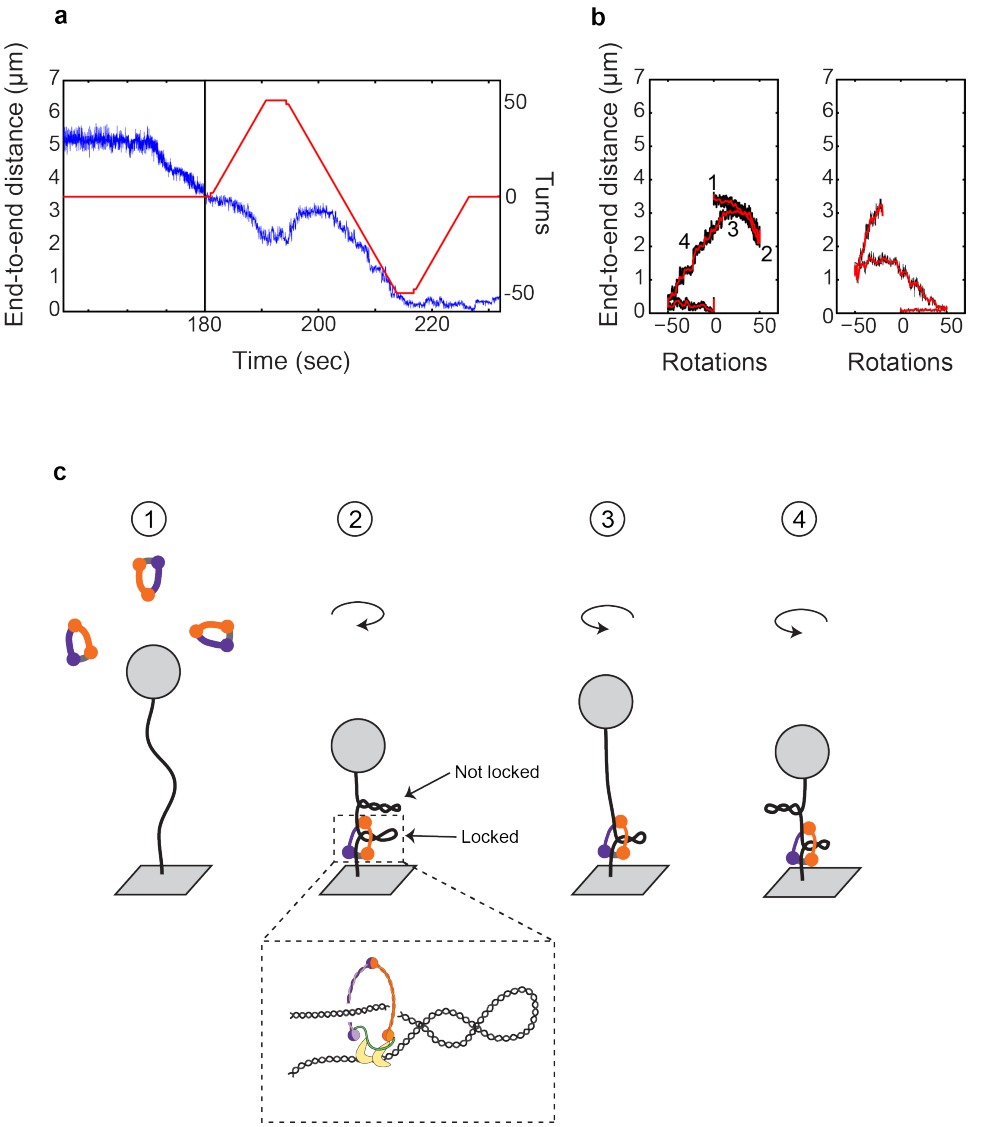

Figure S5.5: **Condensin shifts rotation curves. a.** Example of experiment with the compaction trace shown in blue and the rotations shown in red. Tether was compacted by condensin as usual. After about 50% condensation (at time=180), 50 positive rotations were applied. Then, the magnet was turned to -50 and back to 0. **b.** Rotation curves of condensed DNA at 0.75pN. Left curve shows end-to- end length as a function of rotation, corresponding to the trace in Supplementary Figure 5.4a (after time=180). Right curve shows similar experiment, only here negative turns were applied first. Numbers correspond to the states depicted in B. **c.** Proposed model for condensation curve shifts in condensed molecules. We speculate that condensin is able to lock plectonemes. First, the DNA is "relaxed", as no rotations are introduced yet. Second, the end-to-end length has decreased because 50 turns were absorbed (either positive or negative). Third, the turns are released as the magnet is rotating back to zero, but because condensin has "locked" some plectonemes, the end-to-end length of the DNA cannot be fully recovered. Instead, the rest of the DNA is essentially relaxed before reaching 0 turns. Therefore, the DNA starts absorbing the rotations, and end-to-end length is decreased again. In the shown examples, this shifts the highest point of the rotation curve from 0 to around 25, indicating that condensin has locked about 25 turns into a plectoneme. This process happens regardless of the initial rotation direction, suggesting that condensin can lock both positive and negative supercoils.

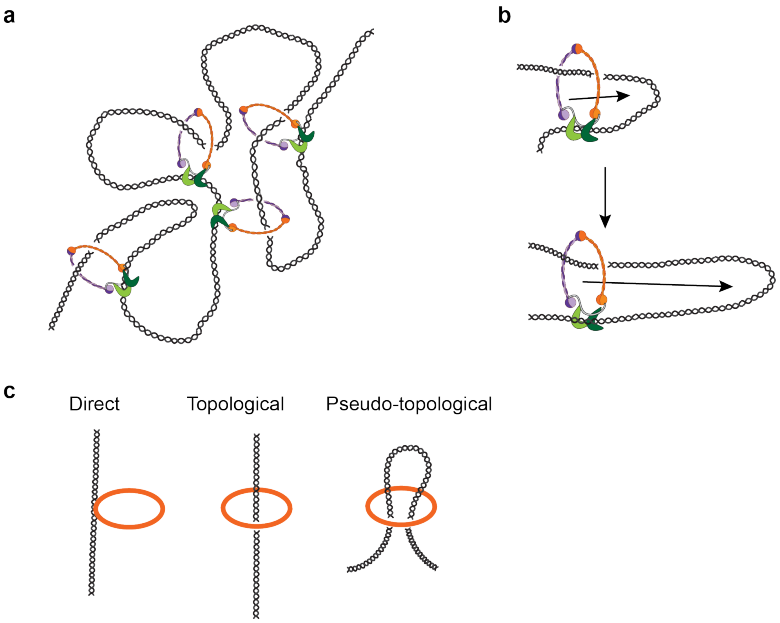

Figure S5.6: **Models for compaction. a.** The random-crosslinking model. **b.** The loop-extrusion model. **c.** Direct, topological, and pseudo-topological loading.

Supplementary methods

Step fitting analysis

We used a user-independent step-finding algorithm that was previously described and which has been abundantly used in many biological studies [39]. Briefly, the method works as follows. With this method, the best step fit is done based on least-square minimization. Then, the same number of steps is applied to the same data, but then deliberately misplaced such that fitted step locations are positioned at places away from the steps, a so-called ?counter-fit?. The more prominent the steps are in a trace, the worse this counter fit is, i.e., the higher the chi-squared. For a featureless trace, the best and worst fit are not that different, however. Therefore, the ratio between the chi-squared value of fit and counter-fit maximizes at the most likely number of steps, whereas this ratio is 1 if there are no steps. We refer to this ratio as the S-value [39]. In our analysis, we reject the fit if this S-value is below 1.15. Thus, as was shown before, by optimizing the S-value, an optimal fit can be found as a function of the number of fitted steps.

For complicated step traces, this procedure tends to underestimate the number of steps. Therefore we performed a two-pass algorithm. To evaluate the variation of step sizes in an objective manner, we improved the implementation of this algorithm to allow for hands-off, batch style analysis. We followed an automated, three-phase analysis workflow:

1. We perform a "major step fit" as described above. Based on the individual errors for these fitted steps, we determine an "error- threshold".
2. This primary step fit is subtracted from the data. The residue may still contain smaller steps.
3. A "minor step fit" is performed on the residue with the same rejection criteria as for the first round, with the addition that the step errors need to be below the "error-threshold".
4. Finally, all accepted step locations are used to build the final fit. All these steps thus have similar error margins.

Figure S5.6 presents an example of the step fitting protocol.

We confirmed the validity of the step fit by evaluating how pronounced the S-value is. For example, as described in [39], for perfect steps of 170 nm with noise comparable to our experiments (102 ± 28 nm, one sigma, mean ± SD), the maximum expected S-value is (1+(170/(2*102))$\hat{2}$)=1.7. For our experimental data, we found a typical ratio maximum of around 1.5 ± 0.3 (mean ± SD), in good agreement with this estimate. We conclude from this that the steps we detect are indeed well-defined, i.e., consisting of sharp transitions and flat plateaus and not just a product of false-positive fits of noise.

Step validation

When we use the step-finder as described, we obtain a wide distribution of steps (Figure 4B). To check how reliable these steps are, we set up a test routine to sporadically inject artificial steps of user-defined size into our experimental data traces, and we subsequently evaluated how well our step-finding algorithm was able to detect these. For this validation routine, we used the experimental curves at standard conditions (0.75pN, 1mM ATP, 8.6nM condensin) as a representative set of 20 curves, which included the typical noise and occasional spikes. To preserve the overall compaction rate, each positive

step was followed by a negative step. We added multiple (~4) up-down pairs per curve (example shown in Figure S5.7). For building statistics, each curve was used 20 times, each time with a different selection of injection steps of defined size. The size for the injected steps was randomly picked from a 0-1500 nm step-size range, thus covering at least the range of originally detected steps.

Consistent with our conservative choices in setting up the step-extraction protocol, we find that only a finite fraction of the steps is detected. For larger-size steps (roughly larger than 500 nm), most steps are detected, but, by contrast, most small steps (~100nm) stay undetected (Figure S5.7BC).

This has important consequences for what can be concluded from our (and others) magnetic tweezer experiments under these low-force condition where such tweezers intrinsically exhibit large noise. Most noteworthy is that small steps easily get drowned by noise or are obscured by nearby neighboring steps, and accordingly we cannot make a firm statement on a characteristic (small) step size associated with the condensin-induced DNA condensation process. At the same time, larger steps are detected reliably, and we can conclude that these indeed occur in the DNA condensation traces. Overall, we conclude that the measurement traces signal a very broad distribution of step sizes, including remarkable large steps.

Response time of the bead

In our magnetic tweezers, the magnetic bead cannot respond infinitely fast to an instant (condensation) step, since it is slowed down by the drag associated with moving the bead through the liquid. Here, we follow a simplified approach to obtain a ballpark estimate of the response time of the bead. This situation is reminiscent of the force-switch experiments performed by Crut et al [34].

We simplify the stretched DNA at an extension e as a linear spring with spring constant $k(e)$. We also assume a mass-less, heavily overdamped system. For determining k, we assume the DNA behaves as a worm-like-chain. We expect the DNA to be stiffer after compaction, as the contour length is decreasing (Supplementary figure S8).

We start out with a stretched tether, where the magnetic force is balanced by the entropic stretching force of the DNA. Then, we assume that a condensation step instantly shortens the DNA by 200 nm. As the bead is initially still in the same position, the DNA is stretched by the same amount of 200 nm. During displacement of the bead following an instant shortening of the DNA, the drag force experienced by the bead is balanced with the DNA spring force:

$$F_{drag} + F_{spring} = 0, \text{ or } \gamma \frac{dx}{dt} + \kappa x = 0$$

with $6\pi\eta r$ characterising the Stokes drag of the bead, η the viscosity of water, and r the radius of the bead (0.5μ). The bead will therefore move according to

$$x(t) = x_0 e^{-t/\tau}$$

with $\tau = \frac{\gamma}{\kappa}$ the response time of the bead.

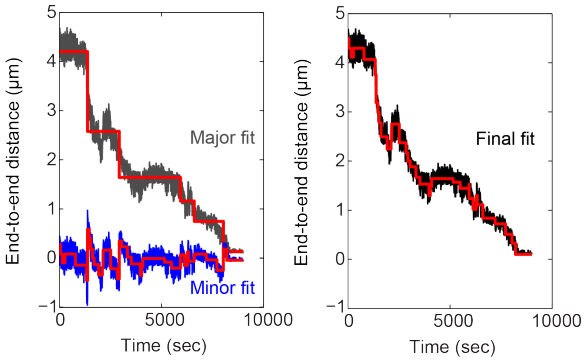

Figure S5.6: **Principle of multi-pass automated step fitting analysis.** First, a major step fit (upper red curve) is done on the data (left panel, gray). This fit is subtracted from the original data. Next, a minor step fit is done on the residue (left panel, blue). Accepted step fits are combined in a final fit (right panel).

We evaluated the response time for three points: near the initial bare DNA extension at the applied pulling force (F=0.3pN, e=4.7μm), at halfway compaction (e=2.0μm), and at nearly complete compaction (e=0.6μm) (see Supplementary Figure S5.8). This yields values of k = 0.2145*10^{-6} to 0.8005*10^{-6}, leading to response times of τ = 100 to 400ms, respectively. This estimate is consistent with experimental measurements [34].

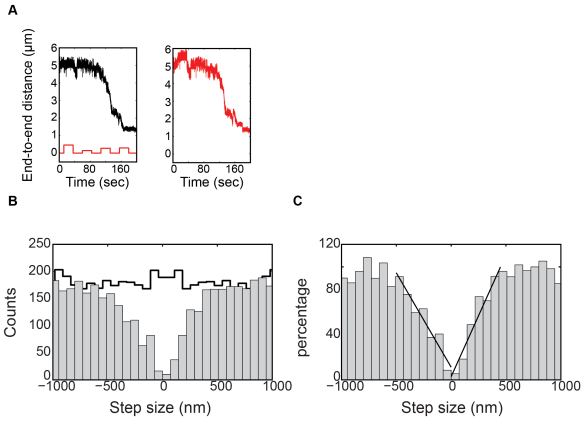

Figure S5.7: **Step validation. a.** On the left side, an experimental trace is shown (black) as well as the "fake" steps (red) that were added to the experimental trace. The right panel shows the combined experimental curve plus injected steps. **b.** Histogram showing the distribution of returned steps (light grey) from all injected steps. For reference, the input distribution is shown with a line in the background. **c.** Histrogram of return percentage per step size. Line is phenomenological fit of the linear regime to the data, which was used for correcting the original step distribution histogram in Figure 5.4B in the main text, see inset to Figure 5.4B.

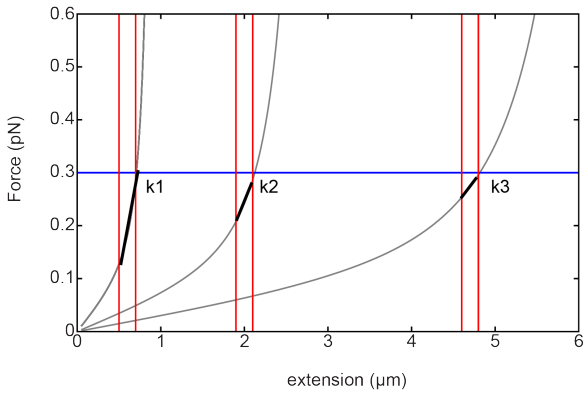

Figure S5.8: **Determining the spring constant of the DNA at three compaction states.**

References

[1] L. Aragon, E. Martinez-Perez, and M. Merkenschlager, *Condensin, cohesin and the control of chromatin states,* Current Opinion in Genetics and Development **23**, 204 (2013).

[2] T. Hirano, *Condensin-Based Chromosome Organization from Bacteria to Vertebrates,* Cell **164**, 847 (2016).

[3] K. Nasmyth and C. H. Haering, *Cohesin: its roles and mechanisms.* Annual review of genetics **43**, 525 (2009).

[4] J. M. Eeftens, A. J. Katan, M. Kschonsak, M. Hassler, L. de Wilde, E. M. Dief, C. H. Haering, and C. Dekker, *Condensin Smc2-Smc4 Dimers Are Flexible and Dynamic,* (2016).

[5] D. E. Anderson, A. Losada, H. P. Erickson, and T. Hirano, *Condensin and cohesin display different arm conformations with characteristic hinge angles.* The Journal of cell biology **156**, 419 (2002).

[6] T. Ono, A. Losada, M. Hirano, M. P. Myers, A. F. Neuwald, and T. Hirano, *Differential Contributions of Condensin I and Condensin II to Mitotic Chromosome Architecture in Vertebrate Cells,* Cell **115**, 109 (2003).

[7] S. Cuylen, J. Metz, and C. H. Haering, *Condensin structures chromosomal DNA through topological links.* Nature structural & molecular biology **18**, 894 (2011).

[8] I. Piazza, A. Rutkowska, A. Ori, M. Walczak, J. Metz, V. Pelechano, M. Beck, and C. H. Haering, *Association of condensin with chromosomes depends on DNA binding by its HEAT-repeat subunits.* Nature structural & molecular biology **21**, 560 (2014).

[9] K. Kinoshita, T. J. Kobayashi, and T. Hirano, *Balancing Acts of Two HEAT Subunits of Condensin I Support Dynamic Assembly of Chromosome Axes,* Developmental Cell **33**, 94 (2015).

[10] D. F. Hudson, K. M. Marshall, and W. C. Earnshaw, *Condensin: Architect of mitotic chromosomes.* Chromosome research : an international journal on the molecular, supramolecular and evolutionary aspects of chromosome biology **17**, 131 (2009).

[11] T. R. Strick, T. Kawaguchi, and T. Hirano, *Real-time detection of single-molecule DNA compaction by condensin I.* Current biology : CB **14**, 874 (2004).

[12] K. Kimura, V. V. Rybenkov, N. J. Crisona, T. Hirano, and N. R. Cozzarelli, *13S Condensin Actively Reconfigures DNA by Introducing Global Positive Writhe,* Cell **98**, 239 (1999).

[13] J. R. Swedlow and T. Hirano, *The making of the mitotic chromosome: modern insights into classical questions.* Molecular cell **11**, 557 (2003).

[14] R. Thadani, F. Uhlmann, and S. Heeger, *Condensin, Chromatin Crossbarring and Chromosome Condensation,* Current Biology **22**, R1012 (2012).

[15] E. Alipour and J. F. Marko, *Self-organization of domain structures by DNA-loop-extruding enzymes,* Nucleic Acids Research **40**, 11202 (2012).

[16] G. Fudenberg, M. Imakaev, C. Lu, A. Goloborodko, N. Abdennur, and L. A. Mirny Correspondence, *Formation of Chromosomal Domains by Loop Extrusion,* Cell Reports **15**, 2038 (2016).

[17] A. Goloborodko, M. V. Imakaev, J. F. Marko, and L. Mirny, *Compaction and segregation of sister chromatids via active loop extrusion,* eLife **5** (2016), 10.7554/eLife.14864.

[18] A. Goloborodko, J. F. Marko, and L. A. Mirny, *Chromosome Compaction by Active Loop Extrusion,* Biophysical Journal **110**, 2162 (2016).

[19] M. Kschonsak and C. H. Haering, *Shaping mitotic chromosomes: From classical concepts to molecular mechanisms,* 10.1002/bies.201500020.

[20] L. Wilhelm, F. Bürmann, A. Minnen, H.-C. Shin, C. P. Toseland, B.-H. Oh, and S. Gruber, *SMC condensin entraps chromosomal DNA by an ATP hydrolysis dependent loading mechanism in Bacillus subtilis,* eLife **4** (2015), 10.7554/eLife.06659.

[21] E. Dolgin, *DNA's secret weapon against knots and tangles,* Nature **544**, 284 (2017).

[22] D. P. Bazett-Jones, K. Kimura, and T. Hirano, *Efficient Supercoiling of DNA by a Single Condensin Complex as Revealed by Electron Spectroscopic Imaging,* Molecular Cell **9**, 1183 (2002).

[23] K. Kimura and T. Hirano, *ATP-Dependent Positive Supercoiling of DNA by 13S Condensin: A Biochemical Implication for Chromosome Condensation,* Cell **90**, 625 (1997).

[24] J. St-Pierre, M. Douziech, F. Bazile, M. Pascariu, É. Bonneil, V. Sauvé, H. Ratsima, and D. D'Amours, *Polo Kinase Regulates Mitotic Chromosome Condensation by Hyperactivation of Condensin DNA Supercoiling Activity,* Molecular Cell **34**, 416 (2009).

[25] I. F. Davidson, D. Goetz, M. P. Zaczek, M. I. Molodtsov, P. J. Huis in 't Veld, F. Weissmann, G. Litos, D. A. Cisneros, M. Ocampo-Hafalla, R. Ladurner, F. Uhlmann, A. Vaziri, and J. Peters, *Rapid movement and transcriptional re-localization of human cohesin on DNA,* The EMBO Journal **35**, 2671 (2016).

[26] H. Kim and J. J. Loparo, *Multistep assembly of DNA condensation clusters by SMC,* Nature Communications **7**, 10200 (2016).

[27] J. Stigler, G. Ö. Çamdere, D. E. Koshland, and E. C. Greene, *Single-Molecule Imaging Reveals a Collapsed Conformational State for DNA-Bound Cohesin*, Cell Reports **15**, 988 (2016).
[28] T. Terakawa, S. Bisht, J. M. Eeftens, C. Dekker, C. H. Haering, and E. Greene, *The condensin complex is a mechanochemical motor that translocates along DNA*, , 1 (2017).
[29] Y. Cui, Z. M. Petrushenko, and V. V. Rybenkov, *MukB acts as a macromolecular clamp in DNA condensation*, **15**, 411 (2008).
[30] M. Kschonsak, F. Merkel, S. Bisht, J. Metx, J. Rybin, M. Hassler*, and C. Haering, *Structural basis for a safety-belt mechanism that anchors condensin to chromosomes*, Cell (2017).
[31] R. Seidel, J. G. Bloom, J. van Noort, C. F. Dutta, N. H. Dekker, K. Firman, M. D. Szczelkun, and C. Dekker, *Dynamics of initiation, termination and reinitiation of DNA translocation by the motor protein Eco R124I*, The EMBO Journal **24**, 4188 (2005).
[32] Y. Murayama and F. Uhlmann, *Biochemical reconstitution of topological DNA binding by the cohesin ring*. Nature **505**, 367 (2014).
[33] Y. Murayama and F. Uhlmann, *Chapter 2 An In Vitro Assay for Monitoring Topological DNA Entrapment by the Chromosomal Cohesin Complex*, **1515**, 23 (2017).
[34] A. Crut, D. A. Koster, R. Seidel, C. H. Wiggins, and N. H. Dekker, *Fast dynamics of supercoiled DNA revealed by single-molecule experiments*. Proceedings of the National Academy of Sciences of the United States of America **104**, 11957 (2007).
[35] T. M. K. Cheng, S. Heeger, R. A. G. Chaleil, N. Matthews, A. Stewart, J. Wright, C. Lim, P. A. Bates, and F. Uhlmann, *A simple biophysical model emulates budding yeast chromosome condensation*. eLife **4**, e05565 (2015).
[36] N. Zhang, S. G. Kuznetsov, S. K. Sharan, K. Li, P. H. Rao, and D. Pati, *A handcuff model for the cohesin complex*. The Journal of cell biology **183**, 1019 (2008).
[37] K. Nasmyth, *Disseminating the Genome: Joining, Resolving, and Separating Sister Chromatids During Mitosis and Meiosis*, Annual Review of Genetics **35**, 673 (2001).
[38] J. M. Eeftens, J. van der Torre, D. R. Burnham, and C. Dekker, *Copper-free click chemistry for attachment of biomolecules in magnetic tweezers*, BMC Biophysics **8**, 9 (2015).
[39] J. W. J. Kerssemakers, E. L. Munteanu, L. Laan, T. L. Noetzel, M. E. Janson, and M. Dogterom, *Assembly dynamics of microtubules at molecular resolution*. Nature **442**, 709 (2006).

III

Force spectroscopy on the cohesin complex

6

Copper-free click chemistry for the attachment of biomolecules in magnetic tweezers

Background: Single-molecule techniques have proven to be an excellent approach for quantitatively studying DNA-protein interactions at the single-molecule level. In magnetic tweezers, a force is applied to a biopolymer that is anchored between a glass surface and a magnetic bead. Whereas the relevant force regime for many biological processes is above 20pN, problems arise at these higher forces, since the molecule of interest can detach from the attachment points at the surface or the bead. Whereas many recipes for attachment of biopolymers have been developed, most methods do not suffice, as the molecules break at high force, or the attachment chemistry leads to nonspecific cross reactions with proteins.
Results: Here, we demonstrate a novel attachment method using copper-free click chemistry, where a DBCO-tagged DNA molecule is bound to an azide-functionalized surface. We use this new technique to covalently attach DNA to a flow cell surface. We show that this technique results in covalently linked tethers that are torsionally constrained and withstand very high forces (> 100pN) in magnetic tweezers.
Conclusions: This novel anchoring strategy using copper-free click chemistry allows to specifically and covalently link biomolecules, and conduct high-force single-molecule experiments. Excitingly, this advance opens up the possibility for single-molecule experiments on DNA-protein complexes and molecules that are taken directly from cell lysate.

This chapter has been published as: J.M. Eeftens, J. van der Torre, D.R. Burnham, C. Dekker (2015) Copper-free click chemistry for the attachment of biomolecules in magnetic tweezers. *BMC Biophysics* 8:9

6.1. Background

Single-molecule methods have become increasingly popular to study biomolecules [1]. With techniques such as atomic force spectroscopy, or optical or magnetic tweezers, one is able to study the mechanical properties of single DNA molecules, single proteins, or individual DNA-protein complexes. The effect of applied force on biomolecules is a particularly relevant topic, as mechanical forces play a crucial role in many cellular processes [2–4]. The relevant forces range from a few pN, like the force produced by an RNA polymerase during transcription (14pN)[5], to tens of pN, as in, for instance, viral packaging motors that use forces of 40pN to compact genomes [6]. Even higher forces are needed in the process of chromosome segregation in eukaryotic cells, where microtubules pull on sister chromatids to segregate them to opposite sides of the spindle pole [7–10]. Many studies using magnetic tweezers have been published that probe the behavior of DNA-protein complexes under applied force and torque [11–16]. For studying biomolecules across the full relevant force range, it is necessary to also measure at higher forces (>20pN). In this regime, however, many traditional anchoring methods fail, thus limiting such single-molecule experiments.

For efficient tethering of biomolecules, it is essential to use orthogonal anchoring chemistries on both ends of the molecule, i.e. at the surface and at the bead. To achieve this, a DNA molecule is constructed that has different reactive groups incorporated, on both ends. To complete the anchoring, the bead and surface are functionalized with the corresponding reacting group. A commonly used technique is the binding of biotin to streptavidin. The bond between these functional groups has been shown to resist forces of 150pN [17, 18]. This is a high rupture force compared to a second commonly used method; the binding of a digoxygenin (dig) functionalized nucleotide and a surface coated with antibodies against digoxygenin (anti-dig) (Fig. 6.1A). This forms a stable non-covalent bond, but a limitation of this binding technique is its low stability under an applied force [19]. Depending on the force-loading rate applied to such a molecule, the dig/anti-dig bond breaks at around 20pN.

Other, much stronger, anchoring methods have been developed [20–24] by functionalizing DNA with amine (Fig. 6.1B) or thiol groups (Fig. 6.1C) that are covalently linked to the surface or bead. Although these bonds indeed resist high forces, these techniques have an important limitation in that significant nonspecific binding occurs when studying systems that are more complicated than bare DNA. For example, when studying proteins, native lysines (amine) or cysteines (thiol) in the protein can bind nonspecifically (blue arrows in Fig. 6.1B+C). For controlled single-molecule measurements, it is however important that the force is being applied at a consistent and known location [25].

A new and exciting challenge is to study DNA-protein complexes that are extracted from cell lysate. For controlled single-molecule experiments, it is essential to anchor these complexes in a stable, strong, and specific way. As the anchoring methods developed so far are unsuitable, studying DNA-protein complexes or complexes from cell lysate remains challenging [26].

Here, we present a novel method for covalent attachment of a DNA tether to a surface, based on copper-free click chemistry. Click reactions are defined as those that are selective, with favorable reaction kinetics, a high yield, and good physiological stability. Early click chemistry reactions required copper as a catalyst [27]. Copper is cytotoxic

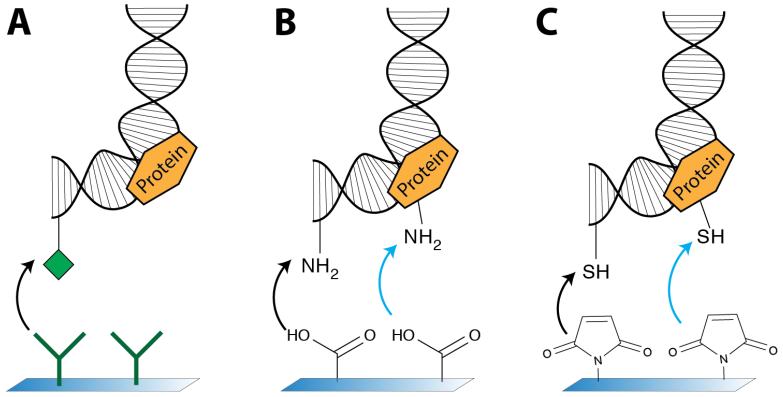

Figure 6.1: **Common DNA tethering techniques. A.** Binding of a digoxygenin-functionalized DNA-protein complex to an anti- digoxygenin-coated surface. This reaction is specific, but unstable when high forces are applied. **B.** Binding of an amine-functionalized DNA-protein complex to a carboxyl-coated surface. Both the functionalized DNA (black arrow) and native lysine groups in the protein (blue arrow) bind the surface. **C.** Binding of a thiol-functionalized DNA-protein complex to a maleimide-coated surface. Both the functionalized DNA (black arrow) and native cysteine groups in the protein (blue arrow) bind the surface.

and thus limits application of click reactions in cells. More recently, copper-free methods became available, for instance the Strain Promoted Azide-Alkyne Click (SPAAC) reaction, of which the reaction between dibenzocyclooctyl (DBCO) and azide is an example [28]. These click reactions are bio-orthogonal, i.e. they can occur within organisms without interfering with native biochemical processes.

As mentioned above, a specific and high-force-compatible anchoring technique is essential for studying DNA-protein complexes in magnetic tweezers. The reactions have to be specific, biocompatible, and able to withstand experimental conditions such as an applied high force. We develop a novel technique for covalent attachment that meets these criteria using copper-free click chemistry, based on the reaction of DBCO with azide (scheme 1). By functionalizing DNA with DBCO on one end (R1), we can covalently link it to an azide-functionalized surface (R2). As we will show below, this protocol results in a high-yield of DNA tethers, that are torsionally constrained and able to withstand very high forces (>100pN). This method is thus found to be suitable for specifically anchoring DNA-protein complexes and measuring in the relevant force regime.

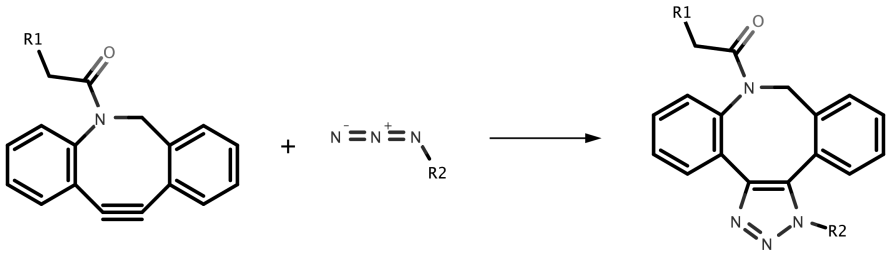

Scheme 1: **Cycloaddition between dibenzocyclooctyl and azide.**

6.2. Materials and Methods

Magnetic tweezers

We used multiplexed magnetic tweezers [29], as illustrated in Fig. 6.2A. Two 5mm cube magnets (Supermagnete, N50) are mounted in vertical orientation [30], with a very small (0.3mm) gap in between them. A red LED provides illumination through the magnet holder onto the flow cell. We use a 50x objective (Nikon) with an achromatic doublet tube lens (200mm) to provide 50x magnification and image the focal plane onto a CCD camera (Dalsa Falcon 4M60). Beads are tracked in real time with custom software (Labview, National Instruments) and images are also saved for later analysis [31]. Reference beads are used to correct for drift. The applied force is determined from the Brownian motion of the magnetic bead [32, 33]. For force-extension curves, we perform dynamic force microscopy where the force is increased over time with a constant loading rate of 1 pN/second.

DNA constructs

A 20678 bp pSupercos1 plasmid was made by removal of the MluI fragment from pSupercos1 (Stratagene) and insertion of two lambda fragments. This Plasmid DNA was isolated with midiprep (Qiagen), restricted with XhoI and NotI.HF (New England Biolabs), and purified (Wizard SV Gel and PCR Clean-Up System, Promega), resulting in a 20kb fragment. DBCO and biotin labeled handles were prepared by PCR on a pbluescriptIISK+ template (Stratagene) with a taq polymerase (GoTaq, Promega) and the addition of Biotin-16-dUTP (Roche), or 5-DBCO-dUTP (Jenabioscience) to the nucleotide mixture respectively. The forward primer was: GACCGAGATAGGGTTGAGTG, and reverse primer: CAGGGTCGGAACAGGAGAGC. The biotin-handle was digested with XhoI resulting in 554 bp and 684 bp fragments. The DBCO-handle was digested with NotI.HF resulting in 624 bp and 614 bp fragments. The handles were purified (Wizard SV Gel and PCR Clean-Up System, Promega), combined with the restricted plasmid DNA and ligated with T4 DNA ligase (Promega) overnight at 16°C. The tweezer-construct was then purified again (Wizard SV Gel and PCR Clean-Up System, Promega).

Surface functionalization and flow cell assembly

For making amine-coated flow cells, coverslips (Menzel Glaser, 24x60mm, thickness #1) were cleaned in an O2 plasma cleaner for 30 seconds, which ensures activation of the

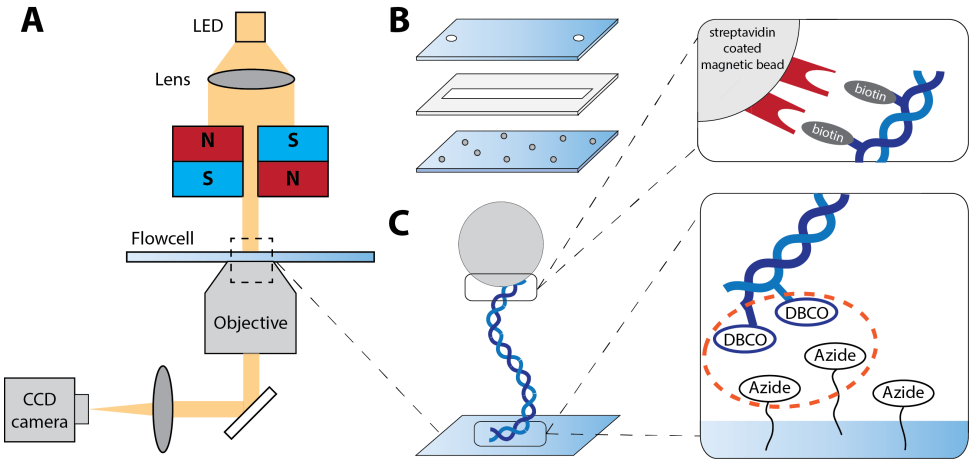

Figure 6.2: **Magnetic tweezers set-up for measuring on a tethered DNA molecule. A.** Schematic of the set-up. A LED illuminates the flow cell through a lens and the magnet holder. Imaging is done with a 50x Nikon objective onto a CCD camera. Magnets manipulate a magnetic bead attached to the DNA. **B.** A flow cell is constructed with 24x60mm coverslips. The bottom coverslip is amine- coated and has reference beads bound to it. The top coverslip has sandblasted holes to allow fluid flow. Parafilm is used to seal the coverslips and to create a ~50µl flow cell volume. **C.** Schematic of a tethered DNA molecule. A DNA molecule is linked to a streptavidin-coated magnetic bead with biotin, and to azide groups on the surface with DBCO at the other end.

silanol groups. Coverslips were then treated with 2% APTES in acetone for 10 minutes, rinsed with MilliQ and air-dried. Before flow cell assembly, polystyrene beads (Polysciences Europe GmbH) were pipetted onto the coverslip and spread with the side of a pipette tip. These non-motile surface-bound beads serve as reference beads for drift correction. The amine-coated coverslips were then aligned with a pre-cut parafilm gasket and another coverslip (Fig. 6.2B). The assembled flow cell was put on a hot plate at 90°C until the parafilm was sufficiently melted to prevent fluid leakage. The applied heat also firmly binds the polystyrene reference beads to the surface.

DNA anchoring

To anchor the DBCO-functionalized DNA to the amine-coated flow cell, we used bi-functionalized PEG_4-linkers with an N-hydroxysuccimide (NHS) ester on one end and an azide group on the other (CLK-AZ103, Jenabioscience GmbH, Germany). We mixed azide-functionalized PEG-linkers with CH_3- terminated PEG-linkers of the same length ($MS(PEG)_4$, Life technologies) in PBS buffer to passivate the surface and prevent aspecific binding. Both PEG- linkers were dissolved in DMSO before further diluting in PBS. To prevent hydrolysis of the NHS ester, the PEG mixture in PBS was prepared shortly before filling the flow cell via capillary action through pipetting the fluid into one flow cell hole of the amine-coated flow cell. The MS-PEG-linker concentration was held constant at 50mM, while the Azide-PEG concentration was varied (0-50mM). PEG-linkers incubated in the amine-coated flow cell for 1 hour at room temperature, to allow the

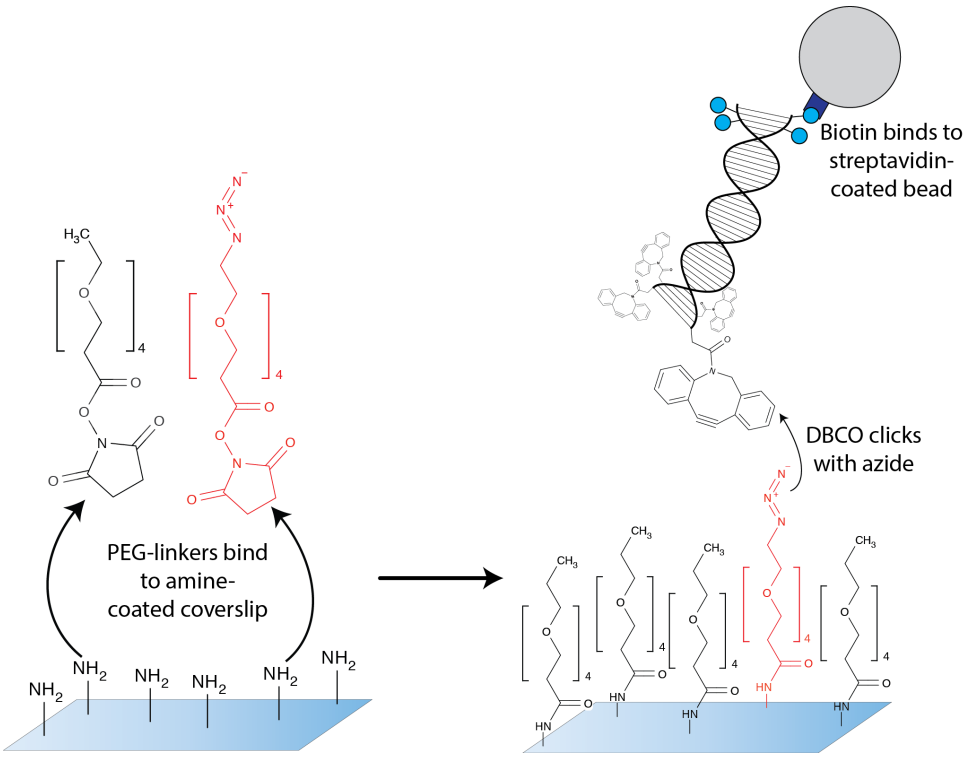

Figure 6.3: **Stepwise linkage of DNA to the surface with copper-free click chemistry.** Bifunctionalized PEG-linkers are attached to an amine-coated surface via their NHS group. The NHS ester on the PEG conjugates to the amine on the surface. Non-reactive PEG linkers (terminated with a CH^3-group) are used to passivate the surface. Finally, a DBCO group on DNA clicks with the azide and thus forms a covalent bond between the DNA and the surface.

NHS-ester group to attach to the amine groups in the flow cells (Fig. 6.3). Next, the flow cell was flushed with washing buffer (20mM Tris, 5mM EDTA, pH7.4), to stop the reaction and remove excess PEG. Streptavidin-coated beads (M270 Streptavidin coated, Life Technologies) were incubated with the biotin-functionalized DNA for 20 minutes. After incubation, the beads were washed 3 times with washing buffer with 0.05% Tween. An overabundance of DNA-bound beads was then dissolved in 50µl washing buffer with 0.05% Tween and flushed into the flow cell. Beads were incubated for 1 hour, to allow the DBCO to click with the azide (Fig. 6.3). Finally, the flow cell was washed with washing buffer until no more unbound beads were visible.

Control experiment

For control experiments, we used a dig-functionalized DNA construct. The dig handle was constructed in the same matter as the DBCO handle described above, but instead dig-11-dUTP was used (Digoxygenin-11-dUTP, Roche). Coverslips were cleaned in acetone for 30 minutes in a sonicator for creating the flow cells. After air-drying, they were coated with 1% nitrocellulose (Invitrogen) in amylacetate (Sigma Aldrich). Application of reference beads and assembly of flow cells proceeded as described above. Next, nitrocellulose-coated flow cells were incubated with 100mM anti-dig antibodies (Fab-fragment, Roche) for 30 minutes. After washing as described above, the surface was passivated with 10mg/ml BSA (Bioke) for 1 hour. Preparation of beads proceeded as described above. Beads with digoxygenin-functionalized DNA then incubated in the flow cell for 10 minutes. Finally, the flow cell was washed with washing buffer until no more unbound beads were visible.

6.3. Results and Discussion

We developed a protocol to covalently attach biomolecules in a magnetic tweezers flow cell using copper-free click chemistry. As described in Materials and Methods, we coat the glass surface with azide-functionalized PEG- linkers, and attach DBCO-tagged DNA through the azide-group, thereby covalently linking the DNA molecule at one end to the surface.

The DBCO-functionalized DNA thus covalently attaches to the azide-coated flow cell while the biotin groups at the other end of the DNA attach to the bead. The amount of these DNA tethers is expected to scale with the amount of clickable groups on the surface. To verify the protocol, we varied the density of the azide groups on the surface by using different concentrations of the PEG-linking groups. We determined the tether density by manually counting the number of successful DNA tethers in our field of view ($0.02mm^2$), for different azide-PEG concentrations. As expected, we found that the number of tethers increased linearly with increasing azide-PEG concentrations, see Fig. 6.4. Importantly, when no azide-functionalized PEG- linkers were added, no tethers of the expected length were observed. This shows that the steps in the protocol are specific and that, conveniently, the tether density is tunable.

Our DNA tethers anchored with copper-free click chemistry are able to withstand high force. We anchored 20kb DNA molecules using copper-free click chemistry and tracked the position of the magnetic beads (corresponding to the end-to-end length of

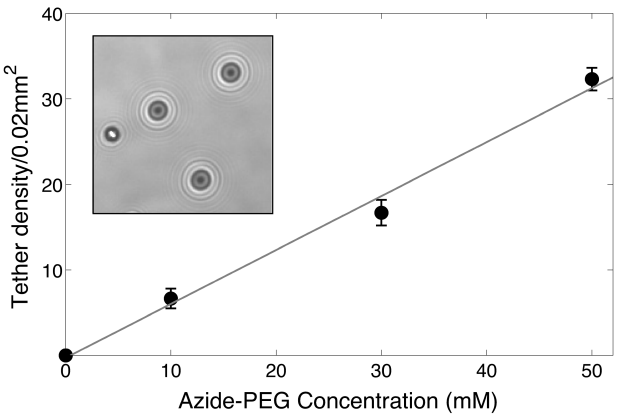

Figure 6.4: **Tether density as a function of PEG concentration.** DNA tether density for different Azide-PEG concentrations. The number of tethers increases linearly with increasing PEG concentration. Inset shows an example of a reference bead (left) and three beads that signal 20kb DNA molecules tethered with click chemistry.

the DNA) while applying a force ramp of 1pN/sec. As shown in Fig. 6.5, the tethered double-stranded DNA molecules show the expected behavior, viz., with increasing end-to-end distance we observe a strongly rising force, a plateau as the DNA overstretches, and a further rise. As expected, for torsionally unconstrained molecules, overstretching of the double-stranded DNA is observed at about 65pN [34]. Torsionally constrained DNA molecules (depicted in grey in Fig. 6.5A) are expected to show overstretching at a force of about 110pN, a force that, unfortunately, is just beyond the reach of our set-up [35]. We find an average contour length of 6.75± 0.04µm (as measured from the extension just before the overstretching plateau), indicating correct attachment of the DNA molecules at the functional end groups. Most importantly, the tethers can withstand a force of >100pN (Fig. 6.5A). The tethers remain stable at this high force for over 12 hours, allowing ample time for measurements. By contrast, DNA molecules attached with the conventional anti-dig tag break off well before the overstretching force (cf. the black line in Fig. 6.5A). In addition, as shown in Fig. 6.5B, the click- chemistry-assembled DNA tethers can be torsionally constrained, which allows for DNA supercoiling studies with magnetic tweezers. For the described conditions, we found half of the tethers to be coilable. Loss of torsional constrain is likely induced by nicking of the DNA. The new attachment strategy is thus found to be suitable for both high force and torque measurements.

In contrast to the binding of DBCO to azide, the bond between biotin and streptavidin on the other end of the DNA is not covalent. Yet, as can be observed from Figure 6.5, this bond also withstands forces of >100pN, which is consistent with earlier reports [17, 18]. For a wide range of applications, the current method, with tethers that contain a mutually orthogonal DBCO/azide bond on one end and biotin/streptavidin on the other, will suffice. Double copper-free click chemistry (with orthogonal click reactions at both bead and surface) can be considered in future applications if even much higher forces are desired.

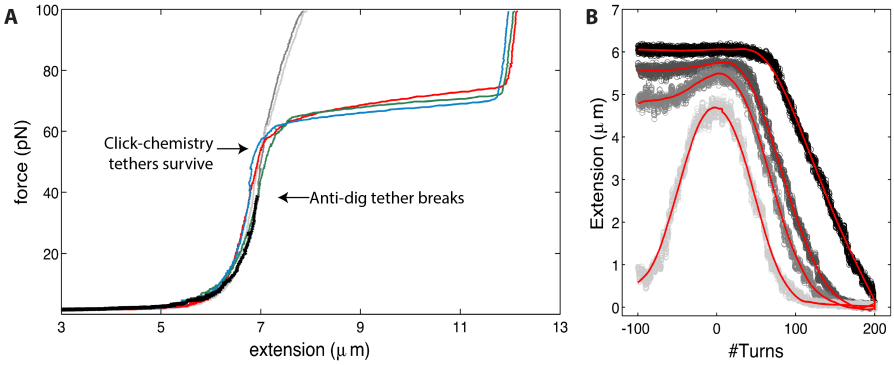

Figure 6.5: **Anchored DNA molecules can be torsionally constrained and withstand forces of >100pN. A.** The DNA molecules anchored with click chemistry show the expected behavior (a strongly rising force, and for unconstrained molecules, a plateau near 65pN as DNA overstretches and a further rise) in a slow force ramp of 1pN/sec. Different colors represent different tethers. All tethers that were bonded by click chemistry withstand forces of over 100pN. By contrast, the DNA anchored with digoxygenin/anti-dig (black) breaks off near 40pN, well before the overstretching point. **B.** Rotation curves at constant forces of (light to dark) 0.5, 1, 3 and 5pN, indicating that this 20kb DNA molecule anchored with click chemistry is torsionally constrained.

The copper-free click chemistry attachment strategy presents many advantages. The reaction between DBCO and azide is relatively fast, specific, it does not require a catalyst, and, importantly for some applications, it can be performed in physiological conditions. Furthermore, azide and DBCO groups are relatively small and inert to biological moieties [27] and thus easy to incorporate. There are already numerous examples of the application of SPAAC reactions in biological systems and even living cells [28, 36]. Examples include use of copper-free click chemistry in non-canonical amino acids [37], imaging in live cells [38], joining of DNA strands [39], and DNA- functionalized nanoparticles [40].

Above, we demonstrated the use of a new DNA-attachment method in magnetic tweezers. We note that it can easily be applied to other single- molecule methods as well. For example, in the same manner, polystyrene beads could be coated with click chemistry functional groups for use in optical tweezers. By immobilizing the PEG linkers on the surface, the same copper-free click chemistry can also be used in atomic force microscopy [41], flow stretching and DNA combing.

Single-molecule force spectroscopy opens up the possibility to apply and measure forces on biomolecules, and study DNA-protein interactions. These *in vitro* experiments with bare DNA and purified protein give great insights into the cell machinery, but purified complexes are taken out of their cellular context. As our new method does not cross-react, it is possible to anchor and measure complexes that are directly extracted from cell lysate. Measuring on this native state of biomolecules can be expected to yield new insight into interactions between biomolecules.

6.4. Conclusions

Traditional methods for anchoring biomolecules have encountered limitations in studying DNA-protein complexes in magnetic tweezers related to low force stability and cross reactivity. Here, we developed a method for covalently anchoring biomolecules with copper-free click chemistry, using the reaction between DBCO and azide. This reaction is bio-orthogonal and no catalyst is needed. Furthermore, it is highly specific and it resists high force (>100pN). The protocol is reproducible, fast and uses commercially available reagents. Perhaps most excitingly, covalently linking molecules with copper-free click chemistry opens up the possibility to measure on a wide variety of DNA- protein complexes and complexes isolated from cell lysate.

References

[1] K. C. Neuman and A. Nagy, *Single-molecule force spectroscopy: optical tweezers, magnetic tweezers and atomic force microscopy.* Nature methods **5**, 491 (2008).

[2] V. Vogel and M. Sheetz, *Local force and geometry sensing regulate cell functions.* Nature reviews. Molecular cell biology **7**, 265 (2006).

[3] J. H.-C. Wang and B. P. Thampatty, *An introductory review of cell mechanobiology.* Biomechanics and modeling in mechanobiology **5**, 1 (2006).

[4] A. D. Rape, W.-H. Guo, and Y.-L. Wang, *The regulation of traction force in relation to cell shape and focal adhesions.* Biomaterials **32**, 2043 (2011).

[5] H. Yin, M. D. Wang, K. Svoboda, R. Landick, S. M. Block, and J. Gelles, *Transcription Against an Applied Force,* Science **270**, 1653 (1995).

[6] Y. R. Chemla, K. Aathavan, J. Michaelis, S. Grimes, P. J. Jardine, D. L. Anderson, and C. Bustamante, *Mechanism of force generation of a viral DNA packaging motor.* Cell **122**, 683 (2005).

[7] R. B. Nicklas, *The forces that move chromosomes in mitosis.* Annual review of biophysics and biophysical chemistry **17**, 431 (1988).

[8] R. B. Nicklas, *Measurements of the force produced by the mitotic spindle in anaphase.* The Journal of cell biology **97**, 542 (1983).

[9] G. Jannink, B. Duplantier, and J. L. Sikorav, *Forces on chromosomal DNA during anaphase.* Biophysical journal **71**, 451 (1996).

[10] J. Brock and K. Bloom, *A chromosome breakage assay to monitor mitotic forces in budding yeast,* J. Cell Sci. **107**, 891 (1994).

[11] I. D. Vlaminck and I. Vidic, *Torsional regulation of hRPA-induced unwinding of double-stranded DNA,* Nucleic acids ... (2010).

[12] B. Xiao, R. Johnson, and J. Marko, *Modulation of HU–DNA interactions by salt concentration and applied force,* Nucleic acids research (2010).

[13] A. Revyakin, R. H. Ebright, and T. R. Strick, *Promoter unwinding and promoter clearance by RNA polymerase: detection by single-molecule DNA nanomanipulation.* Proceedings of the National Academy of Sciences of the United States of America **101**, 4776 (2004).

[14] R. Vlijm, J. S. J. Smitshuijzen, A. Lusser, and C. Dekker, *NAP1-assisted nucleosome assembly on DNA measured in real time by single-molecule magnetic tweezers.* PloS one **7**, e46306 (2012).

[15] M. T. J. van Loenhout, T. van der Heijden, R. Kanaar, C. Wyman, and C. Dekker, *Dynamics of RecA filaments on single-stranded DNA.* Nucleic acids research **37**, 4089 (2009).

[16] R. Vlijm, M. Lee, J. Lipfert, A. Lusser, C. Dekker, and N. H. Dekker, *Nucleosome Assembly Dynamics Involve Spontaneous Fluctuations in the Handedness of Tetrasomes.* Cell reports **10**, 216 (2015).

[17] M. de Odrowaz Piramowicz, P. Czuba, M. Targosz, K. Burda, and M. Szymoński, *Dynamic force measurements of avidin-biotin and streptavdin-biotin interactions using AFM.* Acta biochimica Polonica **53**, 93 (2006).

[18] R. Janissen, B. a. Berghuis, D. Dulin, M. Wink, T. van Laar, and N. H. Dekker, *Invincible DNA tethers: covalent DNA anchoring for enhanced temporal and force stability in magnetic tweezers experiments.* Nucleic acids research , 1 (2014).

[19] G. Neuert, C. Albrecht, E. Pamir, and H. E. Gaub, *Dynamic force spectroscopy of the digoxigenin-antibody complex.* FEBS letters **580**, 505 (2006).

[20] M. K. Walsh, X. Wang, and B. C. Weimer, *Optimizing the immobilization of single-stranded DNA onto glass beads,* Journal of Biochemical and Biophysical Methods **47**, 221 (2001).

[21] R. Janissen, L. Oberbarnscheidt, and F. Oesterhelt, *Optimized straight forward procedure for covalent surface immobilization of different biomolecules for single molecule applications.* Colloids and surfaces. B, Biointerfaces **71**, 200 (2009).

[22] L. Wildling, B. Unterauer, R. Zhu, A. Rupprecht, T. Haselgrübler, C. Rankl, A. Ebner, D. Vater, P. Pollheimer, E. E. Pohl, P. Hinterdorfer, and H. J. Gruber, *Linking of sensor molecules with amino groups to amino-functionalized AFM tips.* Bioconjugate chemistry **22**, 1239 (2011).

[23] C. K. Riener, F. Kienberger, C. D. Hahn, G. M. Buchinger, I. O. Egwim, T. Haselgrübler, A. Ebner, C. Romanin, C. Klampfl, B. Lackner, H. Prinz, D. Blaas, P. Hinterdorfer, and H. J. Gruber, *Heterobifunctional crosslinkers for tethering single ligand molecules to scanning probes,* Analytica Chimica Acta **497**, 101 (2003).

[24] M. Grandbois, *How Strong Is a Covalent Bond?* Science **283**, 1727 (1999).

[25] R. B. Best, E. Paci, G. Hummer, and O. K. Dudko, *Pulling direction as a reaction coordinate for the me-*

chanical unfolding of single molecules. The journal of physical chemistry. B **112**, 5968 (2008).

[26] Y. F. Dufrêne, E. Evans, A. Engel, J. Helenius, H. E. Gaub, and D. J. Müller, *Five challenges to bringing single-molecule force spectroscopy into living cells.* Nature methods **8**, 123 (2011).

[27] E. M. Sletten and C. R. Bertozzi, *Bioorthogonal chemistry: fishing for selectivity in a sea of functionality.* Angewandte Chemie (International ed. in English) **48**, 6974 (2009).

[28] N. J. Agard, J. a. Prescher, and C. R. Bertozzi, *A strain-promoted [3 + 2] azide-alkyne cycloaddition for covalent modification of biomolecules in living systems.* Journal of the American Chemical Society **126**, 15046 (2004).

[29] I. De Vlaminck, T. Henighan, M. T. J. van Loenhout, D. R. Burnham, and C. Dekker, *Magnetic forces and DNA mechanics in multiplexed magnetic tweezers.* PloS one **7**, e41432 (2012).

[30] A. J. W. te Velthuis, J. W. J. Kerssemakers, J. Lipfert, and N. H. Dekker, *Quantitative guidelines for force calibration through spectral analysis of magnetic tweezers data.* Biophysical journal **99**, 1292 (2010).

[31] M. T. J. van Loenhout, J. W. J. Kerssemakers, I. De Vlaminck, and C. Dekker, *Non-bias-limited tracking of spherical particles, enabling nanometer resolution at low magnification.* Biophysical journal **102**, 2362 (2012).

[32] J. Lipfert, X. Hao, and N. H. Dekker, *Quantitative modeling and optimization of magnetic tweezers.* Biophysical journal **96**, 5040 (2009).

[33] W. P. Wong and K. Halvorsen, *The effect of integration time on fluctuation measurements: calibrating an optical trap in the presence of motion blur.* Optics express **14**, 12517 (2006).

[34] S. B. Smith, Y. Cui, and C. Bustamante, *Overstretching B-DNA: The Elastic Response of Individual Double-Stranded and Single-Stranded DNA Molecules,* Science **271**, 795 (1996).

[35] J. F. Léger, G. Romano, A. Sarkar, J. Robert, L. Bourdieu, D. Chatenay, and J. F. Marko, *Structural Transitions of a Twisted and Stretched DNA Molecule,* Physical Review Letters **83**, 1066 (1999).

[36] J. C. Jewett and C. R. Bertozzi, *Cu-free click cycloaddition reactions in chemical biology,* Chemical Society Reviews **39**, 1272 (2010).

[37] A. J. Link, M. K. S. Vink, N. J. Agard, J. A. Prescher, C. R. Bertozzi, and D. A. Tirrell, *Discovery of aminoacyl-tRNA synthetase activity through cell-surface display of noncanonical amino acids.* Proceedings of the National Academy of Sciences of the United States of America **103**, 10180 (2006).

[38] J. M. Baskin, J. a. Prescher, S. T. Laughlin, N. J. Agard, P. V. Chang, I. a. Miller, A. Lo, J. a. Codelli, and C. R. Bertozzi, *Copper-free click chemistry for dynamic in vivo imaging.* Proceedings of the National Academy of Sciences of the United States of America **104**, 16793 (2007).

[39] J. Qiu, A. H. El-Sagheer, and T. Brown, *Solid phase click ligation for the synthesis of very long oligonucleotides.* Chemical communications (Cambridge, England) **49**, 6959 (2013).

[40] A. Heuer-Jungemann, R. Kirkwood, A. H. El-Sagheer, T. Brown, and A. G. Kanaras, *Copper-free click chemistry as an emerging tool for the programmed ligation of DNA-functionalised gold nanoparticles.* Nanoscale **5**, 7209 (2013).

[41] P. Hinterdorfer, H. J. Gruber, F. Kienberger, G. Kada, C. Riener, C. Borken, and H. Schindler, *Surface attachment of ligands and receptors for molecular recognition force microscopy,* Colloids and Surfaces B: Biointerfaces **23**, 115 (2002).

7

Determining the rupture force of the cohesin complex

The alignment of duplicated chromosomes in the middle of the cell is an essential process in the cell cycle, which needs to be tightly regulated. In particular, while microtubules are already pulling the chromosomes towards the spindle poles in metaphase, pre-mature separation of the sister chromatids needs to be prevented. The cohesin complex provides the essential linkage between sister chromatids, presumably by trapping them inside its ring, hereby preventing separation until the cell is ready to divide. Cohesin thus withstands the forces of the microtubule pulling. Direct measurements of the strength and stability of cohesin are, however, missing. We designed an experiment to probe the strength of cohesin by measuring its rupture force with magnetic tweezers. This chapter contains preliminary data on the force spectroscopy, as well as recommendations for pursuing this project.

J.M. Eeftens, J. van der Torre, M. van Loenhout, C.H. Haering, C. Dekker, *unpublished*

7.1. Introduction

Faithful chromosome segregation is one of the most important processes in the cell cycle of eukaryotic cells. Structural maintenance of chromosome proteins such as cohesin and condensin play major roles in this process. In preparation for cell division, the duplicated DNA needs to be organized and compacted into chromosomes. The duplicated chromosomes then align in the center of the cell, where the spindle poles start to pull on the DNA. As the processes of aligning and pulling occur simultaneously, it is essential that this process is precisely regulated in order for the DNA to be equally divided over the daughter cells. Cohesin provides the essential linkage between sister chromatids, ensuring the sister chromatids are held together until the cell is ready to divide [1, 2].

Like all SMC complexes, cohesin contains of a heterodimer of SMC proteins (Smc1-Smc3, Figure 7.1A)[3]. SMC proteins consist of ~50nm long coiled coil structures, interacting at the hinge on one side, and with ATPase heads on the other side. Although essential in vivo, the role of ATP binding and hydrolysis is largely unknown. The ring is closed by protein from the kleisin family, in the case of cohesin Scc1. A fourth subunit, Scc3, interacts with Scc1. Numerous other proteins have been found to contribute to cohesion more indirectly (reviewed in [4, 5]).

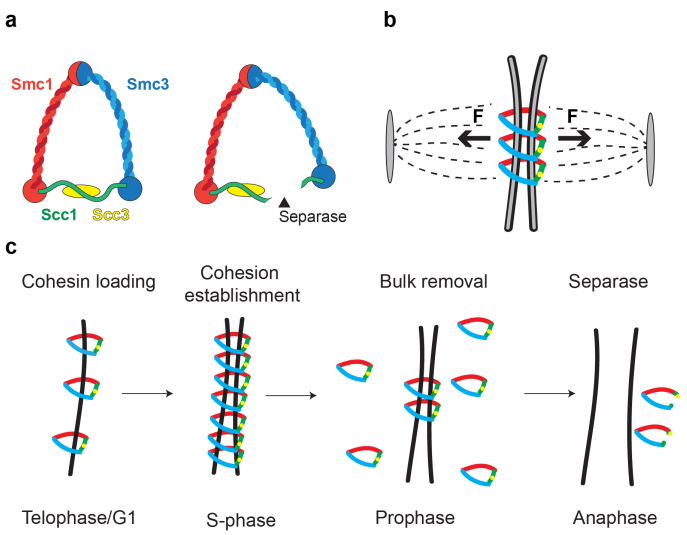

Figure 7.1: **a.** Schematic representation of cohesin and its cleavage by separase. **b.** Cohesin resists the forces exerted by the microtubules while the chromosomes align. **c.** Cohesin is loaded in Telophase. Most of the cohesin is removed from chromosomal arms during prophase, while complexes at the centromere remain associated with the DNA until cleavage by separase.

Eukaryotic chromatid cohesion starts from the moment sister chromatid are generated in S-phase until their segregation in anaphase (Figure 7.1C). In vertebrates, the bulk of the cohesin is already removed during prophase [6]. Only a small percentage remains, mainly near the centromere. The destruction of cohesion at the metaphase to anaphase transition depends on the cleavage of the Scc1 subunit by separase [7]. Besides its role in sister chromatid cohesion, cohesin also has function in DNA damage pathways and gene regulation [8]. It is presumed that cohesin links sister chromatids by entrapping their DNA within its tripartite ring structure, and it has been shown that cohesin embraces DNA topologically rather than physically [9, 10]. Cohesin must withstand the large microtubule forces that align chromosomes by pulling towards opposite spindle poles (Figure 7.1B). Note that in female oocytes, DNA can spend over 40 years stably cohesed [14, 15].

Cohesin rings are thus expected to be remarkably strong and stable, but direct measurements of its mechanical strength are missing [16]. We try to probe this mechanical strength by pulling on the cohesin complex with magnetic tweezers, in a conformation that closely mimics the *in vivo* geometry. In this chapter, we list the various strategies and results, working towards this goal. We end with recommendations for pursuing this project.

7.2. Experimental procedures

To measure the rupture force of the cohesin complex, we need to design a geometry of the protein in complex with DNA that we can tether in our magnetic tweezers set-up. We used two different strategies for isolating the cohesed minichromosomes from yeast. First, we purify cohesed mini-chromosomes by pulling down the plasmid DNA, where we use the interaction of TetO with TetR to pull out the protein-DNA complex (Figure 7.2). Second, we purify cohesin loaded onto a mini chromosome by pulling down the protein, where we use a SNAP-tagged cohesin to pulldown the protein loaded onto the plasmid (Figure 7.3). The final experimental geometry is pictured in the last panel of both figures.

In both strategies, a 6kb plasmid was introduced into the strain. While the complex is on the bead, we nick the plasmid twice, which removes a short piece of DNA, thereby creating a single strand DNA gap to which we then ligate DBCO- and biotin-functionalized oligos. We will stepwise describe these the protocols for these purifications and for control experiments in the section below.

Purification of cohesed mini-chromosomes by DNA pulldown

This protocol is schematically described in Figure 7.2. Strain 4117 was grown on SD-W plates at 30°C. One colony was inoculated in YPAD medium and grown until OD600=0.8. Then, 2.5ml of 1mg/ml nocodazole was added, and grown for 2 hours at 30°C. Cells were spun down (4000 rpm, 4°C) and resuspended in cold water twice. Cells were spun down again and resuspended in 0.1M Tris-HCl, 10mM DTT, 0.01mg/ml nocodazole, pH 9.4, and incubated for 15 minutes at room temperature. Cells were spun down and resuspended in cold water once more. Next, cells were spun down and resuspended in prewarmed spheroblasting buffer (1M sorbitol, 50mM Tris-HCl, 1mM CaCl2, 1mM MgCl2,

0.08mg/ml lyticase, 0.01mg/ml nocodazole, pH7.5), and incubated in the shaker at 30°C, 100rpm. After 30 minutes, it was checked if spheroblasts were formed under the microscope (with 2% sarcosyl). Spheroblasts were spun down at 4000rpm for 6 minutes, carefully resuspended in cold 1M sorbitol, and spun down again. Spheroblasts were then lysed on ice for 30 minutes in 2.5 lysis buffer (25mM HEPES-KOH, 50mM KCl, 200mM NaCl, 10mM MgSO4, 0.25% Triton X-100, 1mM PMSF, 1mM DTT, 2x Complete protease inhibitor, 100μg/ml DNAse-free RNAse A). Lysate was spun down at 10000 rpm for 5 minutes in 2ml eppendorf tubes at 4°C. 50μl extract was put on hold to load on gel as "input".

For immunoprecipitation, the Life Technologies Dynabeads Prot G kit was used. Meanwhile, 75μl beads were washed with the Ab-binding buffer provided by the kit. Beads were resuspended in 225μl Ab-bindin buffer with 7.5μl anti-PK antibody, and incubated on a wheel for 1.5 hours at room temperature. Beads were then resuspended in 75μl washing buffer (provided by the kit). 25μl beads were added to 1ml lysate. This was incubated overnight at 4°C on a wheel. The next day, 50μl unbound lysate was put on hold, and beads were washed 3 times with lysis buffer, on a wheel at 4°C.

Next, beads were combined in a single tube and resuspended in 650μl NEB buffer 3.1 (50mM Tris-HCl, 100mM NaCl, 10mM MgCl2, 100μg/ml BSA, 1mM DTT, 1x Complete), nicking enzymes were added (8μl Nb.BbvCl+8μl Nt.BspQ1), and incubated 2 hours at room temperature on a wheel. After incubation, beads were washed three times with lysis buffer. For ligation, beads were resuspended in 50μl pre-warmed Promega lysis buffer, and 2.5μl of each handle (1μg/ml) were added. This was incubated for 10 minutes at 37°C on a wheel, then the temperature was ramped in 20 minutes to 16°C. After reaching 16°C, 3μl T4 ligase was added and this was incubated 4 hours at 16°C. Then beads were washed three times with lysis buffer again. For elution, beads were resuspended in 250μl lysis buffer with 50μl anhydrotetracycline (1μg/ml). This was incubated for 40 minutes at 16°C on a wheel. Supernatant was stored at -20°C and used for tweezer experiments. Strain 3261, containing TEV cleavable cohesin, was grown and treated in the same way.

Purification of cohesed mini chromosomes by protein pulldown

The second strategy (purification by protein pulldown) is schematically described in Figure 7.3. Strain 2874 was grown on SD-W plates at 30°C (Figure 7.3). One colony was inoculated in YPAS medium and grown and lysed as described above, with the exception that cells were not arrested (no nocodazole was added).

Meanwhile, an 8kb DNA molecule with a SNAP-catcher tag was prepared by linking an NHS-benzylguanine linker (NEB) to an amine/biotin-tagged DNA molecule. During lysing, M270 streptavidin coated beads were incubated with this construct for 20 minutes. Beads were then washed with T20E5+Tween. Lysate was then added to the beads and incubated for 1 hour at roomtemperature. Lastly, 50μl supernatant was kept as "unbound" and beads were washed with lysis buffer. These beads could directly be used as tweezer constructs.

For control experiments, after washing the beads with lysis buffer, the construct was treated with restriction enzyme NaeI for 1 hour at 37°C. This enzyme cut the 8kb linear molecule close to the attachment to the cohesin. Some of the eluate was then used to do

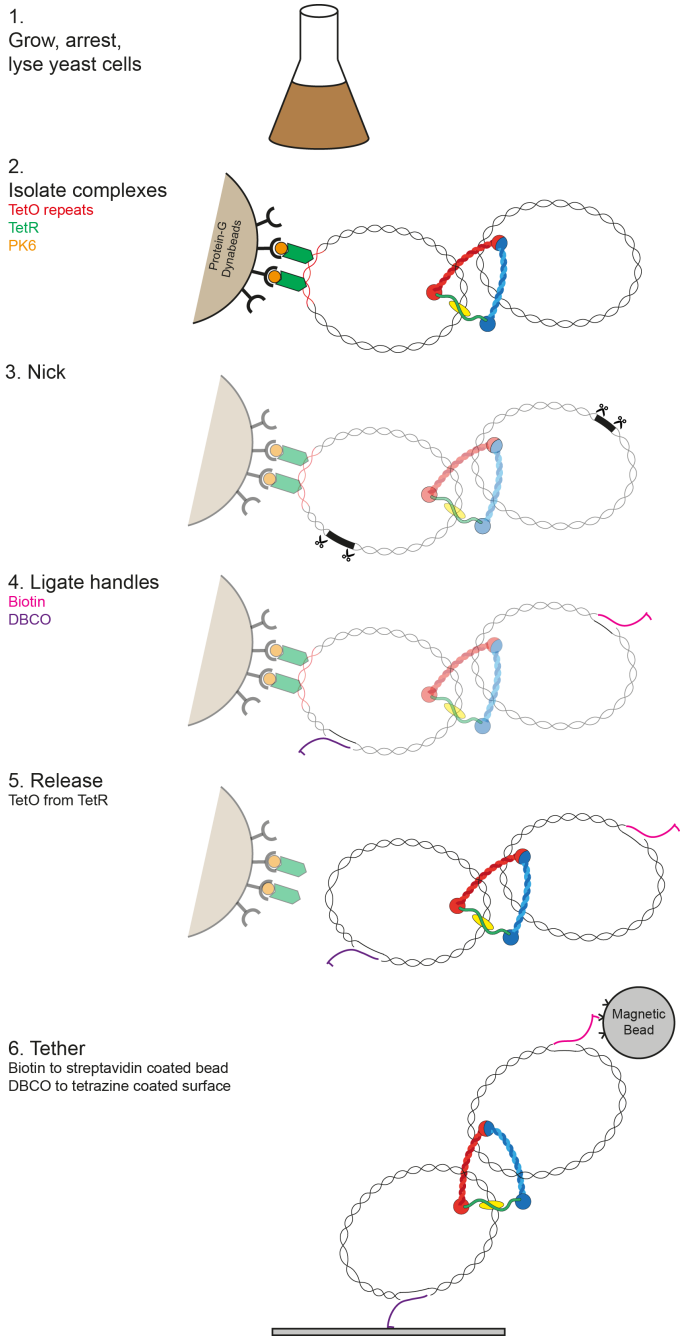

Figure 7.2: **Purification of cohesed mini chromosomes by pulldown of the plasmid.**

a PCR (to check for presence of the plasmid). The rest of the eluate was treated with 1μl DNAse for 1 hour at 37°C and subsequently ran on a protein gel to check for presence of cohesin.

Southern blot

This protocol was adapted from an earlier protocol [9]. All samples of interest were ran on a regular 0.8% agarose gel in 1x TAE. For the control, we used plasmid BN2202. The agarose gel was then depurinated upside down in 0.13M HCl while gently shaking for 10 minutes. The gel was then washed with MQ, followed by denaturing buffer (1.5M NaCl, 0.5M NaOH) for 30 minutes, followed by neutralisation buffer (1.5M NaCl, 0.5M Tris-HCl, pH7.5) for 30 minutes, and lastly with blotting buffer (20x SSC). Meanwhile the blotting chamber was prepared. Three pre-wetted (in blotting solution) Whatman blot papers (20x40cm) were placed on a pvc-plate, sides of the paper hangin into the tank. There should be no bubbles between the papers. On top, three more pre-wetted Whatman papers were placed (20x25), again preventing bubbles. On top of this the (still upside down) agarose gel was placed. Next, 20x25cm Millipore Immobilon NY+ (positive charged) membrane was placed on top of the gel. This should not be pre-wet, the membrane should suck itself on the gel. Next, again, three pre-wetted 20x25 Whatman papers. The tank was filled with sufficient blotting solution and the sides were sealed with parafilm. A big stack of paper towels was placed on top, with a weight on top to strengthen the capillary power of the plot. This was blotted overnight. DNA was crosslinked to the membrane for 1 minute in a UV-tray. The blot was then treated with pre-hybridisation buffer (35ml block/hybmix from Amersham, 1g NaCl, 1.4g blocking powder) for 1 hour at 55°C. We used 6 specific PCR probes containing biotin-dUTPs using Promega GoTaq (primers shown in Table 1). The probes were denatured for 5 minutes at 100°C, before adding 100ng it to the membrane and incubating overnight at 55°C. The next day, the membrane was washed twice with SSC buffer (twice, 5 minutes each), then with 1x SSC buffer with 0.1%SDS (twice, 30 minutes each), then with 0.1x SSC with 0.1% SDS (twice, 30 minutes each). All washed were done at 55°C. Detection was done using the Thermo Fisher Chemiluminescent Nucleic Acid Detection module. Finally, the membrane was scanned using the Typhoon scanner.

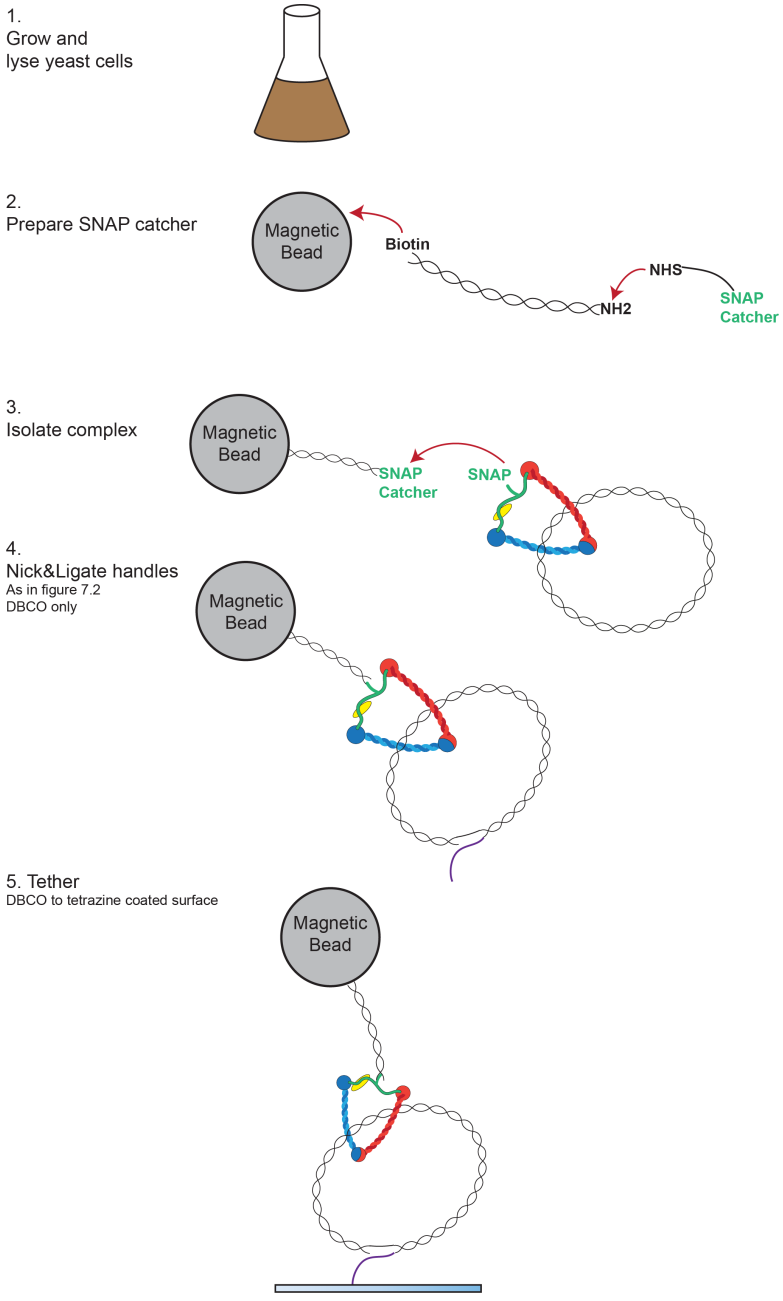

Figure 7.3: **Purification of cohesed mini chromosomes by pulldown of the SNAP-tagged protein.**

Table 1: Primers used to make PCR probes

PCR probe	Primer sequence
PCR probe 1	GGCGGGTGTCGGGG GGCGGGTGTCGGGG
PCR probe 2	AATTTCAAGTCTTGTAAAAGCATATAAAAATAGTTCAGGCA AGTAATAACCTATTTCTTAGCATTTTTGACGAAATTTGC
PCR probe 3	GGGGGTTGACTTTTACCATTTCACC GGTAATACCGACCAATGCATTGTTTTACG
PCR probe 4	TGATCTATGTAAGAAATGGAAGTTTTCTCCCTTAGT CAATACAGCCCACCTCTCCTTAGC
PCR probe 5	TTTTCAAAGATGACTAAAATAAGTGAAATTTCAACATTAACTTCG TGAGCAAAACTTCCACCAGTAAACGT
PCR probe 6	CGACAGCGAAGATAACGGTTACACA ATCAAAATTGAAATTTCTAACCACTGTGTCATCC

PCR detection

We set up a specific PCR to detect the plasmid in different purification sales. We used PCR probe 3 (Table 1) as primers. The PCR was always done on diluted samples (dilution range as shown in the figures). The PCRs were performed using KOD Xtreme Polymerase (Novagen) using the standard reaction conditions and the following cycling conditions: denaturing 94°C for 2 minutes, followed by 40 cycles of 98°10 seconds, 60°C 30 seconds, 68°C 30 seconds. The PCR product was detected on a 1% agarose gel ran with 1x TAE buffer, and detection by ethidium bromide.

Magnetic tweezers

We used a multiplexed magnetic tweezers as described in [17]. Azide-coated flowcells were prepared as described in [18]. Constructs, prepared as described above, were incubated in the flowcells for 1 hour. The applied force was determined by Brownian motion of the bead. A force calibration curve was made to correlate the magnet height to the force. For force ramp experiments, force was increased linearly, and kept constant after reaching maximum. For force clamp experiments, force was increased instantly and kept constant, either until rupture or to a maximum measurement time of 20 minutes.

7.3. Results

Isolation and detection of cohesed minichromosomes

We used two different strategies for isolating the cohesed minichromosomes from yeast. With various controls described below, we attempted to convince ourselves that we were purifying the correct construct. First, throughout the protocol we saved sample at various stages for analysis on southern blot. We chose this detection method because ideally, this would enable us to detect single and cohesed plasmids. Unfortunately, we could never detect our samples with Southern blot, while the positive control (the bare plasmid) was detected to low concentrations (0.0625ng). This indicates that the concentration of our isolated constructs was too low to detect, or the probe was unable to hybridize

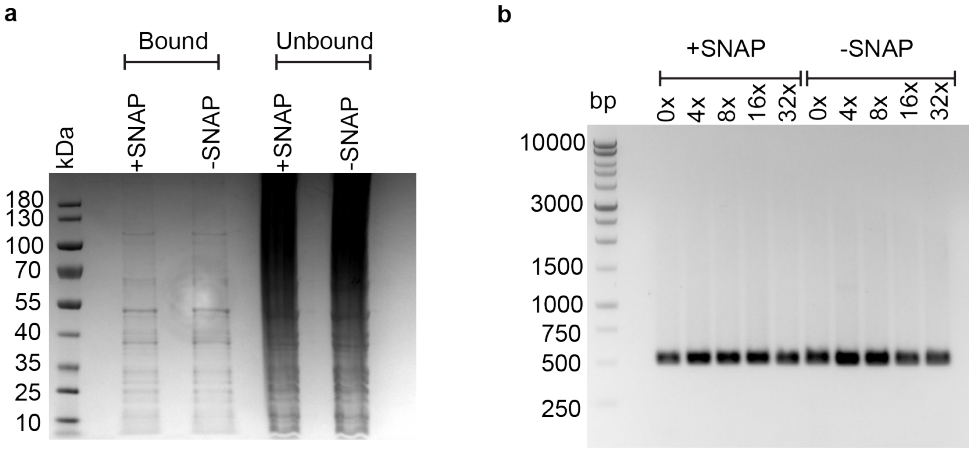

Figure 7.4: **a.** Protein gel from purification with SNAP-tagged and untagged strains. **b.** PCR product from purification with SNAP-tagged and untagged strains. The PCR product is expected to run at 500bp.

to our isolated samples, or the purification simply did not work. We also tried to visualize the constructs with AFM, but never found any recognizable structures.

We wondered if the samples that we isolated were cohesed plasmids. To check this, we used Strain 3261, which contains a TEV-cleavable cohesin. If we would load cohesed minichromosomes onto beads, enzymatic cleavage of cohesin should result in release of one of the cohesed plasmids. We ligated oligos to the plasmids as described, and attached them to streptavidin-coated beads. Half of the complexes should be bound with only one plasmid, the other one presumably attached by cohesin. If we then added TEV (kindly donated by Simon Lindhoud), this second plasmid was expected to release. We did a PCR on the released samples but could never detect the presence of DNA. This could either indicate that the TEV cleavage failed, or that the complex is not as we draw it in Figure 7.2.

As we did not succeed to isolate cohesed minichromosomes as described above, we were not convinced that this purification strategy worked. Therefore, we tried a second strategy by purifying via cohesin itself, as indicated in Figure 7.3. We used strain 2874, that contains a SNAP-tagged cohesin. To test if we were specifically pulling out the tagged cohesin protein, we compared the SNAP-tagged strain to the non-tagged strain. When purifying with the SNAP-catch construct, the strain with untagged cohesin should not give any yield. Strikingly, when we ran the proteins on a protein gel, we found the same product for both the tagged and the untagged cohesin (Figure 7.4a). We could also detect the plasmid in both strains with PCR (Figure 7.4b). This indicates that our purification was not working as designed.

Force spectroscopy

Although we could not show that we isolated cohesed mini-chromosomes, we nevertheless tried to tether the DNA-isolated constructs in a magnetic tweezers set-up. We did

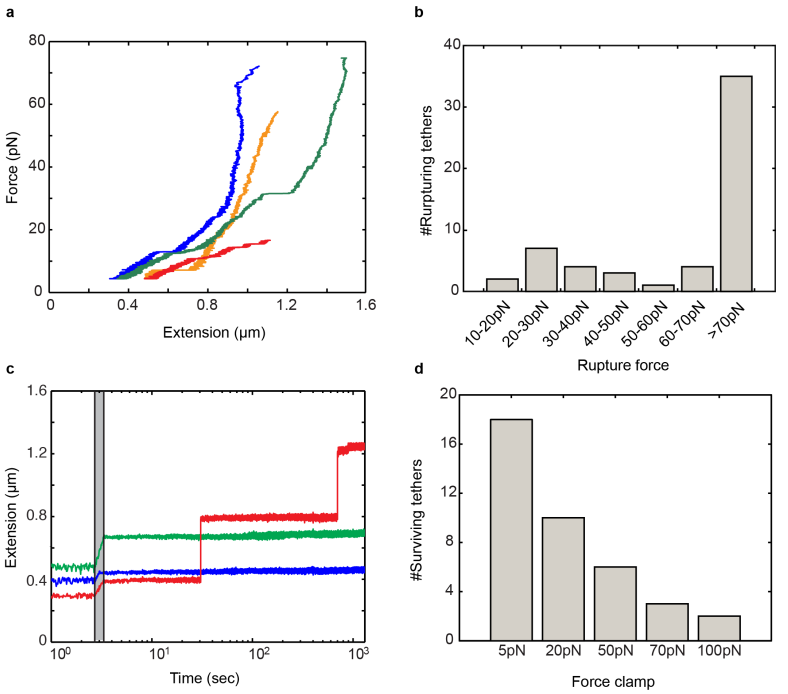

Figure 7.5: **a.** Histogram of rupturing tethers in a force-ramp experiment. **b.** Examples of traces in a force ramp experiment. The red tether already ruptured at about 20pN, while the green tether survived until 75pN. **c.** Histrogram of surviving tethers in a force-clamp experiment. **d.** Examples of traces in a 20pN force clamp. The grey area represents the time where the magnet was moved from 5pN to 20pN. All tethers depicted here survived the clamp. The red trace shows large steps.

force spectroscopy on the tethers of the expected length (~2μm). We took two different approaches: a force ramp and force clamp. In force ramp experiments, we applied ramps of 1pN/sec and measured the force at which the tether ruptured. Examples of rupture traces are shown in Figure 7.5a. About half of the tethers did not rupture up to a force of 70pN (Figure 7.5b, N=56). For the tethers that did rupture before 70pN, a very broad distribution was found. There is no clear peak for a certain force.

In force-clamp experiments, we used force clamps of 20, 50, 70, and 100pN, and measured the lifetime of the tethers at that force. Examples of traces at the 20pN clamp are shown in Figure 7.5d. If the tethers had not ruptured after 20 minutes, the force clamp was moved to the next level. All tethers survived the 5pN clamp, and about half survived the 20pN clamp (Figure 7.5c, N=18). Surprisingly, two tethers survived a force clamp of 100pN. Note that the dataset is too small to analyze the lifetime distribution within a clamp.

7.4. Discussion and Outlook

The biochemical controls showed that we were unable to successfully isolate the constructs as we pictured them. The PCR on the plasmid showed higher yields for the

protein-purified samples than for the DNA-purified samples, but also here we could not convincingly show that we had obtained the right construct. It is important to remember that when isolating from live cells, we purify everything that is associated with the DNA as well. Accordingly, there will be many other proteins associated with the DNA, e.g. nucleosomes. The rupture-force dataset is very limited and shows a wide variety. As we could not confirm we were pulling on cohesed mini chromosomes, this data is difficult to interpret. Because of the complexity and the lack of convincing controls, we would not recommend pursuing this direction of isolating from live cells.

Fortunately, the field of protein purification, and more specifically *in vitro* loading of cohesin, has progressed a lot in the past years [10, 19]. This approach is significantly simpler, easier to control, and the DNA is free of unwanted proteins. With *in vitro* loading, one could still take the two directions described above. Pulling on two cohesed plasmids resembles the *in vivo* situation best, but controlling the number of cohesin rings between the two rings is an uncertainty. Alternatively, one could pull on a cohesin protein that is loaded onto a single plasmid. For this approach, it is important to consider the position of the label on the protein, and check if the rupture-force depends on the position of this tag.

After succeeding to get a basic idea about the rupture force, a good approach would be to incorporate fluorescent tags at various places within the tweezer construct. In this way, if one fluorophore leaves the field of view and another stays, one can determine where the rupture happened. It would also be interesting to use cohesin complexes with crosslinks between the subunits. If the distribution of rupture forces shifts and becomes much higher when a certain link is introduced, this interface might be responsible for opening up. It would also be interesting to investigate the influence of other factors on cohesin stability, for example, the cohesin loading complex.

References

[1] T. Tanaka, J. Fuchs, J. Loidl, and K. Nasmyth, *Cohesin ensures bipolar attachment of microtubules to sister centromeres and resists their precocious separation.* Nature cell biology **2**, 492 (2000).

[2] K. Nasmyth, *How might cohesin hold sister chromatids together?* Philosophical Transactions of the Royal Society of London B: Biological Sciences **360** (2005).

[3] C. H. Haering, J. Löwe, A. Hochwagen, and K. Nasmyth, *Molecular Architecture of SMC Proteins and the Yeast Cohesin Complex,* Molecular Cell **9**, 773 (2002).

[4] J.-M. Peters, A. Tedeschi, and J. Schmitz, *The cohesin complex and its roles in chromosome biology.* Genes & development **22**, 3089 (2008).

[5] K. Nasmyth and C. H. Haering, *Cohesin: its roles and mechanisms.* Annual review of genetics **43**, 525 (2009).

[6] I. Sumara, E. Vorlaufer, C. Gieffers, B. H. Peters, and J.-M. Peters, *Characterization of Vertebrate Cohesin Complexes and Their Regulation in Prophase,* The Journal of Cell Biology **151** (2000).

[7] K. Nasmyth, F. Uhlmann, and F. Lottspeich, *Sister-chromatid separation at anaphase onset is promoted by cleavage of the cohesin subunit Scc1,* Nature **400**, 37 (1999).

[8] K. S. Wendt and J.-M. Peters, *How cohesin and CTCF cooperate in regulating gene expression.* Chromosome research : an international journal on the molecular, supramolecular and evolutionary aspects of chromosome biology **17**, 201 (2009).

[9] D. Ivanov and K. Nasmyth, *A physical assay for sister chromatid cohesion in vitro.* Molecular cell **27**, 300 (2007).

[10] Y. Murayama and F. Uhlmann, *Biochemical reconstitution of topological DNA binding by the cohesin ring.* Nature **505**, 367 (2014).

[11] R. B. Nicklas, *How Cells Get the Right Chromosomes,* Science **275**, 632 (1997).

[12] R. B. Nicklas,
textit The forces that move chromosomes in mitosis. Annual review of biophysics and biophysical chemistry **17**, 431 (1988).

[13] J. G. Ault and R. B. Nicklas, *Tension, microtubule rearrangements, and the proper distribution of chromosomes in mitosis,* Chromosoma **98**, 33 (1989).

[14] T. Chiang, F. E. Duncan, K. Schindler, R. M. Schultz, and M. A. Lampson, *Evidence that Weakened Centromere Cohesion Is a Leading Cause of Age-Related Aneuploidy in Oocytes,* (2010).

[15] R. Jessberger, *Age-related aneuploidy through cohesion exhaustion.* EMBO reports **13**, 539 (2012).

[16] M. V. Loenhout, *Single-molecule studies of the twisted, knotted, and broken genome,* (2012).

[17] I. De Vlaminck, T. Henighan, M. T. J. van Loenhout, D. R. Burnham, and C. Dekker, *Magnetic forces and DNA mechanics in multiplexed magnetic tweezers.* PloS one **7**, e41432 (2012).

[18] J. M. Eeftens, J. van der Torre, D. R. Burnham, and C. Dekker, *Copper-free click chemistry for attachment of biomolecules in magnetic tweezers,* BMC Biophysics **8**, 9 (2015).

[19] Y. Murayama and F. Uhlmann, *Chapter 2 An In Vitro Assay for Monitoring Topological DNA Entrapment by the Chromosomal Cohesin Complex,* **1515**, 23 (2017).

Summary

Every cell deals with the challenge of organising its DNA. First, the DNA needs to be compacted in size by several orders of magnitude. For example, in each human cell, 2 meters of DNA need to fit inside a micron-sized cell nucleus. Second, the DNA needs to stay accessible for cellular processes such as transcription and replication. To achieve these goals, cells are assisted by proteins that organise the DNA by locally bending the DNA, wrapping DNA around them, or by making DNA loops. A prime example are the Structural Maintenance of Chromosomes (SMC) family of proteins, which is known to be essential for DNA organisation. In eukaryotes, the SMC complex cohesin is responsible for keeping sister-chromatids together until the cell is ready to divide. Without cohesin, division might occur prematurely, leading to unevenly divided DNA. The SMC complex condensin is responsible for compacting the DNA into mitotic chromosomes. Indeed, without condensin, the DNA does not form properly organised chromosomes. This thesis describes a series of experiments that aim to understand the molecular mechanism of these SMC proteins.

In part I of this thesis, SMC proteins are introduced. Despite the fact that both cohesin and condensin are essential proteins that were discovered decades ago, their molecular mechanism is still unknown. **Chapter 1** gives an introduction into DNA organisation, as well as a short history of SMC proteins. How do these SMC proteins use their large ring structure to mechanistically organise the DNA? To answer this question, we believe that biophysical experiments are key. **Chapter 2** reviews the insights obtained so far with biophysical methods such as single-molecule imaging, force spectroscopy, and fluorescent imaging techniques. As crystal structures are difficult to obtain from the large and flexible SMC subunits, most of the information on their conformation originates from imaging studies with electron microscopy and atomic force microscopy. However, the abundance of imaging studies has not resulted in a consensus uniform conformation. With magnetic tweezers, the DNA condensation activity of several SMC complexes has been investigated, all observing compaction with remarkably large steps (70-200 nm). With DNA-flowstretching and DNA-curtain experiments, SMC proteins' ability to move on the DNA can be monitored.

Part II of this thesis focuses on investigating the structure and mechanism of the eukaryotic condensin complex. In **chapter 3**, we probed the topology of the Smc2-Smc4 dimers of the *S. cerevisiae* condensin complex with high-speed atomic force microscopy. With this technique, we visualised the dynamics of condensin dimers in real-time in near-physiological conditions. The conformation of SMC complexes is of great interest, as it is likely to mechanistically determine their biological function. We showed that the Smc2-Smc4 dimers are remarkably flexible, with coiled-coils with a persistence length of only~4nm. We furthermore found that the dimers can adopt various conformations.

The heads can dynamically engage and disengage with each other, as well as with the hinge. Our combined findings indicate that condensin complexes have the structural flexibility for DNA entrapment.

Chapter 4 describes a single-molecule fluorescence imaging study where we demonstrated the ability of the *S. cerevisiae* condensin holocomplex to translocate along DNA. In a DNA-curtain assay, DNA is stretched between barriers. By labelling condensin fluorescently and imaging with total internal reflection fluorescent microscopy, we visualised condensin binding to DNA at a single-molecule level. We found that condensin was able to move along the DNA in the presence of ATP, consistent with what would be expected for a DNA-translocating motor protein. Condensin traveled an average distance of 10 kb, with an average velocity of 60 basepairs per second. When we used an ATPase mutant condensin complex, we did not observe this translocation activity. Similary, when a non-hydrolyzable form of ATP was used, no translocation was observed. Condensin was also able to move a second DNA molecule along the stretched DNA, indicating that condensin is able to interact with two DNA molecules simultaneously. Combined, these results provide support for the loop-extrusion model of DNA compaction, for which motor activity of SMC proteins is a prerequisite.

The DNA compaction activity of condensin was further investigated in **chapter 5** with magnetic tweezers. This assay is especially suitable to monitor the end-to-end length of DNA, and we can study the condensin-mediated compaction in real-time. We found that the rate of compaction is dependent on the force applied. Forces above 2pN completely abolished compaction. Higher concentrations of protein or ATP resulted in faster compaction. While initial binding of condensin to DNA did not require DNA, we did not see compaction at all without the addition of ATP. Upon ATP hydrolysis, condensin associated with DNA in a salt-resistant manner, suggesting a topological binding mode. Our results lead us to propose a multi-step binding model for condensin. We also included a discussion on the implications our findings on the various models of DNA compaction.
Cohesin is expected to be a remarkably strong and stable molecule, but direct measurements of this property are missing. Part III works towards answering this question. In **chapter 6**, we describe a novel method for attaching biomolecules in magnetic tweezers: with copper-free click chemistry. The relevant force regime for many biological processes is above tens of pN, but with conventional attachment methods, problems arise as the molecule can detach from the attachment points at the bead or the surface. An additional problem arises when one wants to measure on protein-DNA complexes, as the attachment chemistry might lead to aspecific reactions with the proteins. Our new method uses copper-free click chemistry: the reaction of a DBCO-tagged molecule with a azide-functionalized surface. This technique leads to covalently linked DNA tethers that are torsionally constrained. These tethers can withstand high forces, and since DBCO is not a native protein group, it is highly specific. This new technique opens up the possibility to anchor DNA-protein complexes taken directly form cell-lysate.

In **chapter 7**, we present our initial efforts to develop an experimental set-up to probe the strength of the cohesin complex by measuring its rupture force with magnetic tweezers force spectroscopy. First, we needed to design a geometry of the protein in complex with DNA that closely resembles the *in vivo* situation, and that we can tether in our

magnetic tweezers flow cell with copper-free click chemistry. We describe two different strategies: purifying cohesed mini chromosomes by pulldown of the DNA from cells, and purifying loaded cohesin by pulldown of SNAP-tagged cohesin. We present biochemical controls that, unfortunately, showed that our efforts could not yield a sufficiently clean sample to use in single-molecule experiments. Nevertheless, we show results of our pilot experiments with pulling on cohesed mini chromosomes. We end with recommendations for pursuing this project.

Samenvatting

Elke cel staat voor dezelfde uitdaging: hoe organiseer ik al dat DNA in het kleine celvolume? Eerst moet het DNA opgevouwen worden. In elke menselijke cel zit bijvoorbeeld 2 meter DNA, dat in een celkern van een micrometer moet passen. Ten tweede moet het DNA toegankelijk blijven voor cellulaire processen als transcriptie en replicatie. Om dit te bewerkstelligen wordt het DNA geholpen door eiwitten die het DNA organiseren, bijvoorbeeld door het DNA lokaal te buigen, DNA om het eiwit te winden, of door lussen in het DNA te maken. Een belangrijk voorbeeld van zulke eiwitten is de SMC familie ("structureel onderhoud van DNAëiwitten). Deze eiwitten zijn essentieel voor de DNA organisatie. In eukaryoten is het SMC eiwit cohesin verantwoordelijk voor het bij elkaar houden van zuster chromatiden tot het moment dat de cel klaar staat om te delen. Zonder cohesin kan er premature celdeling voorkomen, wat kan leiden tot ongelijk verdeelde chromosomen. Het SMC eiwit condensin is verantwoordelijk voor het opvouwen van DNA in chromosomen die klaar gemaakt worden voor de celdeling. Zonder condensin wordt het DNA niet netjes georganiseerd en opgevouwen. Dit proefschrift beschrijft experimenten die als doel hebben meer te begrijpen over het moleculaire mechanisme van deze SMC eiwitten.

In deel I van dit proefschrift worden SMC eiwitten geïntroduceerd. Hoewel zowel cohesin als condensin al decennia geleden ontdekt zijn, en beide essentieel zijn voor elke vorm van leven, weten we nog weinig over hun moleculaire mechanisme. **Hoofdstuk 1** introduceert de DNA organisatie en beschrijft de geschiedenis van SMC eiwitten. Hoe gebruiken SMC eiwitten hun grote ringstructuur om DNA te organiseren? Om deze vraag te beantwoorden, denken wij dat biofysische experimenten de sleutel kunnen zijn. In **hoofdstuk 2** worden de inzichten beschreven die tot dusver zijn verworven met biofysische technieken zoals enkel-molecuul microscopie, krachtspectroscopie en fluorescentie microscopie. Omdat ze zo groot zijn is het is lastig om de kristalstructuren van SMC eiwitten op te lossen. De meeste informatie die we hebben over de structuur van SMC eiwitten komt dus van studies met electronenmicroscopie of atomaire kracht microscopie. De overvloed aan beeldmateriaal heeft echter niet geresulteerd in een consensus over de conformatie. Met een magnetisch pincet kan de DNA condensatie-activiteit van SMC eiwitten worden onderzocht. Alle studies op dit gebied vinden zeer grote condensatiestappen (70-200nm). Met DNA dat gestrekt is door stroming en zogenaamde "DNA-gordijn"technieken kan de mogelijkheid van SMC eiwitten om op DNA te bewegen worden bekeken.

De focus van deel II van dit proefschrift ligt op het onderzoeken van de structuur en het mechanisme van het eukaryotische condensin complex. In **hoofdstuk 3** kijken we naar de topologie van Smc2-Smc4 dimeren uit *S. cereviseae* (bakkersgist) met hoge snelheid atomaire krachtmicroscopie. Met deze techniek kunnen we de dynamica van deze condensin dimeren visualiseren op snelheid en in fysiologische condities. De con-

formatie van SMC complexen is interessant omdat het zeer waarschijnlijk gekoppeld is aan de biologische functie. Wij laten zien dat de Smc2-Smc4 dimeren verrassend flexibel zijn, en dat de zogenaamde "coiled coils"(opgerolde spoel subeenheden) een persistentie lengte van maar ~4nm hebben. Verder vinden we dat de dimeren verschillende conformaties aannemen. De "koppen"(uiteinden van de opgerolde spoel subeenheden) kunnen dynamisch met elkaar en met het "scharnier"domein interacteren. Onze bevindingen wijzen erop dat de condensin complexen de intrinsieke flexibiliteit hebben om DNA te vangen.

Hoofdstuk 4 beschrijft een enkel-molecuul fluorescentie microscopiestudie waarin we laten zien dat het *S. cerevisiae* condensin complex het vermogen heeft om zich over DNA te verplaatsen. In de DNA-gordijn techniek is DNA opgespannen tussen twee barrières. Door condensin een fluorescent label te geven en dit in beeld te brengen met totale interne fluorescentiemicroscopie, kunnen we visualiseren hoe condensin bindt aan DNA op het enkel-molecuul niveau. We vinden dat condensin zich over DNA kan verplaatsen in de aanwezigheid van ATP. Dit is consistent met de verwachting voor een DNA-translocatie motor eiwit. Condensin verplaatst zich gemiddeld over een afstand van 10kb, met een gemiddelde snelheid van 60 baseparen per seconde. Als we een AT-Pase mutant gebruiken, zien we geen translocatie. We zien ook geen translocatie als we een niet-hydrolyseerbare vorm van ATP gebruiken. Condensin kan ook een tweede molecuul meetrekken over het gestretchte DNA. Dit wijst erop dat condensin met twee DNA moleculen tegelijkertijd kan binden. Deze resultaten ondersteunen het "lus-verdrijf"model voor DNA condensatie.

Het DNA condensatiemechanisme wordt verder onderzocht in **hoofdstuk 5** met een magnetisch pincet. Deze techniek is zeer geschikt voor het monitoren van de mate waarin DNA gestrekt is. Met deze techniek kunnen we de condensatie van DNA door condensin volgen. We vinden dat de snelheid waarmee DNA gecondenseerd wordt afhankelijk is van de kracht op het DNA. Het DNA kan niet meer condenseren bij krachten boven de 2pN. Hogere eiwitconcentraties en meer ATP zorgen voor snellere condensatie. Voor de initiële binding van condensin aan DNA is geen ATP vereist, maar we zien geen condensatie als er geen ATP aanwezig is. Als ATP gehydrolyseerd wordt, kan condensin aan DNA binden op een manier die resistent is tegen hoge zoutconcentraties. Dit wijst op een topologische binding. Onze resultaten leiden tot een model waarin we voorstellen dat condensin meerdere stappen neemt om DNA te condenseren. We voeren ook een discussie over de implicaties van onze bevindingen voor de verschillende modellen van DNA condensatie.
De verwachting is dat cohesin een zeer sterk en stabiel molecuul is, maar er zijn geen directe metingen van deze eigenschappen. Deel III werkt toe naar het beantwoorden van deze vraag. In **hoofdstuk 6** beschrijven we een nieuwe methode voor het ankeren van biomoleculen in een magnetisch pincet: met koper-vrije klikchemie. Het relevante krachtregime van veel biologische processen is tientallen piconewtons, maar met conventionele anker technieken kan de aanhechting breken bij deze krachten. Extra problemen ontstaan als men wil meten aan DNA-eiwit complexen, omdat de ankertechniek kan zorgen voor aspecifieke interacties met het eiwit. Onze nieuwe methode gebruikt koper-vrije klikchemie: de reactie van een DBCO groep met een azide oppervlak. Deze techniek leidt tot covalent gelinkte DNA moleculen die torsioneel belemmerd zijn. Deze

gebonden DNA moleculen kunnen hoge krachten weerstaan en omdat DBCO geen native groep is, is deze methode zeer specifiek. Deze nieuwe techniek geeft de mogelijkheid om te meten aan DNA-eiwit complexen die direct uit cel lysaat geïsoleerd zijn.

In **hoofdstuk 7** presenteren we onze progressie in het ontwikkelen van een experimentele opstelling om de sterkte van het cohesin complex te onderzoeken door het meten van de kracht waarom het complex breekt met een magnetisch pincet. Eerst hebben we een construct ontwikkeld van cohesin in complex met DNA die lijkt op de *in vivo* situatie. Dit construct moet ook bruikbaar zijn in ons magnetisch pincet en geankerd worden met koper-vrije klik chemie. We beschrijven twee strategiën: purificatie van minichromosomen in cohesie door het DNA uit cellen te trekken, en purificatie van cohesin op DNA door aan cohesin met een SNAP-label te trekken. We presenteren biochemische controles die laten zien dat onze inspanningen helaas niet hebben geleid tot een bruikbaar construct voor enkel molecuul experimenten. Desalniettemin laten we de resultaten van onze eerste metingen zien. We eindigen met een discussie en aanbevelingen voor het voortzetten van dit project.

Curriculum Vitæ

Jorine Mirjam Eeftens

31-07-1990	Born in Breda, the Netherlands.
2002–2008	Secondary school Newman College Breda
2008–2011	B.Sc. Molecular Life Science Radboud Universiteit Nijmegen
2011–2013	M.Sc. Molecular Life Science Radboud Universiteit Nijmegen
2013–2017	PhD. Department of Bionanoscience Technische Universiteit Delft *Thesis:* Single-molecule approaches to unravel the mechanism of SMC proteins *Promotor:* Prof. dr. C. Dekker

Publications

1. **J.M. Eeftens**, C. Dekker, Catching DNA with hoops - clarifying the mechanism of SMC proteins through single-molecule biophysics. *submitted* (2017)

2. **J.M. Eeftens**, S. Bisht, J. Kerssemakers, C.H. Haering, C. Dekker, Real-time detection of condensin-driven DNA compaction reveals a multistep binding mechanism. *submitted* (2017)

3. T. Terakawa*, S. Bisth*, **J.M. Eeftens***, C. Dekker, C.H. Haering, E. Greene, The Condensin Complex Is A Mechanochemical Motor That Translocates Along DNA. *Science*, published online 7 september (2017)

4. **J.M. Eeftens***, A.J. Katan*, M. Kschonsak, M. Hassler, L. de Wilde, E.M. Dief, C.H. Haering, C. Dekker, Condensin Smc2-Smc4 dimers are flexible and dynamic. *Cell Reports* 14, 1813-1818 (2016)

5. **J.M. Eeftens**, J. van der Torre, D.R. Burnham, C. Dekker, Copper-free click chemistry for the attachment of biomolecules in magnetic tweezers. *BMC Biophysics* 8:9 (2015)

6. M.K. Herbert, **J.M. Eeftens**, M.B. Aerts, R.A.J. Esselink, B.R. Bloem, H.B. Kuiperij, M.M. Verbeek, CSF levels of DJ-1 and tau distinguish MSA patients from PD patients and controls. *Parkinsonism Related Disorders*, 20, 112:5 (2014).

7. M.C.M. Balemans, N. Nadif Kasri, M.V. Kopanitsa, N.O. Afinowi, G. Ramakers, T.A. Peters, A.J. Beynon, S.M. Janssen, R.C.J. van Summeren, **J.M. Eeftens**, N. Eikelenboom, M. Benevento, M. Tachibana, Y. Shinkai, T. Kleefstra, H. van Bokhoven, C.E.E.M. Van der Zee, Hippocampal dysfunction in the Euchromatin histone methyltransferase 1 heterozygous knockout mouse model for Kleefstra syndrome. *Human Molecular Genetics* 22, 852–866 (2013).